

**Nieuwe concepten voor golflengte-afstembare laserdiodes  
voor toekomstige telecommunicatienetwerken**

**New concepts of wavelength tunable laser diodes  
for future telecom networks**

Reinhard Laroy

Proefschrift tot het verkrijgen van de graad van  
Doctor in de Ingenieurswetenschappen: Elektrotechniek

Universiteit Gent  
Faculteit Ingenieurswetenschappen  
Vakgroep Informatietechnologie  
Academiejaar 2005-2006



**Promotoren:**

Prof. dr. ir. G. Morthier, Universiteit Gent, INTEC  
Prof. dr. ir. R. Baets, Universiteit Gent, INTEC

**Examencommissie:**

Prof. dr. ir. D. De Zutter (voorzitter), Universiteit Gent, INTEC  
Prof. dr. ir. M.-C. Amann, Technical University of Munich  
Dr. E.A.J.M. Bente, Technische Universiteit Eindhoven  
Prof. dr. P. Clauws, Universiteit Gent, Vaste-stofwetenschappen  
Prof. dr. ir. K. Neyts, Universiteit Gent, ELIS  
Prof. dr. ir. D. Van Thourhout, Universiteit Gent, INTEC

Universiteit Gent  
Faculteit Ingenieurswetenschappen

Vakgroep Informatietechnologie (INTEC)  
Sint-Pietersnieuwstraat 41  
B-9000 Gent  
België

Tel.: +32-9-264.33.16  
Fax: +32-9-264.35.93  
<http://www.intec.UGent.be>

Dit werk kwam tot stand in het kader van een specialisatiebeurs van het IWT - Instituut voor de Aanmoediging van Innovatie door Wetenschap en Technologie in Vlaanderen.

This work was carried out in the context of a specialisation grant from the Flemish Institute for the Industrial Advancement of Scientific and Technological Research (IWT).



# Preface - Voorwoord

Vier en een half jaar geleden begon ik aan mijn doctoraatsavontuur. Op de momenten dat Murphy toesloeg of ik weer eens in een sukkelstraatje beland was, leek het een eeuwigheid te duren maar als ik nu terugkijk lijkt het voorbij voor ik het goed en wel besef. Dat heb ik te danken aan heel wat mensen.

Allereerst wil ik Geert en Roel als promotoren bedanken om mij met raad bij te staan en mij door de knelmomenten heen te loodsen.

Voor de praktische kant waren er gelukkig Hendrik, Dirk en Bart die me uit de nood hielpen met meetproblemen, Steven en Liesbet die mijn processing tot een goed einde brachten en handige Luc die mijn rare ontwerpen fysisch vorm gaf.

De boog kan niet altijd gespannen staan, dus gelukkig had ik fantastische bureaugenootjes die af en toe voor de broodnodige afleiding zorgden. Ons gezellig 39-burootje met Bert, Peter, Björn en Alberto waar het altijd wel te warm of te koud was. Maar ook de verpozing tijdens het schrijven dankzij Sam, Olivier, John, Wim, Peter en Freddie heeft voor een aangename verpozing gezorgd bij het tot stand komen van dit boekje. En hoe kan ik de legendarische koffiepauzes vergeten waar alles eens lekker gerelativeerd werd.

Eigenlijk zou ik alle andere collega's hier ook kunnen opnoemen, want elk van hen heeft me wel iets bijgebracht de laatste jaren. Eén iemand verdient evenwel een aparte vermelding. Lieven was de gangmaker, de ambiencebrenger maar ook de toeverlaat waar ik tijdens de werkuren en erna even met mijn frustraties of problemen terecht kon.

Khad ook het geluk (en soms ongeluk) om een aantal thesisstudentjes te hebben die een deel van de weg samen met mij afgelegd hebben.

Diederik die samen met mij de wondere wereld van de roosters ontdekte, Dominique en zijn sensoren en Stijn<sup>2</sup> die de laatste maanden voor wat schwung zorgden.

I would also like to thank my Newton project partners from Munich, Stockholm and Dublin. A special thanks goes to Rene for the interesting discussions, the sharing of frustrations and the funny moments.

Naast toffe collega's had ik ook een resem toffe vrienden om op terug te vallen. In het bijzonder wil ik hier Matthias, Joost, Stefan en Hilke vermelden die elk op hun eigen speciale manier als steunpilaar gediend hebben. Hoe had ik de laatste jaren doorgekomen zonder vrienden zoals jullie.

Last but not least verdienen mijn ouders en familie ook heel wat dank want zonder hen was ik niet de man geworden die ik nu ben. Bedankt voor alles!

Reinhard Laroy  
Gent, 14 februari 2006

# Contents

<b>Preface - Voorwoord</b>	<b>i</b>
<b>Contents</b>	<b>iii</b>
<b>Dutch summary - Nederlandstalige samenvatting</b>	<b>ix</b>
<b>English summary</b>	<b>xiii</b>
<b>1 Introduction</b>	<b>1</b>
1.1 Why widely tunable lasers? . . . . .	3
1.1.1 WDM applications . . . . .	3
1.1.2 Sensor applications . . . . .	4
1.2 Specifications for WDM applications . . . . .	6
1.3 Goals of this work . . . . .	8
1.4 Outline of this thesis . . . . .	9
1.5 Publications . . . . .	10
1.5.1 International Journals . . . . .	10
1.5.2 International Conferences . . . . .	11
<b>2 Tuning mechanisms and laser concepts</b>	<b>13</b>
2.1 Laser basics . . . . .	14
2.2 Basic tuning mechanisms . . . . .	16
2.2.1 Electrical tuning . . . . .	16
2.2.2 Thermal tuning . . . . .	17
2.2.3 Mechanical tuning . . . . .	18
2.3 Tunable laser concepts . . . . .	19
2.3.1 Distributed Bragg Reflector (DBR) laser . . . . .	19
2.3.2 Tunable Twin-Guide (TTG) laser . . . . .	19
2.4 Existing concepts of Widely Tunable Lasers . . . . .	21
2.4.1 Different types of widely tunable lasers . . . . .	21

2.4.2	Superstructure Grating or Sampled Grating Distributed Bragg laser . . . . .	25
2.4.3	Digital-Supermode Distributed Bragg Reflector . . . . .	26
2.4.4	Grating-assisted coupler with rear sampled reflector . . . . .	26
2.5	Two New Concepts . . . . .	27
2.5.1	Widely Tunable Twin Guide(TTG) Laser . . . . .	27
2.5.2	Widely Tunable Y-Branch Laser . . . . .	28
<b>3</b>	<b>Diffraction Gratings</b> . . . . .	<b>31</b>
3.1	Uniform Gratings . . . . .	31
3.1.1	Fresnel approach . . . . .	32
3.1.2	Coupled-mode theory . . . . .	33
3.1.3	Transfer matrix method . . . . .	34
3.2	Sampled Gratings . . . . .	36
3.3	Superstructure Gratings . . . . .	39
3.4	Fabrication . . . . .	41
3.4.1	Holography . . . . .	42
3.4.2	E-beam lithography . . . . .	42
3.4.3	Controlling the depth of overgrown gratings . . . . .	44
3.4.4	Creating a $\pi$ phase shift . . . . .	45
3.5	Measurements of overgrown gratings . . . . .	46
3.6	Influence of gain . . . . .	50
3.6.1	Effects on Reflection Spectra . . . . .	50
3.6.2	Optimisation . . . . .	51
3.7	Influence of facet reflections . . . . .	53
3.8	Conclusions . . . . .	55
<b>4</b>	<b>Widely Tunable Twin-Guide Lasers</b> . . . . .	<b>57</b>
4.1	Device Principle . . . . .	57
4.1.1	The widely tunable twin-guide laser . . . . .	58
4.1.2	Layer Structure . . . . .	60
4.1.3	Leakage Currents . . . . .	61
4.2	Design Rules for wide tuning . . . . .	62
4.2.1	Quasi-continuous tuning . . . . .	62
4.2.2	Large tuning range . . . . .	63
4.2.3	High side-mode suppression . . . . .	64
4.3	Simulations . . . . .	65
4.3.1	Limitations and Design choices . . . . .	66
4.3.2	Threshold analysis of SG-TTGs . . . . .	66

4.3.3	Threshold analysis of SSG-TTGs . . . . .	68
4.4	Fabrication . . . . .	68
4.5	Measurements . . . . .	71
4.6	Alternative thermal designs . . . . .	76
4.6.1	Thermally tunable sampled grating DFB laser . . . . .	77
4.6.2	BCB-bonded thermally tunable SGDFB . . . . .	78
4.7	Conclusions and further research . . . . .	79
<b>5</b>	<b>Modulated Grating Y-Branch Laser</b>	<b>81</b>
5.1	Device Principle . . . . .	81
5.2	Design . . . . .	82
5.2.1	High side-mode suppression . . . . .	83
5.2.2	High output power and low power variation . . . . .	84
5.2.3	Reducing the number of control currents . . . . .	84
5.3	Fabrication . . . . .	85
5.4	Measurements . . . . .	86
5.5	Conclusions . . . . .	90
<b>6</b>	<b>Control and Stabilisation</b>	<b>91</b>
6.1	Existing Methods . . . . .	92
6.1.1	Frequency stabilisation . . . . .	92
6.1.2	Mode stabilisation . . . . .	94
6.2	Calibration of an MG-Y laser . . . . .	95
6.3	Stabilisation of an MG-Y laser . . . . .	99
6.3.1	Mode Stabilisation Scheme . . . . .	99
6.3.2	Control experiments . . . . .	101
6.3.3	Ratio of right detector currents . . . . .	105
6.4	The widely tunable twin-guide lasers . . . . .	105
6.4.1	Characterisation . . . . .	106
6.4.2	Control . . . . .	106
6.5	Conclusions . . . . .	109
<b>7</b>	<b>Modulation</b>	<b>111</b>
7.1	Noise characteristics of an SG-TTG laser . . . . .	111
7.1.1	Relative intensity noise . . . . .	112
7.1.2	Extracting the modulation bandwidth . . . . .	113
7.1.3	Indication of actual bandwidth . . . . .	114
7.2	Small-Signal Modulation of an SG-TTG laser . . . . .	116
7.3	The Modulated Grating Y-branch laser . . . . .	119
7.4	Comparison with other widely tunable lasers . . . . .	120

<b>8</b>	<b>Conclusions and Perspectives</b>	<b>121</b>
8.1	Conclusions . . . . .	121
8.2	Perspectives and Future Directions . . . . .	122
<b>A</b>	<b>Acronyms</b>	<b>125</b>
	<b>List of figures</b>	<b>127</b>
	<b>Bibliography</b>	<b>131</b>

# **Summary**

# **Samenvatting**



# Dutch summary

## Samenvatting

### **Nieuwe concepten voor golflengte-afstembare laserdiodes voor toekomstige WDM-netwerken**

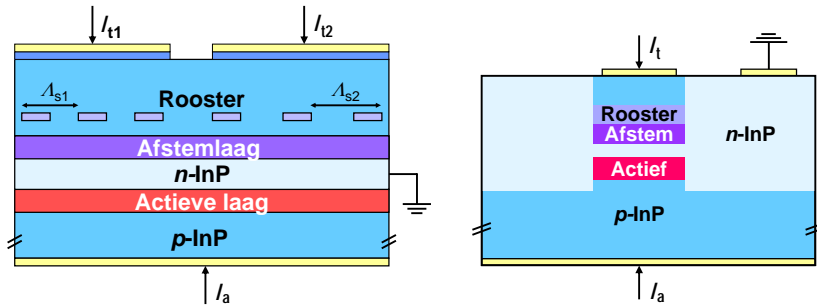
Breed-afstembare halfgeleiderlaserdiodes met een afstembereik van verschillende tientallen nanometers zijn belangrijke componenten voor toekomstige optische telecommunicatienetwerken en sensorapplicaties. De breed-afstembare lasers zullen telecomoperatoren helpen om aan de steeds groter wordende bandbreedtevrage te voldoen tegen een aanvaardbare prijs en daarnaast maken ze de introductie van nieuwe functionaliteit en hogere flexibiliteit in het netwerk mogelijk.

Het hoofddoel van dit doctoraatsonderzoek was het ontwerpen en onderzoeken van nieuwe types van breed-afstembare laserdiodes die dezelfde eigenschappen hebben als (niet afstembare) DFB lasers, d.w.z. een hoog uitgangsvermogen en een hoge zijmode-onderdrukking en daarnaast beschikken over een breed afstembereik, een gemakkelijk fabricage en een eenvoudige controle.

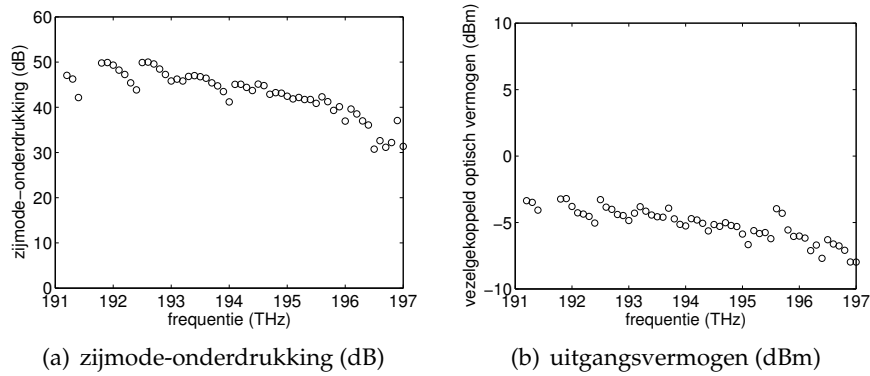
#### **Breed afstembare TTG laser**

Een breed afstembare twin-guide (TTG) laser [1, 2] bestaat uit twee TTG secties waarvan enkel de superperiode van de diffractieroosters verschillend is. De TTG lagenstructuur (Fig. 1) bevat twee dubbele heterostructuren met een n-scheidingslaag tussenin die de afstemlaag en de actieve laag van elkaar scheiden zodat de versterking en de filtering onafhankelijk kunnen aangepast worden.

Door de verschillende superperiode liggen de reflectiepieken van de roosters op een verschillende afstand t.o.v. elkaar. De frequentie



**Figuur 1:** Breed afstembare TTG laser met bemonsterde roosters

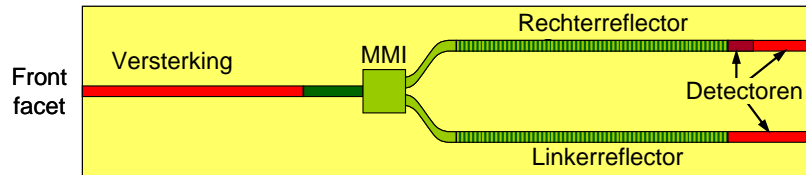


**Figuur 2:** Meetresultaten van de breed-afstembare TTG laser. Voor elke gestandaardiseerde ITU frequentie wordt de beste meetwaarde getoond.

waarbij de pieken van beide roosters overlappen, zal het eerst de laserdrempel bereiken en daar zal laserwerking optreden.

Door één afstemstroom te verhogen, zal het reflectiespectrum van de betreffende sectie naar hogere frequenties opschuiven en de overlappende pieken treden nu op bij een andere frequentie. Dit is het Vernier-effect. De frequenties tussen die sprongen worden bereikbaar door beide afstemstromen samen te verhogen, want de overlappende pieken verschuiven dan continu naar hogere frequenties. Slechts twee afstemstromen zijn nodig om over een breed frequentiebereik af te stemmen. Dit maakt de karakterisatie minder tijdrovend dan bij andere breed-afstembare concepten. De laser kan met bestaande technologieën gefabriceerd worden.

De performantie van de breed-afstembare twin-guide lasers (Fig. 2) is vergelijkbaar met die van andere breed-afstembare monolitische la-



**Figuur 3:** Breed afstembare Y laser met geïntegreerde detectoren

sers. Een afstembereik van 6THz (meer dan 40nm) werd waargenomen terwijl de zijmode-onderdrukking boven 40dB blijft voor de meeste ITU frequenties. Een hoog uitgangsvermogen van meer dan 20mW werd ook aangetoond.

De maximale theoretische bandbreedte voor directe modulatie ligt boven de 20GHz, wat de hoogste waarde is die tot nu toe gerapporteerd werd. De 3dB-bandbreedte bij 250mW geeft een indicatie dat de praktisch haalbare bandbreedte in de buurt van 12GHz zal liggen. Aangezien de huidige lasers niet ontworpen waren voor modulatie bij hoge frequenties was maar 1GHz haalbaar.

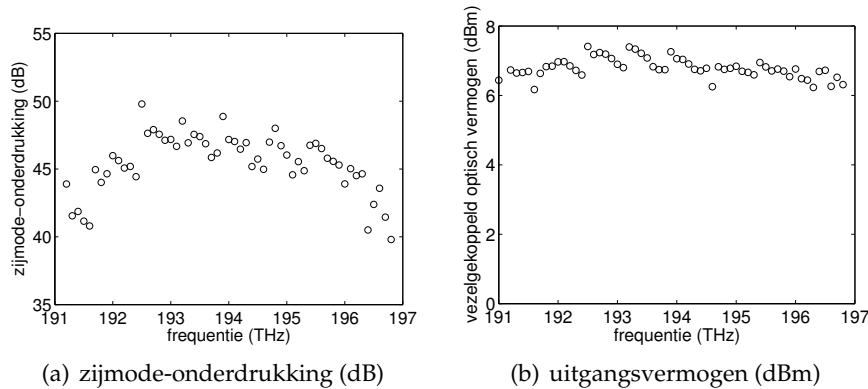
### Breed-afstembare Y laser

In de breed afstembare Y laser [3, 4] worden de reflectoren met licht verschillende piekspatiëring achteraan geplaatst (Fig. 3). De gereflecteerde signalen worden via een multi-mode interferentiekoppelaar coherent opgeteld (additief Vernier-effect). De frequentie waar twee reflectiepieken perfect overlappen wordt de emissiefrequentie als ook de cavitteitsmode daar overlapt.

Een hogere zijmode-onderdrukking wordt bekomen dan bij het multiplicatieve Vernier-effect (bijv. bij een (S)SG-DBR laser) omdat de naburige pieken die hier ook gedeeltelijk overlappen uit fase zijn.

Dankzij een goed roosterdesign en een nauwkeurige fabricage van de armen zijn er enkel 3 onafhankelijke afstemstromen nodig om de laser te controleren. De twee reflectorstromen veranderen de frequentie over een breed bereik en de fasestroom zorgt ervoor dat de cavitteitsmode overlapt met die reflectorpieken.

De breed afstembare MG-Y lasers (Fig. 4) zijn afstembaar over een breed frequentiebereik (191.05-196.80THz) dat de volledige C- of L-frequentieband overspant terwijl een hoge zijmode-onderdrukking van minstens 40dB bewaard blijft. Het uitgangsvermogen van 30 à 40 mW was het hoogste dat ooit voor een monolitische afstembare laser zonder



**Figuur 4:** Meetresultaten van de breed-afstembare MG-Y laser. Voor elke ge-standardiseerde ITU frequentie wordt de beste meetwaarde getoond.

geïntegreerde versterker gerapporteerd werd, want bij het verlaten van de caviteit moet het licht geen verliesrijke reflector passeren.

Aangezien er slechts drie controlestromen nodig zijn, heeft de MG-Y laser dezelfde controlecomplexiteit als SG-DBR of GCSR lasers. Voor modestabilisatie werden er detectoren geïntegreerd achter de reflectoren. Een hoge zijmode-onderdrukking en een hoog uitgangsvermogen wordt bekomen als de caviteitsmode overlapt met reflectorpieken van beide diffractieroosters, dus een optimaal werkingpunt wordt gevonden bij minimale detectorstromen. Op basis hiervan kan een stabilisatieschema uitgewerkt worden dat het werkingpunt stabiliseert in het midden van de werkingscel en een modesprong voorkomt.

Een 8GHz directe modulatiebandbreedte voor de MG-Y laser werd opgemeten [5, 6] bij 80mA actieve stroom. Het theoretische maximum geeft aan dat dit nog kan verdubbeld worden door een beter ontwerp dat aangepast is aan hoge frequenties.

## Besluit

Twee types van breed-afstembare lasers diodes werden ontwikkeld en experimenteel onderzocht tijdens dit doctoraatsonderzoek. Beide ontwerpen voldoen aan alle telecomspecificaties en vertonen een beloftevol dynamisch gedrag. De twee ontwerpen zijn waardige competitie voor de reeds bestaande lichtbronnen voor optische telecommunicatienetwerken.

# English summary

## **New concepts of wavelength tunable laser diodes for future telecom networks**

Widely tunable semiconductor laser diodes with tuning ranges of several tens of nanometers are considered key components in optical telecommunication networks and sensor applications. Those widely tunable lasers can help telecom operators worldwide to respond to the increasing bandwidth demand at a low price, while introducing new functionality and higher flexibility in the network.

The primary goal of this doctoral research was to develop and experimentally investigate new types of widely tunable laser diodes that have the same qualities as (non-tunable) DFB lasers, i.e. high output power and high side-mode suppression, and are widely tunable, easily controllable and easily manufacturable.

### **Widely Tunable Twin Guide Laser**

A widely tunable twin-guide (TTG) laser [1, 2] is a two section TTG laser [7]. The device structure of a TTG laser (Fig. 5) consists of two double heterojunctions with an n-separation layer in the middle that electronically decouples the active layer and tuning layer, so gain and filtering can be controlled independently.

Both sections contain a sampled grating or a superstructure grating with different superperiod resulting in reflection spectra with slightly different reflection peak spacing. The frequency where peaks of both reflectors perfectly overlap will reach the laser threshold first and start lasing.

By increasing one reflector current, its reflection spectrum will move to higher frequencies and the overlapping peaks will occur at another frequency. This is called the Vernier effect. The frequencies in between

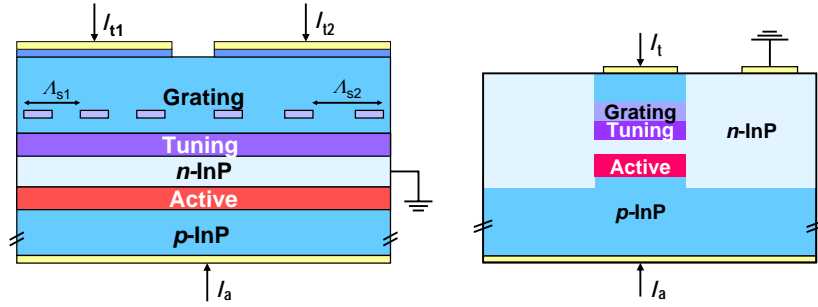


**Figure 5:** Sampled Grating Tunable Twin Guide Laser

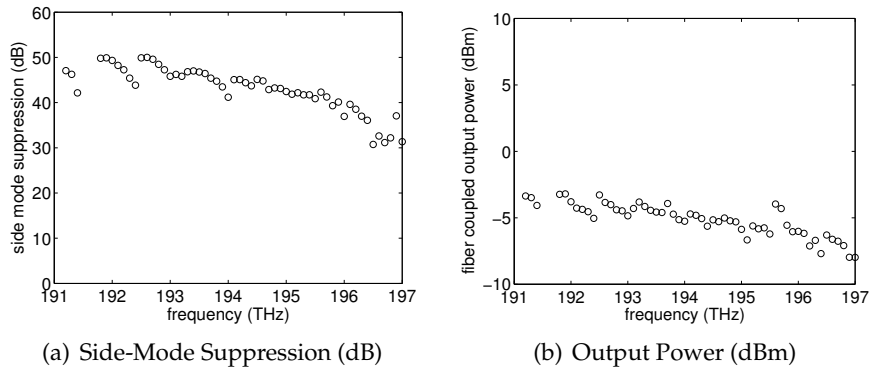


**Figure 6:** Measurement characteristics of a widely tunable twin-guide laser. For each standardised ITU frequency the best measurement point is shown.

the frequency jumps are reachable by increasing both reflector currents together, causing a continuous move of the overlapping peaks to higher frequencies. Only two tuning currents are required to obtain tuning over a large wavelength range, which makes the characterisation substantially less time consuming. The device can easily be manufactured with conventional DFB laser fabrication technology.

The performance of the widely tunable twin-guide lasers (Fig. 6) is comparable with that of other monolithic widely tunable lasers. A tuning range of 6THz (over 40nm) while maintaining a side-mode suppression of more than 40dB for most ITU channels was demonstrated during this PhD research. A high output power of more than 20mW was obtained as well.

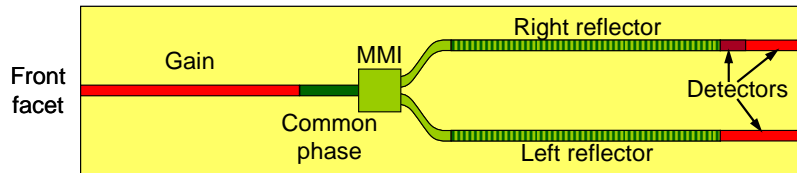


**Figure 7:** A Modulated Grating Y-Branch Laser Diode with integrated photo detectors

The widely tunable twin-guide laser has a promising dynamic behavior. It has a maximum theoretical bandwidth above 20GHz which is the highest value reported so far and the 3dB bandwidth at 250mA indicates that an actual bandwidth of 12GHz should be possible. The current batch of lasers were not designed for high-speed modulation, so only a 1GHz modulation can be reached at the moment.

### Widely Tunable Y-Branch Laser

A schematic of a Modulated Grating Y-Branch (MG-Y) laser [3, 4] is shown in Figure 7. Two reflectors with slightly different peak spacing are placed at the back. The reflected signals are added up coherently by the multi-mode interference coupler. The frequency where both peaks overlap perfectly will be the output frequency if the cavity mode coincides as well. This is called the additive Vernier effect.

A higher side mode suppression than with the multiplicative Vernier effect (used with the (S)SG-DBR laser) is obtained, because the neighboring peaks that only overlap partly, add partly out of phase.

Thanks to a careful design of the gratings and a careful processing of the branches, only 3 independent tuning currents are necessary to control the device. The two reflector currents are changed to tune the frequency, while the phase current guarantees an overlap of the cavity mode and the perfectly overlapping reflection peaks.

State-of-the-art MG-Y lasers (Fig. 8) show a wide tuning range (191.05-196.80THz) with full C or L-band frequency coverage while maintaining a high side-mode suppression ratio of more than 40dB. The output power was the highest measured and reported for a monolithic tunable laser (without integrated amplifier) because the light does not have to pass a lossy reflector section before exiting the laser cavity.

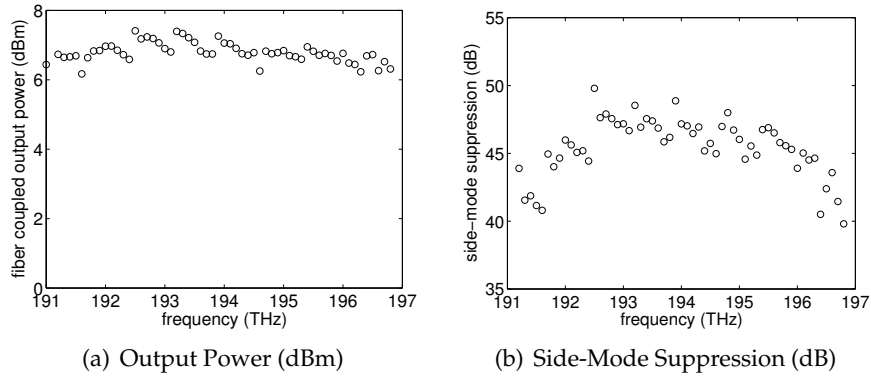


**Figure 8:** Measurement characteristics of a widely tunable MG-Y laser

With three control currents it has the same control complexity as SG-DBR or GCSR lasers. For mode stabilisation purposes an integrated photo detector was added after each reflector. A high side-mode suppression and high output power are obtained when the cavity mode overlaps with a reflection peak of both reflectors, so an optimal operating point coincides with a minimum in both detector currents. This stabilisation scheme guarantees that the operating point of an MG-Y remains in the center of the cell preventing a mode hop.

The MG-Y laser shows good dynamic behaviour [5, 6]. An 8GHz bandwidth was measured at 80mA active current. One of the highest reported so far, while the intrinsic modulation bandwidth indicates that that number can be doubled through a better high frequency design.

## Conclusions

Two new types of widely tunable laser diodes were developed and experimentally investigated during this doctoral research. Both concepts satisfy all the telecom specifications and they have a promising dynamic behavior. Both designs are worthy competitors with other transmitters for optical telecom networks.

**English text**



# Chapter 1

## Introduction

Downloading music and video for your iPod, video conferencing over the internet, renting and watching a video online, ... are bandwidth consuming internet applications that are gaining more popularity every day. Internet has become a daily consumer item in many households and several Terabits of bandwidth are generated every day [8].

All these bits are sent over an optical fiber based telecom network using wavelength division multiplexing (WDM) [9, 10]. Several signals transmitted by different laser diodes at different wavelengths (frequencies) are combined onto one optical fiber without interfering with each other (Fig. 1.1). The principle can be compared to different radio stations broadcasting at different frequencies in the same air space. Just like radio frequencies, the telecom frequencies have been standardised by the International Telecommunication Union. This ITU-grid [11] consists of equally spaced frequencies centered around 193.1THz.

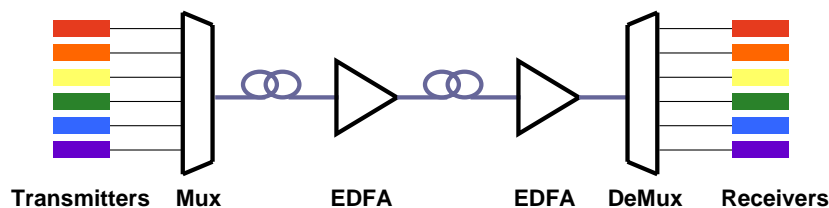


**Figure 1.1:** Principle of wavelength division multiplexing (WDM): Different optical signals that are transmitted at different frequencies are multiplexed and transported over an optical fiber. EDFAs are used to amplify the signals and after de-multiplexing the different optical signals are translated to electrical signals through receivers.

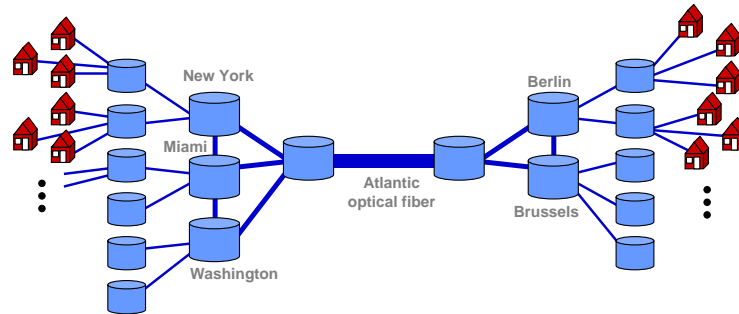


**Figure 1.2:** Example of a telecom network connecting Europe with the United States

When the maximum installed capacity of a link is reached, it is easier and cheaper to install a new laser diode on the same optical fiber transmitting at a previously unused ITU frequency than installing a new optical fiber. Each optical fiber has a potential bandwidth of 25THz. This corresponds to the frequency windows at 1300nm and 1500nm where low loss signal propagation is possible.

Due to the introduction of broadband internet, the bandwidth demand is still growing every year. The internet data traffic is consuming more and more capacity of the telecom networks. Even though the bandwidth increase is slowing down, the available network capacity will run out at some point. For example, the capacity of the optical fibers over the Atlantic Ocean (Fig. 1.2) is expected to saturate between 2007-2015 [12]. Next-generation equipment like optical add-drop multiplexers and cross-connects should be able to handle network traffic more efficiently and will thus postpone this saturation of the capacity.

However, the increasing bandwidth demand isn't the only driving force in the optical industry. The introduction of new functionality that reduces the operating and installing cost and simplifies the network management is gaining more interest from telecom operators worldwide [13]. Widely tunable lasers can help those operators in adding more flexibility and functionality to the telecom network, because their operating frequency can easily be changed.

Since the collapse of the telecom market at the beginning of this millennium, telecom operators have been more careful in employing new network technologies. So the first section of this chapter will concentrate on why widely tunable lasers can be of commercial interest for telecom operators and other markets. The second part of this chapter

will go into more detail about the telecom specifications that the new designs have to satisfy in order to be of commercial interest. Section three will describe the goals of this PhD research and section four will give an outline of the other chapters. This chapter is concluded with an overview of the published papers related to this doctoral research.

## **1.1 Why widely tunable lasers?**

Widely tunable lasers can be used in a multitude of applications ranging from telecom oriented purposes to the sensor market.

### **1.1.1 WDM applications**

Telecom data carriers are very careful in adopting new technologies, but cost reduction is still one of their main driving forces. Widely tunable lasers can help them reduce the cost of installing and running networks. However, new functionality and more flexibility has been the main driving force for the research into widely tunable lasers. Both application areas are discussed in detail below.

#### **Reducing cost**

Telecom operators offer a qualitative service to their customers guaranteeing a certain uptime of their network. If a laser breaks down, the network should be up and running as soon as possible. For every operating laser a spare laser is installed in the network, so a spare laser takes over when a laser breaks down.

Widely tunable lasers can be used as spare laser in the network. When one of the DFB lasers fails, the widely tunable laser temporarily takes over until the failed laser can be replaced. The cost reduction is high because the carriers no longer need a separate spare for every laser in the network, because the widely tunable laser can operate at different operating frequencies and the chances of several lasers breaking down at the same time are very slim. The spare lasers need to have the same performance as any fixed wavelength laser, but a higher price and a limited reliability compared to 'fixed' DFB lasers are acceptable for this application.

A second cost reduction step occurs when widely tunable lasers are used as replacement for failed lasers. Less inventory is needed because

a widely tunable laser can operate at different frequencies. This simplifies the inventory management and reduces the operating cost. For this purpose widely tunable lasers need to have the same quality and reliability as "fixed" lasers, otherwise they won't be interesting as replacement lasers. A price that is 20% higher than fixed-wavelength devices is still competitive.

### **New functionality**

Adding new functionality and more flexibility to the telecom networks has been the main driving force for the research and development of widely tunable lasers in the past. It is still unclear if and when this new functionality will be deployed in real systems, because the topology and the management of the network needs to be changed to take full advantage of these new functionalities. Nevertheless it is interesting to go into more detail about what advantages they can have for telecom operators.

Widely tunable lasers can be used in the creation of reconfigurable dynamic all-optical networks [14] where fast relocation of bandwidth is possible by using optical cross-connects and optical add/drop multiplexers in network nodes. When activating a new connection, a signal is sent over an unused frequency and the optical routing components in every network node are reconfigured to send this new signal to the correct receiver in a matter of minutes. At present, adding bandwidth to a particular line can take days or weeks, because a technician has to intervene to add patch cords and change telecom boards. In these all-optical network applications broad tunability of the lasers is very important otherwise the all-optical cross-connects only work over a very limited bandwidth.

Widely tunable lasers also enable optical switching of data packets [15, 16]. Data is sent in small packets through the network and is routed based on the wavelength/frequency of the packet without making a node to node connection in advance.

#### **1.1.2 Sensor applications**

The use of widely tunable lasers in field-deployable, long-term stable sensor is a new market that has gained much interest after the telecom bubble burst at the end of the nineties. The high speed and long-term accuracy of electronically tunable laser diodes has made them a very



**Figure 1.3:** Optical sensor incorporated in pressure vessel to check the integrity of the vessel.

interesting light source for applications like gas sensing and structural health monitoring [17, 18].

An optical sensor can generate data on a wide range of metrics like temperature, pressure, vibration, distance, gas presence, .... The optical properties change if one of these chosen metrics changes, resulting in a shift of the central wavelength of your transmitted or reflected spectrum.

All this data is then sent back to an intelligent software system that can analyze the incoming data and alert in case of problems. A real-time and correct analysis is only possible when a quick interrogation of the optical sensor with a high accuracy is possible. Electronically tunable lasers provide the fastest interrogation creating more sensor output in a shorter period of time, while a long term reliability in the toughest environments can be guaranteed. An update of the control parameters from time to time can extend the lifetime of the lasers even further.

Widely tunable lasers can also be used for long-distance data transport enabling interrogation of optical sensors that are up to 70 km away. Monitoring of 20km deep oil wells is one of the new applications that is possible thanks to the introduction of electronically tunable lasers.

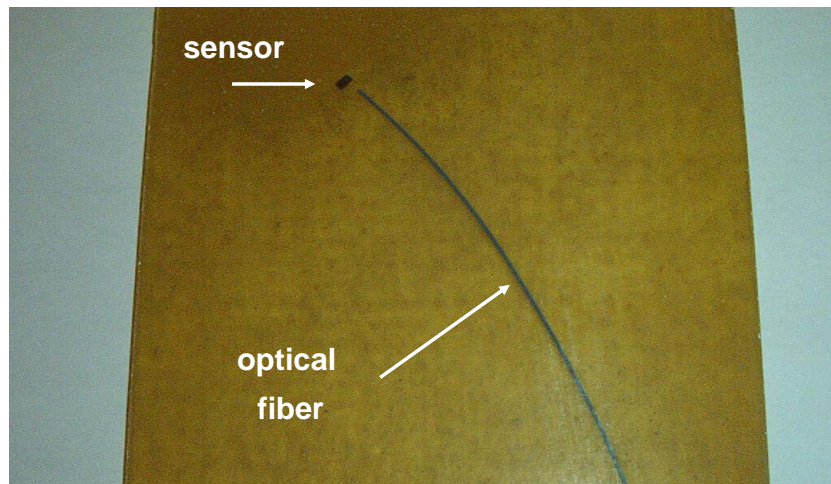


Figure 1.4: Optical sensor incorporated in a plate

## 1.2 Specifications for WDM applications

Wavelength tunable laser diodes have to satisfy a set of requirements to be deployable in WDM networks [19].

### Tuning requirements

Obtaining a large enough tuning range in a widely tunable laser is important. A tuning range that covers the full C-band or the full L-band is a target.

Additionally, the accuracy and the stability of the output wavelength are essential otherwise the developed tunable laser diode won't be commercially interesting. For the accuracy a frequency error smaller than 10% of the channel spacing is acceptable. A feedback scheme can be used to minimize the error. The control and stabilisation possibilities are discussed in chapter 6.

Fast switching is also of commercial interest for all-optical networks. For example, optical cross-connects need laser sources that can be tuned fast over a large tuning range.

### Output power

Wavelength tunable lasers need to have an output power that is at least as high as that of 'fixed' DFB lasers (10mW or more) to be worthy re-

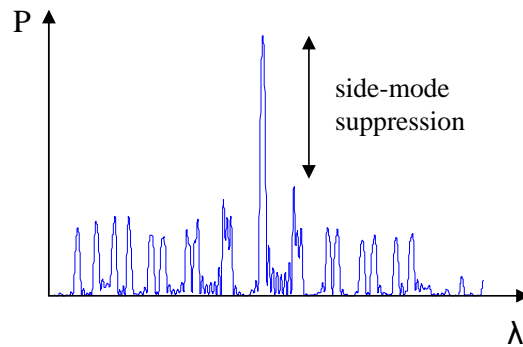


Figure 1.5: Definition of side-mode-suppression

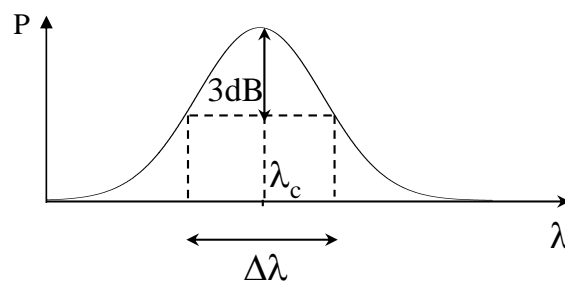


Figure 1.6: Definition of linewidth  $\Delta\lambda$

placements. In the case of low output powers extra amplifiers need to be introduced to the optical network causing a large cost increase for the telecom operators.

The output power of electrically tuned laser diodes varies with tuning current due to the carrier-induced losses. This power variation should be less than 3dB over the full tuning range.

### Monomodal behaviour

The output light needs to be monomodal otherwise the transmitted signal starts interfering with other signals and data will be lost. The side-mode suppression (SMSR) is defined as the ratio of the power in the main mode and that of the strongest side-mode (Fig. 1.5). A side-mode suppression higher than 40dB is required to prevent interference from other channels in telecom networks.

### Linewidth and noise

Communication systems require a laser linewidth that is smaller than a couple of GHz. This linewidth is dependent on the phase noise of the optical signal. The linewidth  $\Delta\lambda$  is defined in Figure 1.6 as the peak width at half maximum.

The noise is typically described by the relative intensity noise (RIN), which compares the intensity fluctuations in the output power to the average output power. Out of the noise characteristics an idea of the maximum modulation bandwidth can be extracted. The noise characteristics and the modulation bandwidth are discussed in chapter 7.

## 1.3 Goals of this work

From the previous sections it is clear that widely tunable lasers with a tuning range of several tens of nanometers are interesting devices for many different applications. The many advantages have led to a multitude of tunable laser concepts in the past years (see chapter 2), but not one of these concepts has the same qualities as (non-tunable) DFB lasers, i.e. high output power and high side-mode suppression, and is widely tunable, easily controllable and easily manufacturable.

The primary goal of this doctoral research was to develop and experimentally investigate new types of widely tunable laser diodes which can be expected not to exhibit the disadvantages of existing types. This thesis includes design, fabrication, characterisation and control related activities for those new concepts.

The widely tunable twin-guide (TTG) laser is based on the concept of a TTG laser that was extensively investigated during the nineties. Some simulation results had already been presented before the start of this PhD but the biggest part of the research, design and development of the new concept still had to be done. The optimisation of the design to satisfy the telecom specifications was done during this doctoral research and the dynamic behavior was investigated as well. This concept was realised in cooperation with the Walter Schottky Institute of the Technical University of Munich (TU Munich). Most of the fabrication was done in Munich and they have a lot of expertise after developing the original TTG lasers.

Diffraction gratings play an important role in every widely tunable laser concept. The grating design is one of the decisive points with respect to the device performance of the laser. Through a good grat-

ing design a large tuning range and a good side-mode suppression can be obtained. The technology and optimisation of different grating concepts were investigated as part of this doctoral research to obtain a good tuning behaviour for the tunable laser concepts.

The widely tunable Y-branch laser is the second concept that was thoroughly investigated during this PhD. This laser concept was patented by IMEC and has been developed in cooperation with the new Swedish start-up Syntune. Our expertise was used in the design phase but the emphasis during this PhD was on the characterisation and the control of the first prototypes.

The control and the stabilisation of widely tunable lasers are key issues, because an accurate and stable light signal is necessary in telecom networks. Developing a control that is quick and easy to use is essential if the laser wants to be commercially interesting. Basic ideas about the control and the stabilisation were already developed for existing widely tunable laser concepts, but they needed to be fine-tuned or adapted to work with the new designs, because the operating principles of the new structures are slightly different. This research has been done in cooperation with Intune Technologies from Dublin.

At the end of the research it was expected that the new concepts of widely tunable laser diodes had a superior performance compared to the existing widely tunable laser diodes on one or more of the key issues like maximum output power, ease of control and tuning range. To this extent a comparison was made between existing types and the new concepts that are presented in this thesis.

## 1.4 Outline of this thesis

Chapter 2 introduces the working principle of widely tunable lasers and gives an overview of the existing concepts and their performance. The main advantages and disadvantages of the existing concepts are discussed and compared with the potential of the new concepts.

An extensive study of diffraction gratings is given in chapter 3. Different simulation methods are investigated and the design, the fabrication and the characterisation of different grating concepts are discussed. The influence of the gain and the facet reflections is also investigated.

The device principle of the widely tunable twin-guide laser is explained in chapter 4. Some design rules for wide tuning are discussed and some simulation results will be given. The fabrication is briefly

mentioned and the characterisation of the fabricated samples is summarised. Finally, some alternative designs are introduced.

The widely tunable Y laser is introduced in chapter 5. The working principle of the new laser concept is explained and some additional design rules are given that are particular to this concept. Finally, the characterisation of the new lasers is shown.

Chapter 6 discusses the control and stabilisation methods of the widely tunable lasers. After explaining the stabilisation algorithm, some experimental results are shown.

The dynamic behavior of the new concepts is investigated in chapter 7. Through noise measurements a theoretical maximum for the direct modulation bandwidth of the widely tunable twin-guide laser is extracted and compared with small-signal modulation measurements. Also the modulation of the widely tunable Y laser is briefly discussed. Finally, the obtained modulation results are compared with the values from other widely tunable lasers.

The results of this PhD research are summarised in chapter 8 and some perspectives on future steps are given.

## 1.5 Publications

The results obtained within this work have been published in various papers and were presented at various conferences. This paragraph gives an overview of the publications.

### 1.5.1 International Journals

- R. Laroy, R. Todt, R. Meyer, M.-C. Amann, G. Morthier, R. Baets, Direct modulation of widely tunable twin-guide lasers, *accepted for publication in Photonics Technology Letters*
- R. Laroy, G. Morthier, T. Mullane, M. Todd, R. Baets, Stabilisation and control of Widely Tunable MG-Y Lasers with Integrated Photodetectors, *submitted to IEE Proceedings-Optoelectronics*
- R. Todt, Th. Jacke, R. Meyer, J. Adler, R. Laroy, G. Morthier, M.-C. Amann, Sampled grating tunable twin-guide laser diodes with wide tuning range ( $\geq 40\text{nm}$ ) and large output power ( $\geq 10\text{mW}$ ), *Phys. Stat. Sol. (c)*, vol. 3(3), p.403-406 (2006)

- R. Todt, Th. Jacke, R. Meyer, J. Adler, R. Laroy, G. Morthier, M.-C. Amann, Sampled Grating Tunable Twin-Guide Laser Diodes With Over 40nm Electronic Tuning Range, *Photonics Technology Letters*, 17(12), p.2514-2516 (2005)
- R. Todt, Th. Jacke, M.C. Amann, R. Laroy, G. Morthier, R. Baets, Demonstration of Vernier effect tuning in tunable twin-guide laser diodes, *IEE Proceedings-Optoelectronics*, 152(2), p.66-71 (2005)
- R. Todt, Th. Jacke, R. Meyer, M.-C. Amann, R. Laroy, G. Morthier, Wide wavelength tuning of sampled-grating tunable twin-guide laser diodes, *Electronics Letters*, 40(23), p.1491-1492 (2004)

### 1.5.2 International Conferences

- R. Todt, Th. Jacke, R. Meyer, J. Adler, R. Laroy, G. Morthier, M.-C. Amann, State-of-the-art performance of widely tunable twin-guide laser diodes, European Semiconductor Laser Workshop (ESLW), United Kingdom, (2005)
- R. Laroy, G. Morthier, R. Todt, R. Meyer, M.C.-Amann, R. Baets, Intrinsic modulation bandwidths of widely tunable SG-TTG lasers, European Semiconductor laser Workshop 2005, United Kingdom, (2005)
- R. Todt, Th. Jacke, R. Meyer, J. Adler, R. Laroy, G. Morthier, M.-C. Amann, Widely tunable twin-guide laser diodes with over 40 nm-tuning range, Proc. of 32nd International Symposium on Compound Semiconductors (ISCS), Germany, p.Tu3.6 (2005)
- R. Todt, Th. Jacke, R. Meyer, J. Adler, R. Laroy, G. Morthier, M.-C. Amann, Widely tunable twin-guide laser diodes at 1.55 $\mu\text{m}$ , Proc. of OptoElectronics and Communications Conference, Post-Deadline Paper PDP07, South Korea, p.13-14 (2005)
- R. Laroy, G. Morthier, R. Baets, Widely Tunable Lasers for future WDM networks, IEEE/LEOS Benelux Annual Workshop 2005 (invited), Netherlands, p.7 (2005)
- R. Todt, T. Jacke, R. Meyer, R. Laroy, G. Morthier, MC. Amann, Wide-wavelength tuning of sampled grating tunable twin-guide laser diodes, SPIE's Photonics West Symposium, 5738, United States, p.253-261 (2005)

- R. Todt, Th. Jacke, R. Meyer, M-C Amann, R. Laroy, G. Morthier, Tunable twin-guide laser diodes for wide wavelength tuning at 1.55 $\mu$ m, SPIE conference Optics East, 5594, United States, p.94-101 (2004)
- G. Morthier, R. Laroy, I. Christiaens, R. Todt, Th. Jacke, M.-C. Amann, J.-O. Wesström, S. Hammerfeldt, T. Mullane, N. Ryan, M. Todd, New widely tunable edge-emitting laser diodes at 1.55 $\mu$ m developed in the European IST-project Newton, Asia-Pacific Optical Communications, China (2004)
- R. Laroy, G. Morthier, R. Baets, Influence of gain on reflection spectra in widely tunable lasers, European Semiconductor Laser Workshop 2004, Sweden, (2004)
- R. Todt, Th. Jacke, R. Meyer, M-C Amann, R. Laroy, G. Morthier, Wide wavelength tuning of sampled-grating tunable twin-guide laser diodes, European Semiconductor Laser Workshop, Sweden, (2004)
- R. Todt, Th. Jacke, R. Meyer, M-C Amann, R. Laroy, G. Morthier, Tuning performance of widely tunable twin-guide laser diodes, 28th WOCSDICE 2004, Slovakia, p.99-100 (2004).
- R. Todt, Th. Jacke, R. Meyer, M-C Amann, R. Laroy, G. Morthier, Design and Fabrication of Widely Tunable Twin-Guide Laser Diodes, Semiconductor and Integrated Opto-Electronics Conference (SIOE), United Kingdom, (2004)
- R. Laroy, G. Morthier, R. Baets, G. Sarlet, J.-O. Wesström, Characteristics of the modulated grating Y laser for future WDM networks, IEEE/Leos Benelux Annual Symposium 2003, Netherlands, p.55-57 (2003)
- R. Laroy, G. Morthier, R. Todt, R. Meyer, M.-C. Amann, Progress on the development of a widely tunable TTG laser, IST-NEWTON Workshop on tunable laser diodes, Italy, (2003)
- J.-O. Wesström, S. Hammerfeldt, J. Buus, R. Siljan, R. Laroy, H. de Vries, Design of a Widely Tunable Modulated Grating Y-branch Laser using the Additive Vernier Effect for Improved Super-Mode Selection, 2002 IEEE International Semiconductor Laser Conference, Germany, p.99-100 (2002)

## Chapter 2

# Tuning mechanisms and laser concepts

It is expected that future optical telecommunication networks will rely on widely tunable lasers to provide extra flexibility, functionality and performance. This has led to a multitude of tunable laser concepts in the past years, but none of these concepts has the same qualities as (non-tunable) DFB lasers, i.e. high output power and high side-mode suppression, and is widely tunable, easily controllable and easily manufacturable.

The main objective of this PhD was to develop and experimentally investigate new types of widely tunable laser diodes which have a number of potential advantages over the existing concepts; e.g. high output powers, simple fabrication, better stability or simple tuning. All the new concepts rely on electronic tuning and offer therefore also the capability of fast wavelength switching.

This chapter will start with an introduction of some basic laser concepts and tuning mechanisms. Afterwards an overview of the existing widely tunable laser concepts and their performance is given. This overview is kept very brief but nevertheless contains the main advantages and disadvantages of the existing concepts. This is followed by an introduction of the new structures that were developed within this PhD research.

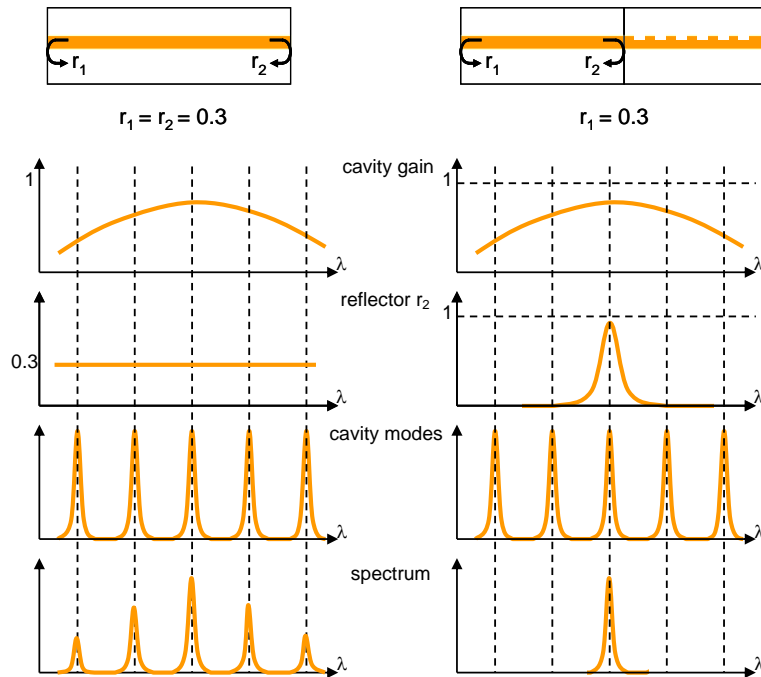


**Figure 2.1:** Lasing in a Fabry-Pérot laser (left column) and a DBR laser with a wavelength selective reflector (right)

## 2.1 Laser basics

Photons are created in the laser cavity through spontaneous emission and then further amplified by stimulated emission. Current is injected into the active layer to obtain enough gain through stimulated emission.

Lasing needs reflection (through mirrors) and amplification of the photons (through stimulated emission) in the laser cavity. Lasing occurs when the round trip gain is unity: the optical field after one round-trip in the cavity should be the same as the original field. The active current at which this resonance condition is met first is called the threshold current.

Gain clamping occurs above threshold and the extra carriers injected above threshold are converted into photons via the stimulated emission process. These photons are partly emitted towards the outside world via the laser facets and partly absorbed.

A laser starts operating at the wavelength where the cavity roundtrip gain  $g(\lambda)$  reaches unity first and where the roundtrip phase  $\phi(\lambda)$  is an integer multiple of  $2\pi$ .

For the cavity roundtrip gain to reach unity, the cavity gain needs to compensate the internal loss  $\alpha_i$  and the mirror loss  $\alpha_m$ , so the gain condition can be written as:

$$\Gamma g_a(\lambda) - \alpha_i - \alpha_m(\lambda) = 0 \quad (2.1)$$

with  $g_a$  the active-medium gain and  $\Gamma$  the confinement factor of the mode in the gain layer. The mirror loss  $\alpha_m$  can be made wavelength dependent by using diffraction gratings (§3) as mirrors.

The phase condition depends on the cavity length  $L$  and the effective refractive index  $n_{eff} = n'_{eff} + jn''_{eff}$ :

$$\lambda_M = \frac{2n'_{eff}L}{M} \quad (2.2)$$

with  $M$  the order of the cavity mode.

The solution gives a set of longitudinal cavity modes at which lasing can occur (Fig. 2.1). The laser will start lasing at the cavity mode that reaches the gain condition 2.1 first. This corresponds with the cavity mode that undergoes the lowest mirror losses. The wavelength can be tuned by changing the phase condition or the wavelength with minimal mirror loss. Both conditions are dependent on the effective refractive index.

A simple example of a wavelength selective mirror is a uniform grating (Fig. 2.1 (right column)). In a uniform grating the effective refractive index of the laser waveguide is periodically modulated. Light traveling through the grating is reflected at every change of the refractive index. Those reflections only interfere constructively in a small frequency range and lasing occurs at only one wavelength, the Bragg wavelength (§3.1):

$$\lambda_{laser} \approx \lambda_{Bragg} = 2\Lambda n'_{eff} \quad (2.3)$$

From formula 2.3, it is clear that tuning can be obtained by changing the real part of the effective refractive index  $n'_{eff}$ :

$$\Delta\lambda = \frac{|\Delta n'_{eff}|}{n'_{eff} \lambda_{B,0}} \quad (2.4)$$

with  $\lambda_{B,0}$  the Bragg wavelength without tuning.

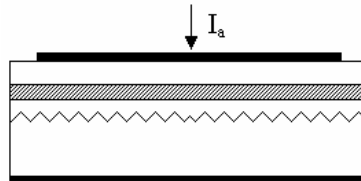


**Figure 2.2:** Distributed Feedback Laser

In a Distributed Feedback (DFB) laser [20, 21] a uniform diffraction grating is placed above or below the active layer (Fig. 2.2) creating a wavelength selective behaviour. The output wavelength is once again given by formula 2.3. Wavelength tuning can be obtained by changing the refractive index  $n_{eff}$  through heating.

Most telecom lasers sold today are DFB lasers due to their low cost, easy manufacturing, high reliability and stability, high output power and high side-mode suppression (SMSR). The DFB lasers set high requirements for the widely tunable laser concepts, if they want to be a worthy replacement for DFB lasers.

## 2.2 Basic tuning mechanisms

### 2.2.1 Electrical tuning

Many widely tunable laser concepts [7, 22, 23, 24, 25] use electrical tuning, where current is injected into the wavelength selective reflector to change the refractive index and thus creating a shift of the peak wavelength.

By injecting current a band-filling effect will occur. The injected electrons will move to the lower bands of the conduction band and the injected holes will occupy the highest bands of the valence band. So higher photon energies will be required to excite an electron from the valence band to the conduction band and the absorption coefficient will decrease.

Additionally the absorption of a photon can move the carrier to a higher energy state within the same band (intra-band) or move holes to another valence band (inter-valence band), while the extra energy is dissipated through lattice vibrations.

All these effects lead to a decrease of the absorption coefficient  $\alpha$  and also the imaginary part of the refractive index  $n_{eff}''$  decreases because both parameters are linked by the following formula:

$$\alpha(\lambda) = -2k_0 n_{eff}''(\lambda) \quad (2.5)$$

Through the Kramers-Kronig equations also the real part of the refractive index is decreased with increasing tuning current and through formula 2.3 the Bragg wavelength is moved to lower values.

Due to recombination a sustained currents needs to be applied to keep the wavelength change. At higher current densities the recombination increases more rapidly ( $\sim N^3$ ) limiting the achievable tuning range:

$$I_t = eV_t R(N) = eV_t \left( \frac{N}{\tau_s} + BN^2 + CN^3 \right) \quad (2.6)$$

with  $R(N)$  the recombination rate,  $e$  the charge of an electron,  $V_t$  the volume of the tuning region,  $\tau_s$  the carrier lifetime (order of a few nanoseconds),  $B$  the constant for the band-to-band radiative recombination,  $C$  the constant for the Auger recombination.

Additionally, the tuning efficiency decreases with increasing tuning current due to two parasitic heating effects. The tuning diode has a series resistance, so power is dissipated when a current runs through it causing heating (Joule effect). There is also heating through non-radiative recombination processes. Heating causes band gap shrinkage leading to an opposite effect on the refractive index decreasing the tuning range.

The wavelength can be switched by changing the amount of tuning current that is injected into the wavelength selective element. From formula 2.6 it is clear that the wavelength tuning speed for electrical tuning is limited by the effective carrier lifetime  $\tau_d$ , which is typically a few nanoseconds.

### 2.2.2 Thermal tuning

With thermal tuning the laser sample is heated to change the refractive index. At increasing temperature there are more hole-hole interactions in the valence band leading to a higher edge of the valence band. The same effect occurs with the electrons in the conduction band leading to a band gap shrinkage that lowers the photon energy needed for absorption. The refractive index enlarges due to this absorption increase.

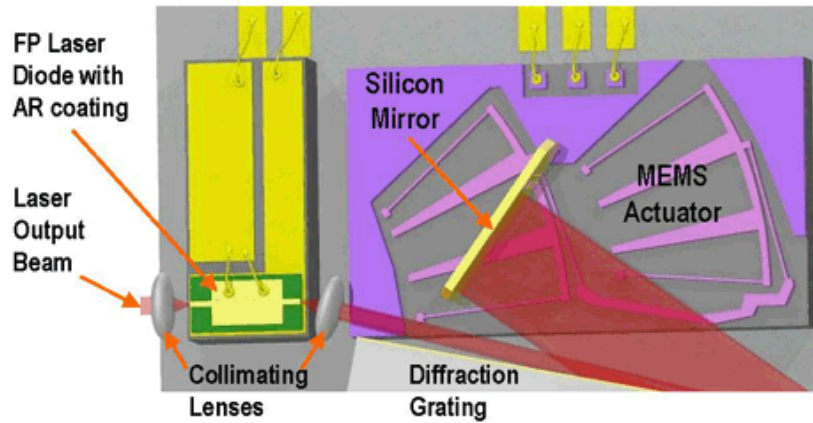


Figure 2.3: Mechanically tuned External Cavity Laser (ECL)

The wavelength increases with about 0.1nm/K for an InP telecom laser emitting around 1550nm.

The increase of threshold current with temperature is exponential, so the temperature increase is limited to around 60 degrees, leading to a limited tuning range of 6nm. By placing the tuning region further away from the active region higher temperatures are possible without increasing the threshold current leading to tuning ranges up to 15nm. In many cases at higher temperature there's also a reduced output power and a degradation of the laser performance.

Fast wavelength switching isn't possible in thermally tuned devices due to their slow thermal response on a timescale of milliseconds. The heat is moved from the waveguide to the chip, then to the subcarrier and finally taken away by the heat sink. The larger the thermal conductivity between those elements, the faster the switching can occur.

### 2.2.3 Mechanical tuning

Mechanical tuning alters the wavelength by mechanically changing the cavity length or the angle of incidence into the reflector (Fig. 2.3), but the switching is very slow (order of milliseconds).

The largest tuning range is obtained through mechanical tuning but the complex fabrication and packaging and the mechanical sensitivity make these devices quite expensive, so they are only used in test and measurement environments.

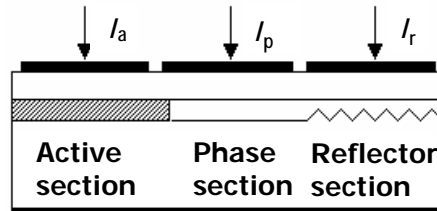


Figure 2.4: Distributed Bragg Reflector Laser

## 2.3 Tunable laser concepts

Before introducing a couple of state-of-the-art widely tunable laser concepts, some basic tunable laser concepts and their tuning mechanisms need to be introduced to understand the working principles of the more complicated widely tunable laser concepts.

### 2.3.1 Distributed Bragg Reflector (DBR) laser

A Distributed Bragg Reflector (DBR) laser [20] is a three or four section device (Fig. 2.4) in which the gain section amplifies the light, the reflector section(s) is responsible for the filtering and the phase section guarantees that the cavity mode is aligned with the reflector peaks so that a high side-mode suppression can be obtained.

A DBR laser has a fast electrical tuning [26, 27]. A limited tuning range of 5 to 10nm can be obtained by electronically tuning a DBR laser [28, 29]. DBR lasers have the disadvantage that an extra phase section is needed to obtain a high SMSR, so the amount of control parameters is increased.

### 2.3.2 Tunable Twin-Guide (TTG) laser

A distributed feedback tunable twin-guide (DFB-TTG) laser [7, 30, 31, 32, 33] is an electronically tunable DFB type laser diode. The device structure of a DFB-TTG laser (Fig. 2.5) consists of two p-n junctions with a n-type separation layer in the middle that electronically decouples the active layer and tuning layer. This prevents the active current from influencing the tuning and the tuning current from influencing the gain. The gain current ( $I_a$ ) that is injected at the bottom, controls the carrier density in the active layer and the refractive index of the layer structure. The tuning current  $I_t$  that is injected at the top of the

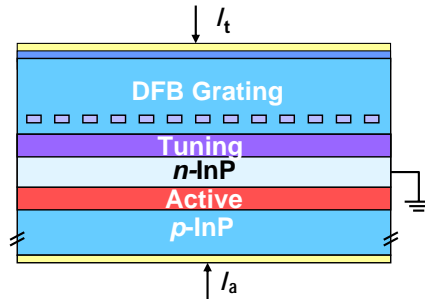


**Figure 2.5:** Device structure of a Tunable Twin Guide (TTG) Laser

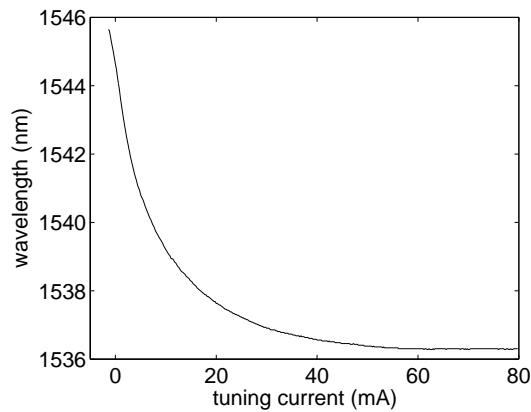


**Figure 2.6:** Tuning characteristics of a DFB-TTG laser

device only changes the refractive index of the tuning layer and can be used to electronically change the wavelength of the laser.

Like any other DFB type laser, this concept has the advantage that in the presence of a  $\pi$  phase shift in the middle of the grating and with good anti-reflection coatings on the facets, the laser cavity mode remains aligned with the reflector peaks and a high side-mode suppression is guaranteed.

DFB-TTGs with a 9nm tuning range (Fig. 2.6) and output powers up to 6mW were reported [34] by the Technical University of Munich.

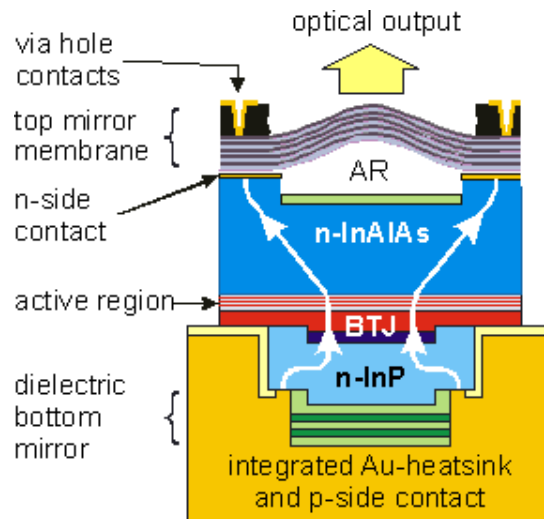


Figure 2.7: Vertical Cavity Surface Emitting Laser (VCSEL)

## 2.4 Existing concepts of Widely Tunable Lasers

Widely tunable laser diodes, with a tuning range of several tens of nm, have been investigated and fabricated since several years now. In the following paragraphs an overview of different widely tunable laser concepts other than those studied in this PhD will be given. This overview is kept very brief but nevertheless contains the main advantages and disadvantages of the existing concepts.

### 2.4.1 Different types of widely tunable lasers

A multitude of widely tunable laser concepts has been investigated in the past few years. A classification can be made depending on a wide range of properties. These classifications will be discussed in the next paragraphs before going into detail about specific laser concepts.

#### Edge-emitting vs. surface-emitting

In addition to the tuning mechanisms, a distinction can be made by the direction of the emitted light. In a vertical cavity surface emitting laser the mirrors are placed above and below the gain layer and the light is emitted from the surface of the device instead of the edge like in conventional laser concepts (Fig. 2.7).

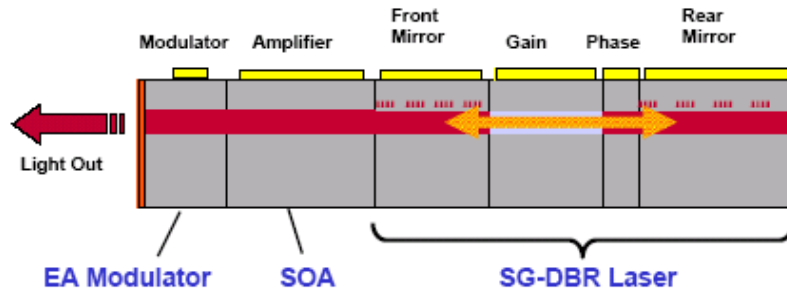


**Figure 2.8:** SG-DBR laser integrated with amplifier and modulator

Surface emitting lasers like Vertical Cavity Surface Emitting Lasers (VCSEL) [35] can be tested before cleaving and packaging speeding up the testing process and reducing the manufacturing costs. The emitted laser beam is circular so it is easier and cheaper to couple the light into the fiber. Widely tunable VCSELs demonstrate low power consumption and a large wavelength range. The tuning is mechanical and the switching is slow (order of milliseconds). The main disadvantage of the VCSEL is the low output power due to the very small active region design that is necessary to maintain single mode operation. Additionally the fabrication can be very complex, certainly in the case where a movable reflector is used as the top reflector.

Edge-emitting laser diodes have two large advantages compared to surface-emitting devices: they can be electronically tuned and without changing the basic manufacturing process they can easily be integrated [36] with other components such as electro-absorption or Mach-Zehnder modulators, semiconductor optical amplifiers (SOA), optical monitoring photodiodes, etc... (Fig. 2.8) There has been a lot of research in this area due to advantages like low cost, low power dissipation, higher reliability and high volume by sharing the same technology for a number of components. However, integrating extra components can have a bad influence on noise, linewidth, side-mode suppression and output power and the design becomes more complicated [37, 38, 39, 40, 41].

### A single laser versus a laser array

In a laser array (Fig. 2.9) several DFB lasers with a limited tuning range of 3 to 5 nanometers are combined through a multimode interference (MMI) coupler [42] to obtain a large quasi-continuous tuning range.

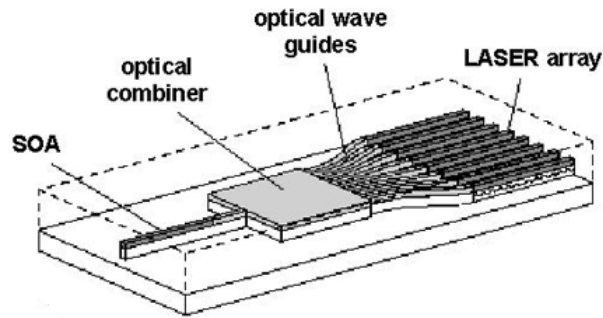


Figure 2.9: Widely tunable DFB laser array

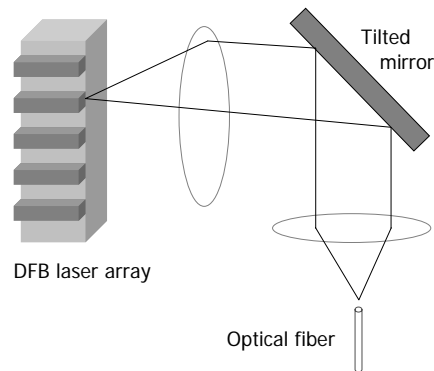
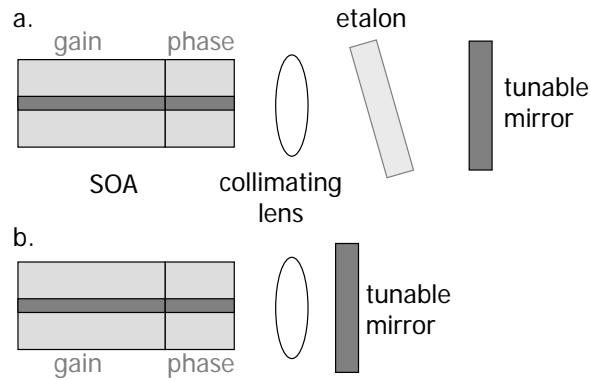


Figure 2.10: Widely tunable DFB laser array with MEMS mirror to couple light into the fiber

The lasers are excited one at a time and they are tuned by heating up the laser sample. Each laser should be fabricated with a slightly different grating design to offset their lasing wavelengths with 3 to 5 nanometers to obtain a large quasi-continuous tuning range. These requirements set very tight fabrication tolerances. Other disadvantages include the significant combiner losses and the high power dissipation to obtain a large tuning range with thermal tuning.

To overcome the high combiner losses another approach for a DFB laser array is used (Fig. 2.10) where a micro-electromechanical systems (MEMS) tilt mirror is placed in the focal plane of a collimating lens to select the appropriate laser [43, 44]. This approach is slower (mechanical tuning) and the processing and the control is more complicated.



**Figure 2.11:** External Cavity Wavelength Tunable Lasers concepts from NEC: (a) mechanically tuned (b) electronically tuned

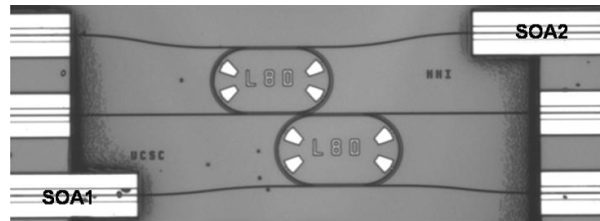


**Figure 2.12:** Widely Tunable Double-Ring Resonator Coupled Laser (Reprinted with permission from IEEE Photonics Technology Letters, Vol. 17, pp. 1770 - 1772 ©2005 IEEE)

### External cavity lasers

Several widely tunable laser concepts incorporate an external element in the laser cavity (Fig. 2.3 and Fig. 2.11). The external element is mechanically [45], thermally [46] or electronically (through liquid crystals) [47] tuned to create an overlap between the cavity mode and the reflection peaks. Biggest concerns are manufacturing and reliability, because several optical elements need to be aligned precisely during manufacturing.

### Wavelength selective elements

Diffraction gratings like sampled gratings and superstructure gratings (chapter 3) are mostly used as wavelength selective element in widely

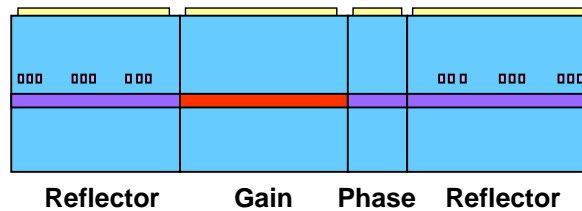


Figure 2.13: Sampled Grating Distributed Bragg laser

tunable lasers. Recently other reflector concepts like ring resonators (fig. 2.12) have received a lot of attention [48].

Different concepts [49, 50, 51] have been presented with a high side-mode suppression, a high output power and an easy fabrication. A much higher tuning range can be obtained because the peak spacing difference can be made much smaller than with diffraction gratings. Lasers with a tuning range higher than 40nm haven't been presented yet. The peaks are also more uniform and much smaller in linewidth.

### Conclusion

The electronically tuned monolithic edge-emitting widely tunable lasers have a wide tuning range, a compact size and fast switching and they can easily be fabricated and integrated with other components. In the following paragraphs some of these laser concepts will be discussed in more detail.

#### 2.4.2 Superstructure Grating or Sampled Grating Distributed Bragg laser

In a Superstructure Grating (SSG) or Sampled Grating (SG) Distributed Bragg (DBR) laser a very stable filter is obtained through two reflectors with slightly different superperiod (Fig. 2.13). Using the Vernier effect (see §4.1.1) a tuning range of more than 40nm is possible [22, 52] through electrical tuning. A phase section is added to guarantee the alignment between the cavity mode and the reflected peaks. Carrier-induced tuning losses in the reflectors cause a low output power (order of 20mW) and a high power variation. Recent research has focused on integrating a Semiconductor Optical Amplifier (SOA) in the design to overcome these problems [36, 40].

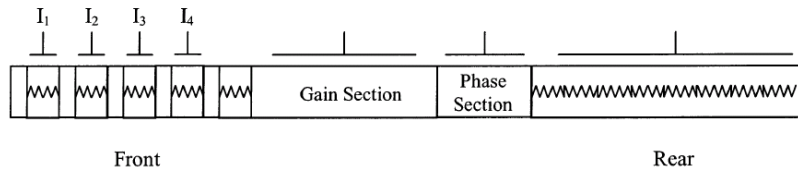


**Figure 2.14:** Digital-Supermode Distributed Bragg Reflector (DS-DBR)

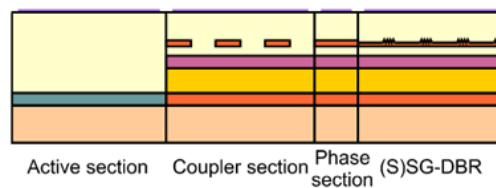


**Figure 2.15:** Grating-assisted coupler with rear sampled reflector (GCSR)

### 2.4.3 Digital-Supermode Distributed Bragg Reflector

A Digital-Supermode Distributed Bragg Reflector (DS-DBR) laser [25, 53] is comparable in performance, fabrication and operation to a 4-section (S)SG-DBR laser. The biggest difference is the front grating section that consists of a concatenation of short Bragg sections with slightly different periods (Fig. 2.14). One of the reflection peaks of the back grating is filtered out by electronically activating one or more of the short front Bragg sections with a low input current. Due to lower tuning-induced losses a larger output power and lower power variation can be obtained compared to an (S)SG-DBR laser. The DS-DBR concept requires many more tuning currents resulting in a more complicated control mechanism. Moreover the front reflector is less selective due to its broader filter characteristic, which hurts the single mode stability.

### 2.4.4 Grating-assisted coupler with rear sampled reflector

A Grating-assisted coupler with rear sampled reflector (GCSR) laser [23, 54] consists of a co-directional coupler that filters out a narrow range of wavelengths from the Bragg reflector (Fig. 2.15). Only small tuning currents are required to tune over a wide quasi-continuous wavelength range (more than 60 nm), so fast wavelength switching is possible (order 5ns). A high output power (larger than 25mW) and a low

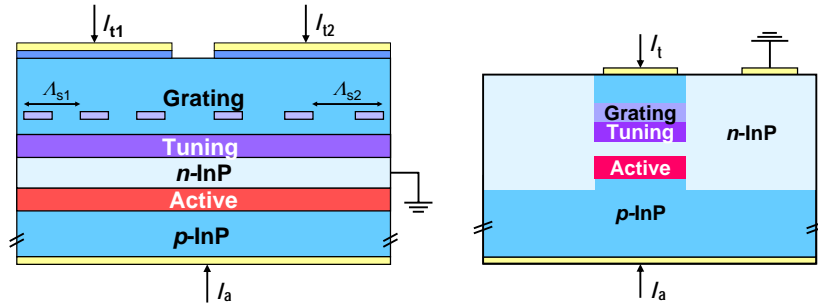


Figure 2.16: Sampled Grating Tunable Twin Guide (SG-TTG) Laser

power variation (lower than 1.4dB) during tuning can be obtained because all (passive) tuning sections are located on one side of the (active) gain section. A large disadvantage is the complex fabrication process causing a lower fabrication yield. Monolithic integration with modulators, amplifiers, etc. is less obvious than for other widely tunable lasers because a reflecting front facet is required for the laser operation. The control and stabilisation of the device is complicated because the feedback is less wavelength-dependent due to the use of a coarse filter.

## 2.5 Two New Concepts

### 2.5.1 Widely Tunable Twin Guide(TTG) Laser

A widely tunable twin-guide (TTG) laser [1, 2] is a two section TTG laser [7]. The device structure of a TTG laser (Fig. 2.16) consists of two double heterojunctions with an n-separation layer in the middle that electronically decouples the active layer and tuning layer, so gain and filtering can be controlled independently.

Both sections contain a sampled grating or a superstructure grating with different superperiod resulting in reflection spectra with slightly different reflection peak spacing. The frequency where peaks of both reflectors perfectly overlap will reach the laser threshold first and start lasing.

By increasing one reflector current, its reflection spectrum will move to higher frequencies and the overlapping peaks will occur at another frequency. This is called the Vernier effect. The frequencies in between the frequency jumps are reachable by increasing both reflector currents

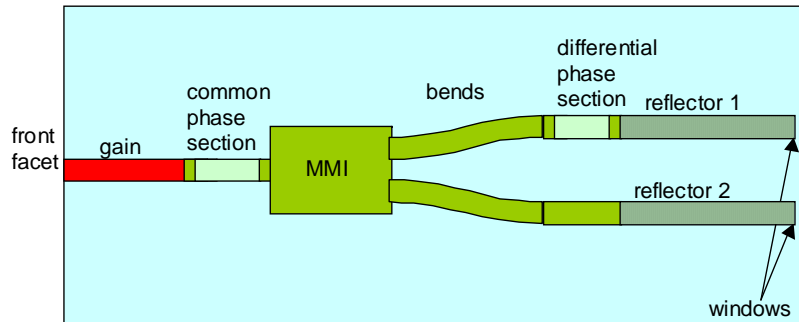


**Figure 2.17:** Modulated Grating Y-Branch (MGY) lasers

together, causing a continuous move of the overlapping peaks to higher frequencies. Only two tuning currents are required to obtain tuning over a large wavelength range, which makes the characterisation substantially less time consuming. The device can easily be manufactured with conventional DFB laser fabrication technology although 3 overgrowth steps are required.

The design, fabrication and characterisation of the Widely Tunable Twin Guide Laser will be discussed in chapter 4.

### 2.5.2 Widely Tunable Y-Branch Laser

In the widely tunable Y-Branch laser concept [3, 4], the different functions are separated into different sections. The gain section amplifies the light. The multi-mode interference (MMI) coupler splits the light into 2 equal beams. The reflectors filter out certain frequencies. The differential phase section guarantees that the reflected beams are added up in phase. And the common phase section is responsible for the alignment between the cavity mode and the reflected peaks.

The need for 4 independent tuning currents in this device is a potential disadvantage, because the characterisation becomes time consuming. Thanks to a careful design of the gratings and a careful processing of the branches the amount of tuning currents needed can be decreased to 3 currents.

A high output power and a lower power variation are expected because the light does not have to pass a lossy reflector section before exiting the laser cavity.

The design, fabrication and characterisation of the Widely Tunable Y-Branch Laser will be discussed in chapter 5. The control and stabilisation of these devices is the subject of chapter 6.



## Chapter 3

# Diffraction Gratings

The grating design is one of the decisive points with respect to the device performance of the laser. Through a good grating design a large tuning range and a good side-mode suppression can be obtained. The aim is to find gratings, which have a reflection spectrum with equally spaced, equally strong reflection peaks over a range of several tens of nanometers and where there is almost zero reflection outside this wavelength range.

Sampled Gratings (SGs) and Superstructure Gratings (SSGs) are the most commonly used grating concepts in widely tunable lasers. Their design, fabrication and characterisation will be discussed in more detail in the next sections, but first the principle of a (uniform) grating is introduced for the ideal case without loss or gain present. At the end of this chapter, the influence of the gain and the facet reflections are also investigated.

### 3.1 Uniform Gratings

A diffraction grating can be obtained by periodically varying the thickness of a passive layer. In a stepwise manner the thickness is changed between two values within each period  $\Lambda$  (Fig. 3.1).

The effective refractive index is different for each thickness, so a wave traveling through the grating will feel a reflection at every change of thickness. Those reflections only interfere constructively in a narrow range around one wavelength and lasing occurs around this Bragg wavelength.

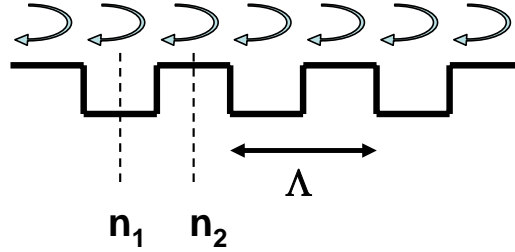


**Figure 3.1:** Longitudinal effective index profile of a uniform grating

In the following paragraphs the wavelength dependent behaviour of uniform gratings is analyzed using different approaches in the ideal case without loss or gain. The effect of gain and loss will be discussed in section §3.6.

### 3.1.1 Fresnel approach

According to the Fresnel formula the reflection  $r$  at each interface can be written in function of the effective refractive index of the layer structure in which a grating is etched ( $n_1$ ) and not etched ( $n_2$ ):

$$r = \frac{n_1 - n_2}{n_1 + n_2} \quad (3.1)$$

Consecutive reflections have a phase difference that depends on the wavelength and the period of the grating so only for certain wavelengths the reflection will add constructively causing a wavelength-dependent filtering.

$$r + (1-r^2)(-r)e^{-jk\frac{\Lambda}{2}} + (1-r^2)^2 r e^{-2jk\frac{\Lambda}{2}} + (1-r^2)^3 (-r)e^{-3jk\frac{\Lambda}{2}} + \dots \quad (3.2)$$

The reflections will only constructively interfere when

$$\frac{k\Lambda}{2} = \pi \quad (3.3)$$

with  $k$  the propagation constant

$$k = k_0 n_{eff} = \frac{2\pi}{\lambda} n_{eff} \quad (3.4)$$

So a uniform grating causes one reflection peak at the Bragg wavelength (Fig. 3.2):

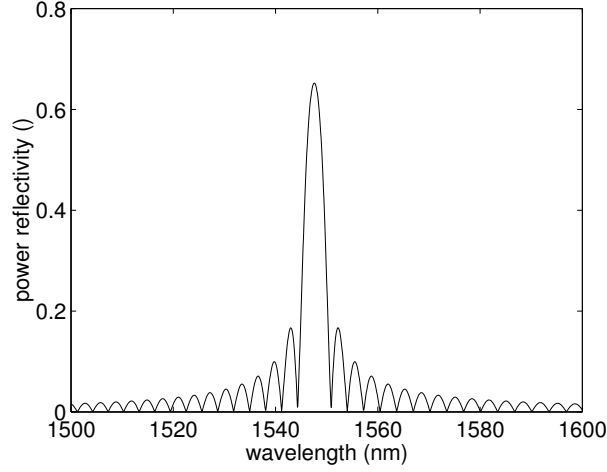


**Figure 3.2:** Reflection Spectrum of a uniform grating with 240nm grating period and 1200  $\mu\text{m}$  grating length

$$\lambda_B = 2 \Lambda n_{eff} \quad (3.5)$$

### 3.1.2 Coupled-mode theory

These results can also be obtained through the coupled-mode theory [26, 55] starting from the scalar wave equation of the electrical field

$$\frac{d^2 E}{dz^2} + [n(z)k_0]^2 E = 0 \quad (3.6)$$

with  $k_0$  the free-space propagation constant. A sinusoidal varying refractive index  $n(z)$  is written as

$$n(z) = n_{eff} + \frac{\Delta n}{2} \cos(2\beta_0 z) \quad (3.7)$$

Neglecting second order variations of the refractive index  $n(z)$  and using the propagation constant in a medium  $\beta = n_{eff} k_0$  one can write

$$[n(z)k_0]^2 = \beta^2 + 4\beta\kappa \cos(2\beta_0 z) \quad (3.8)$$

The coupling factor  $\kappa$  can be interpreted as the amount of reflection per unit length.

$$\kappa = \frac{\pi \Delta n}{2\lambda} \quad (3.9)$$

In the vicinity of the Bragg wavelength ( $\Delta\beta = \beta - \beta_0 \ll \beta_0$ ) the complex amplitude of the electrical field  $E$  can be decomposed in two counter-propagating waves:

$$E(z) = R(z)e^{-j\beta_0 z} + L(z)e^{j\beta_0 z} \quad (3.10)$$

with  $R(z)$  and  $L(z)$  two slowly varying functions. By inserting equations 3.7 and 3.10 in equation 3.6 the following set of coupled-mode equations is obtained:

$$\begin{aligned} \frac{dR}{dz} + (j\Delta\beta)R &= -j\kappa L \\ \frac{dL}{dz} - (j\Delta\beta)L &= j\kappa R \end{aligned} \quad (3.11)$$

Solving these equations leads to the field reflectivity for an uniform grating with length  $L$ :

$$r = \frac{-j\kappa \sinh(\gamma L)}{\gamma \cosh(\gamma L) + j\Delta\beta \sinh(\gamma L)} \quad (3.12)$$

with

$$\gamma^2 = \kappa^2 - \Delta\beta^2 \quad (3.13)$$

This leads once again to only one reflection peak at the Bragg wavelength.

### 3.1.3 Transfer matrix method

The reflection of a uniform grating can be easily calculated through the methods described in the previous paragraphs. When the grating structures become more complex and less periodic the transfer matrix method can be a good alternative. The method is described below for a uniform grating, but it can easily be expanded to more complicated structures like the sampled and superstructure gratings described in the next sections.

The electric field can be written as a superposition of a right and left propagating wave:

$$E(z) = E^R(z) + E^L(z) \quad (3.14)$$

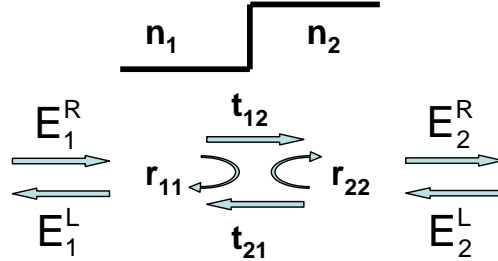


Figure 3.3: Reflection matrix

For the transfer matrix method the relationship is needed between those two propagating waves for every interface where the refractive index changes. Additionally the behaviour of these waves while propagating through a homogeneous medium is needed.

### Reflection matrix

At the interface where the refractive index changes a very simple relation between the right and left propagating waves of both sections can be written thanks to the reflection and transmission coefficients given by the Fresnel equations (Fig. 3.3):

$$r_{11} = r = \frac{n_1 - n_2}{n_1 + n_2} = -r_{22} \quad (3.15)$$

$$t_{12} = \frac{2n_1}{n_1 + n_2} = 1 + r \quad t_{21} = \frac{2n_2}{n_1 + n_2} = 1 - r \quad (3.16)$$

leading to the following expression for the field components:

$$\begin{aligned} E_1^L(z) &= r_{11}E_1^R + t_{21}E_2^L \\ E_2^R(z) &= t_{12}E_1^R + r_{22}E_2^L \end{aligned}$$

from which the following transfer matrix can be derived:

$$\mathbf{R}(n_2|n_1) = \frac{1}{1-r} \begin{bmatrix} 1 & -r \\ -r & 1 \end{bmatrix} \quad (3.17)$$

### Propagation matrix

The propagation of both waves through a homogeneous medium with refractive index  $n$  and length  $L$  can be easily expressed by the following matrix

$$\mathbf{T}(L) = \begin{bmatrix} e^{-jkL} & 0 \\ 0 & e^{jkL} \end{bmatrix} \quad (3.18)$$

where the propagation constant of the waveguide mode  $k = k_0 n$  can be complex in the case of a gain medium.

### Calculating the reflection

By multiplying all those propagation and reflection matrices the effect of the grating on the incoming wave can be calculated. The grating has a period  $\Lambda$  and a length  $L$ .

$$\begin{aligned} \begin{bmatrix} E_N^R \\ E_N^L \end{bmatrix} &= [\mathbf{R}(n_2|n_1) \cdot \mathbf{T}(\frac{\Lambda}{2}, n_2) \cdot \mathbf{R}(n_1|n_2) \cdot \mathbf{T}(\frac{\Lambda}{2}, n_1)]^{\frac{L}{\Lambda}} \\ &= \mathbf{F}_{\text{tot}} \begin{bmatrix} E_0^R \\ E_0^L \end{bmatrix} \end{aligned} \quad (3.19)$$

Out of  $\mathbf{F}_{\text{tot}}$  the complex field reflectivity  $r$  and transmissivity  $t$  can be calculated for this grating structure by setting the left-propagating wave at the right end to zero  $E_N^L = 0$ :

$$\begin{aligned} r &= \frac{E_0^L}{E_0^R} = -\frac{F_{21}^{\text{tot}}}{F_{22}^{\text{tot}}} \\ t &= \frac{E_N^R}{E_0^R} = F_{11}^{\text{tot}} - \frac{F_{12}^{\text{tot}} F_{21}^{\text{tot}}}{F_{22}^{\text{tot}}} \end{aligned} \quad (3.20)$$

The power  $P$  is proportional to  $n|E|^2$ , so the power reflection can be written as:

$$R_{11} = \frac{n_1 |F_{21}^{\text{tot}}|^2}{n_1 |F_{22}^{\text{tot}}|^2} = \frac{|F_{21}^{\text{tot}}|^2}{|F_{22}^{\text{tot}}|^2} \quad (3.21)$$

## 3.2 Sampled Gratings

A sampled grating (SG) [22] is an easy and frequently used grating concept that delivers a reflection spectrum with different reflection peaks

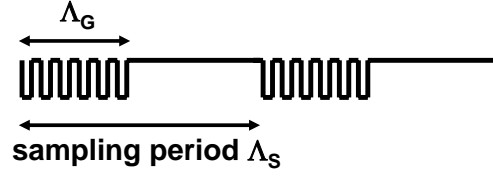


Figure 3.4: Sampled Grating

and constant peak spacing. In a sampled grating some parts of the uniform grating are removed in a periodic fashion (Fig. 3.4). The sampling function has a period  $\Lambda_s$  and a duty cycle  $\delta = \Lambda_g/\Lambda_s$ .

The coupled-mode theory (§3.1.2) can be used once more to obtain the reflection characteristics. This theory says that every spatial Fourier component of the refractive index modulation contributes to a peak in the reflection spectrum. For a sampled grating the single Fourier component of a uniform grating at the Bragg wavelength (3.5) can be convoluted with the Fourier transform of the sampling function to obtain the new Fourier components.

The Fourier components of a sampling function with period  $\Lambda_s$  and duty cycle  $\delta = \Lambda_g/\Lambda_s$  can be written as [27]:

$$F_k = \frac{\Lambda_g}{\Lambda_s} \frac{\sin(\pi k \Lambda_g / \Lambda_s)}{\pi k \Lambda_g / \Lambda_s} e^{-j\pi k \Lambda_g / \Lambda_s} \quad (3.22)$$

So a sampled grating has several reflection peaks  $\nu_k$  centered around the Bragg wavelength of the uniform grating (3.5) with the peak spacing  $\Delta f$  being inversely proportional to the sampling period  $\Lambda_s$ :

$$\nu_k = \frac{c}{2n(\nu_k)} \left( \frac{1}{\Lambda} + \frac{k}{\Lambda_s} \right) \quad (3.23)$$

$$\Delta f = \frac{c}{2n_g \Lambda_s} \quad (3.24)$$

with  $n_g$  the group refractive index.

Sampled gratings that can be used in the widely tunable laser concepts were simulated with software based on the transfer matrix method (§3.1.3) and with the cavity mode solver software CAMFR [56, 57]. The reflection spectrum is shown in Figure 3.5.

The envelope of the reflection spectrum is a sinc function, so the reflection is decreasing with the wavelength deviating from the Bragg wavelength. Therefore, reflection peaks that are too far away from the

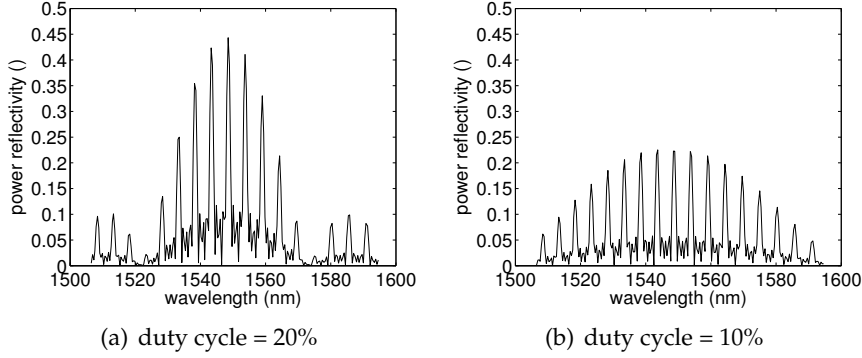


**Figure 3.5:** Reflection Spectrum of Sampled Gratings with two different duty cycles, 240nm grating period, 72 $\mu$ m sampling period and 648 $\mu$ m grating length

Bragg wavelength may not be usable due to too low reflectivity. Only the reflection peaks that have a power reflectivity that is more than the half of the highest reflection peak are usable.

Generally, the envelope of the reflection peaks becomes broader with decreasing sampling duty cycle  $\delta = \Lambda_s/\Lambda_g$  (Fig. 3.5). Therefore, the more reflection peaks are needed, the smaller the sampling duty cycle has to become. However, this happens at the expense of the overall reflectivity of the reflection peaks, which is also decreasing with lower duty cycle because there's a relation between the index modulation of the grating and the duty cycle through the coupling coefficient:

$$\kappa(k) = \kappa_0 F_k \quad (3.25)$$

where  $\kappa_0$  is the coupling coefficient of the unsampled grating and  $F_k$  is the  $k$ th Fourier component of the sampling function (3.22). When waveguide losses are neglected, the dependence between the reflectivity of the reflection peaks and the coupling coefficient  $\kappa$  of the grating is described as

$$R(k) = \tanh^2(|\kappa(k)|L) \quad (3.26)$$

For the zeroth order peak (at the Bragg wavelength) and using equation (3.25), the reflectivity becomes

$$R(\nu_0) = \tanh^2(\kappa_0|F_0|L) = \tanh^2(\kappa_0 L \delta) = \tanh^2(\kappa_0 N_s \Lambda_g) \quad (3.27)$$

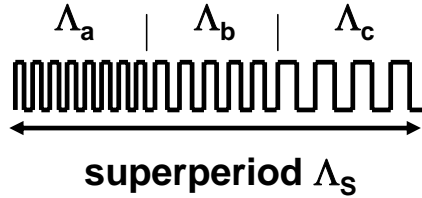


**Figure 3.6:** Superstructure Gratings with one superperiod

with  $N_s$  the number of sampling periods. A duty cycle  $\delta$  of 10 to 15% is typically chosen for sampled gratings to obtain a sufficiently flat spectrum, because only the reflection peaks that have a power reflectivity that is more than the half of the highest reflection peak are usable if a high side-mode suppression is needed in widely tunable lasers.

A sampled grating doesn't have the optimal reflection spectrum. Other index modulations exist [58, 59] that have a more ideal comb like reflection spectrum with equally spaced and equally strong reflection peaks. However sampled gratings have the advantage that they are easy to fabricate in comparison with those other concepts and that they are very robust against frequently occurring fabrication tolerances. One of these concepts, the superstructure gratings will be discussed in the next section.

### 3.3 Superstructure Gratings

Superstructure gratings (SSG) [52, 60] are another way of sampling a uniform grating to obtain multiple reflection peaks by varying the grating frequency (or phase). Within the superperiod  $\Lambda_s$  the grating period is varied continuously or in discrete steps between  $\Lambda_a$  and  $\Lambda_c$  (Fig. 3.6) causing high-reflection peaks between  $\lambda_a (= 2 \Lambda_a n_{eff})$  and  $\lambda_c (= 2 \Lambda_c n_{eff})$ . The peak spacing is dependent on  $\Lambda_s$  just like in a sampled grating (equation 3.23), but the envelope of the reflection peaks is significantly more uniform (Fig. 3.7). The drawback of this method is its fabrication. Superstructure gratings are created through e-beam lithography, which is a very costly and time-consuming method.

A true continuous variation of the grating period is never used due to the limited resolution of e-beam lithography. In practice, the grating period is changed in discrete steps instead of a linearly changing function. Simulations show that the use of only three or four discrete steps

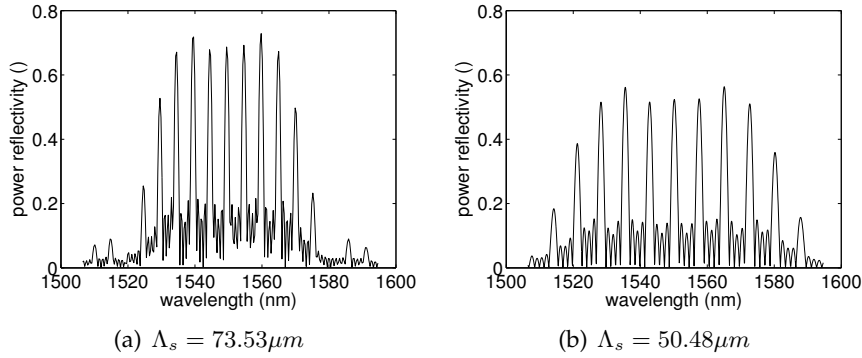


**Figure 3.7:** Effect of a different superperiod on reflection spectrum of superstructure gratings. (a) Superstructure Grating with a  $73.53\mu\text{m}$  superperiod, and  $367.66\mu\text{m}$  grating length. The grating period of the SSG has three discrete steps within a superperiod:  $237.9\text{nm}$ ,  $240.3\text{nm}$  and  $242.7\text{nm}$ . (b) Superstructure Grating with a  $50.48\mu\text{m}$  superperiod, and  $252.42\mu\text{m}$  grating length. The grating period of the SSG has three discrete steps within a superperiod:  $236.9\text{nm}$ ,  $240.4\text{nm}$  and  $243.9\text{nm}$ .

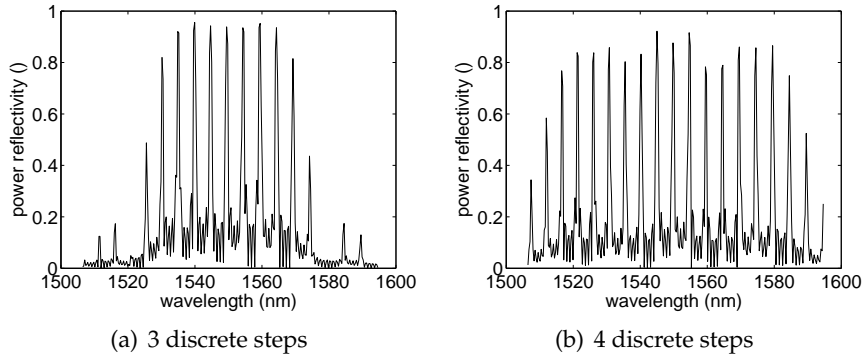


**Figure 3.8:** Effect of discrete steps on the reflection spectrum of superstructure gratings: (a) Superstructure Grating with a  $75.7\mu\text{m}$  superperiod, and  $757\mu\text{m}$  grating length. The grating period of the SSG has three discrete steps within a superperiod:  $238\text{nm}$ ,  $240.3\text{nm}$  and  $242.6\text{nm}$ . (b) Superstructure Grating with a  $76.9\mu\text{m}$  superperiod, and  $769\mu\text{m}$  grating length. The grating period of the SSG has four discrete steps within a superperiod:  $235.8\text{nm}$ ,  $239.1\text{nm}$ ,  $241.6\text{nm}$  and  $244.9\text{nm}$ .

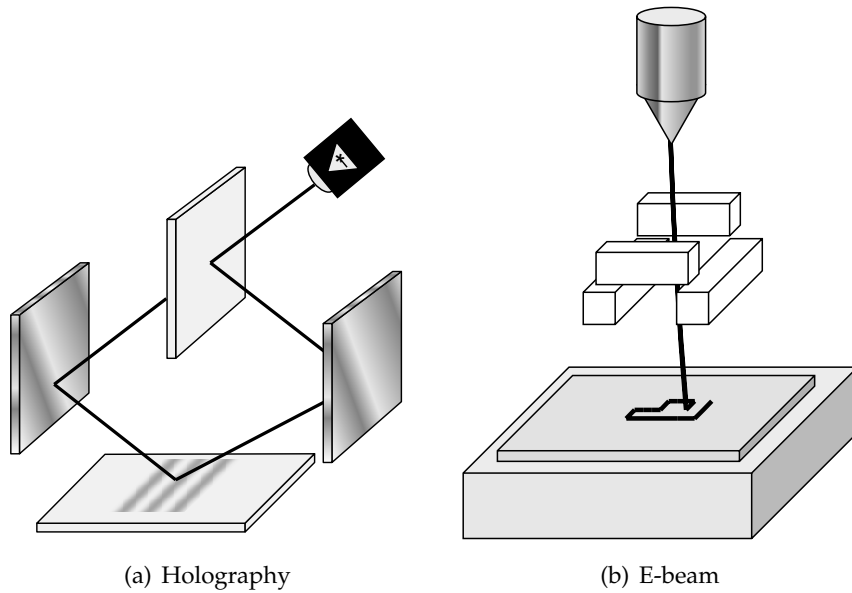


**Figure 3.9:** Definition of grating patterns: (a) holography (b) e-beam lithography

already provides an almost flat envelope over a wavelength range of 40nm. (Fig. 3.8).

Simulations on superstructure gratings with short lengths and only three different grating pitches show that an almost flat reflection spectrum with a reasonable reflection over a large wavelength range can be obtained, as is illustrated in Figure 3.7.

A perfectly flat envelope can be obtained by introducing extra phase shifts in between superperiods [59].

### 3.4 Fabrication

The creation of gratings is complex due to the small feature size of these components: a very stable lithography setup is needed and the presence of dust should be avoided to prevent defects in further processing.

A grating period is typically around 240nm long in InP-based semiconductor lasers and patterns that are only half of that period need to be etched away. Holography and e-beam lithography (Fig. 3.9) are typically used for the definition of grating patterns.

In both cases the samples are first cleaned to remove all possible dirt particles. A photo resist is spun on top of the sample and baked in an oven. A grating pattern is then written in the resist, after which the exposed or unexposed parts (depending on the type of resist used) are removed during development. The developed resist layer can then be used as an etching mask to transfer the grating into the wafer.

### 3.4.1 Holography

Interference lithography or holography uses the interference of two coherent light beams to define patterns into resist. The two beams interfere constructively or destructively depending on their optical pathway difference, so a periodic pattern is obtained in the resist (Fig. 3.10(a)). For holography an anti-reflection coating (ARC) is added under the resist to prevent unwanted reflections at the bottom of the resist. With the Argon laser operating at  $\lambda=363.8\text{nm}$ , the processing of uniform gratings down to 240nm is possible at INTEC [61].

To obtain a sampled grating an extra optical lithography step is added in the process. An UV light lamp and mask are used to create the sampling in a uniform grating (Fig. 3.10(b)). Only the parts of the grating that are covered by the mask during UV exposure will conserve their grating pattern. After which the resist can be developed, removing the exposed resist parts (Fig. 3.10(c)).

Before etching, a small titanium layer is evaporated on top of the resist (Fig. 3.10(d)). Otherwise the pattern in the resist would be destroyed during the  $O_2$  plasma etching, which is used to etch through the ARC (Fig. 3.10(e)).

Afterwards, the grating pattern is transferred into the InGaAsP/InP layer structure through dry etching (Fig. 3.10(f)). Wet chemical etching isn't an option because of the under-etch. Reactive Ion Etching (RIE) and Inductively Coupled Plasma Etching (ICP) are available at INTEC. After removing resist and ARC (Fig. 3.10(g)), a grating as shown in Figure 3.10(h) is obtained.

### 3.4.2 E-beam lithography

With electron-beam lithography the sampled grating or superstructure grating pattern can be directly written in the resist using a focused electron beam (Fig. 3.9(b)). The beam is moved over the resist in a programmed way to generate the grating pattern so no mask is necessary.

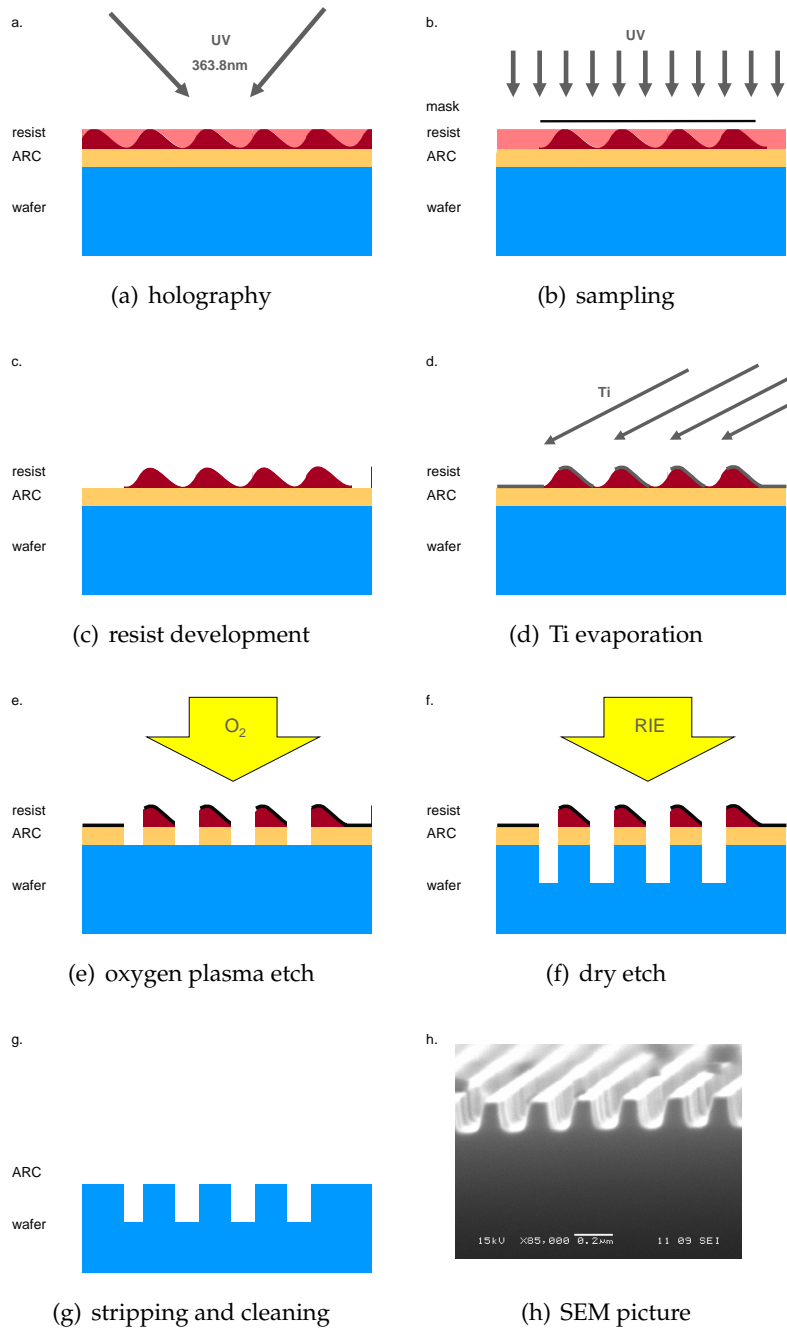
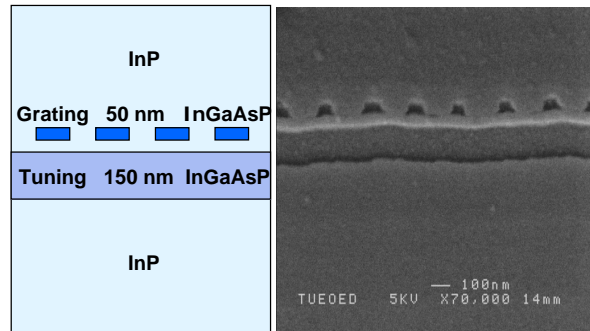


Figure 3.10: Fabrication of Sampled Gratings through holography.



**Figure 3.11:** SEM image of the cross section of an overgrown grating

E-beam lithography is very time-consuming and expensive so it is not frequently used for mass-production, but it is very popular for research purposes due to its high flexibility.

The electron-beam lithography was done at the Technical University of Munich using an upgraded scanning electron microscope (JEOL JSM-6400 with e-beam lithography attachment Elphy Plus from Raith GmbH). The capabilities of this upgraded SEM lack somewhat behind state-of-the-art electron-beam writers. It has a limited writefield of  $600\mu\text{m}$ , because writefield stitching is not possible. Only a low SEM magnification can be used, causing more writefield distortions. These distortions can have a detrimental effect on the reflection spectrum of the grating.

### 3.4.3 Controlling the depth of overgrown gratings

The grating depth is a very critical factor in the fabrication process. The grating depth controls the refractive index change between the etched and unetched areas, so it influences the coupling factor  $\kappa$ . The peak height and the peak width of the reflection spectrum depend on this coupling factor, so it is important to accurately etch the grating to obtain the required grating depth.

A 50nm InGaAsP grating layer was grown above the tuning layer with a 50nm InP buffer layer in between (Fig. 3.11(a)). During the etching process, the gratings are completely etched through the InGaAsP grating layer. By subsequently overgrowing the structure with InP, the height of the grating layer will be determined by the growth process of the InGaAsP grating layer and not by the less accurate etching process.

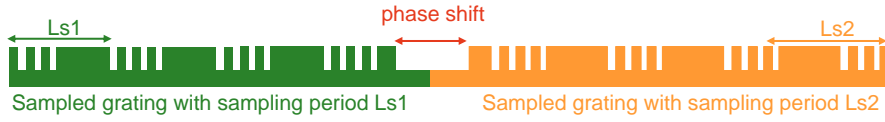


**Figure 3.12:** Cross section showing a phase shift etched between the two grating sections.

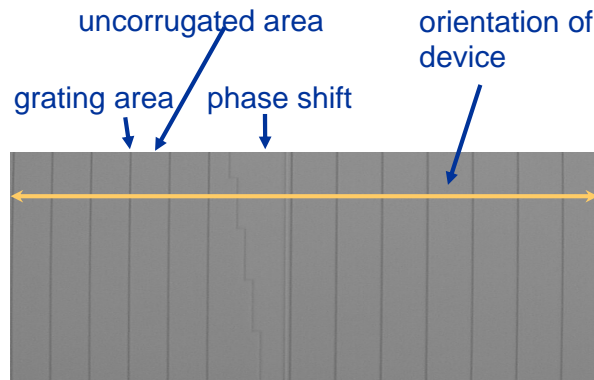


**Figure 3.13:** Top view of two grating sections with phase shift in between

A SEM picture of an overgrown grating is shown in Fig. 3.11(b). No gaps and no cavities are present inside the cavity. The surface of the overgrown grating is observed to be even. So the grating fabrication is suitable for laser fabrication.

#### 3.4.4 Creating a $\pi$ phase shift

A phase shift of  $\pi$  is added between the two grating sections of the (S)SG-TTG laser to obtain a high SMSR and a monomode behaviour. This is in analogy to other DFB lasers, where a  $\pi$  phase shift is used to ensure that the cavity mode coincides with the overlapping reflection peaks [21].

Such a phase shift can be introduced by etching a phase block of length  $L_{phase}$  in the center of the two grating sections (Fig. 3.12-3.13). A refractive index change  $\Delta n = n_1 - n_2$  occurs over the total length of the phase block, so the change of the cavity round trip phase is given by  $\Delta\phi = 2\Delta n L_{phase}$ . The required phase block length  $L_{phase}$  can be extracted out of the condition for the  $\pi$  phase shift:  $\Delta\phi = \pi$ .

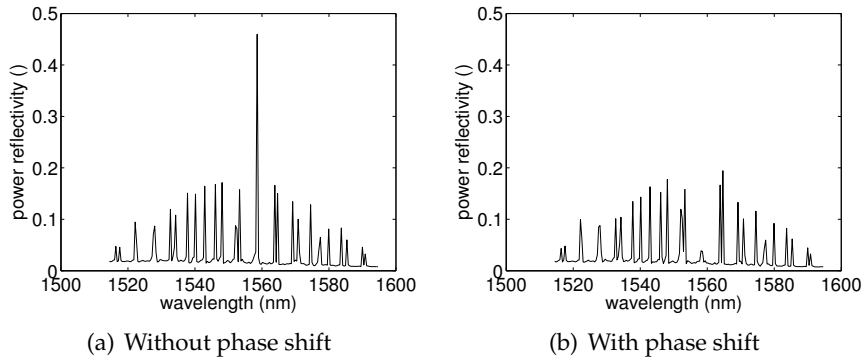


**Figure 3.14:** Simulated reflection spectrum of a sampled grating showing the effect of adding a phase shift: two-section SG-TTG laser with sampling periods of  $72\mu\text{m}$  and  $80\mu\text{m}$  respectively, a section length of  $720\mu\text{m}$ , a duty cycle of 10% and a grating length of  $1440\mu\text{m}$ . The needed phase shift width is  $82.7\mu\text{m}$  in order to obtain a  $\pi$  phase change.

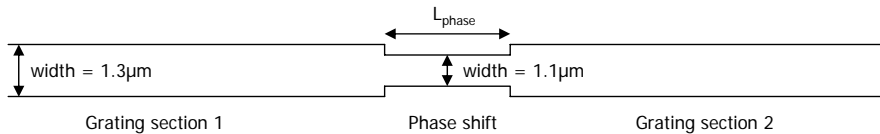


**Figure 3.15:** Top view showing a smaller width of the laser mesa in between two grating sections creating a phase shift.

The simulations shown in figure 3.14 show that the constructive interference of the overlapping peaks of two reflector sections becomes destructive when a phase block is added. This destructive interference proves that a  $\pi$  phase shift was added to the device.

A refractive index change  $\Delta n$  over a length  $L_{phase}$  can also be obtained by changing the width of the laser mesa in between two grating sections (Fig. 3.15). Once again a  $\pi$  phase shift is obtained if the length  $L_{phase}$  is correctly chosen.

### 3.5 Measurements of overgrown gratings

Sampled gratings and superstructure gratings can be characterised by incorporating them in a passive waveguide. The wavelength dependent behaviour of the grating can be checked by sending a light beam with varying wavelength through the waveguide (Fig. 3.16) and mea-

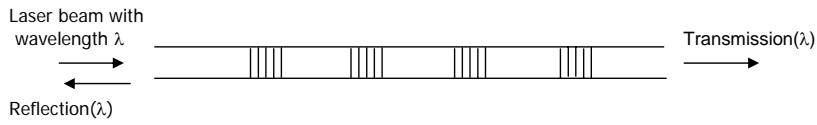


Figure 3.16: Measuring gratings in a passive waveguide structure

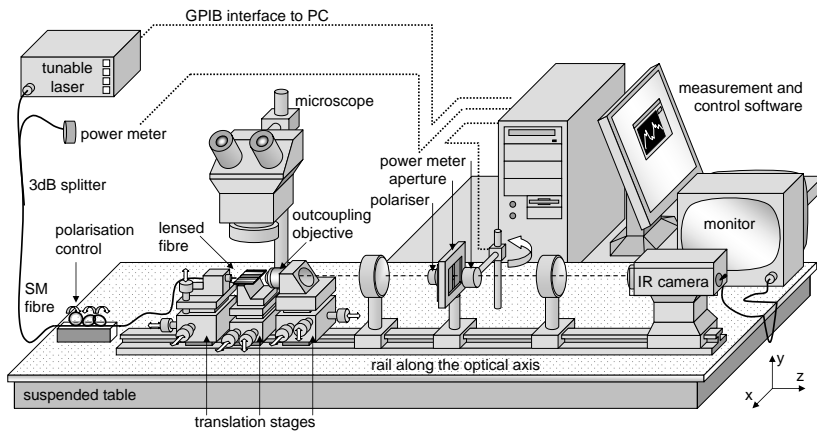


Figure 3.17: Setup for measuring gratings. (Modification of drawing by Wim Bogaerts [62])

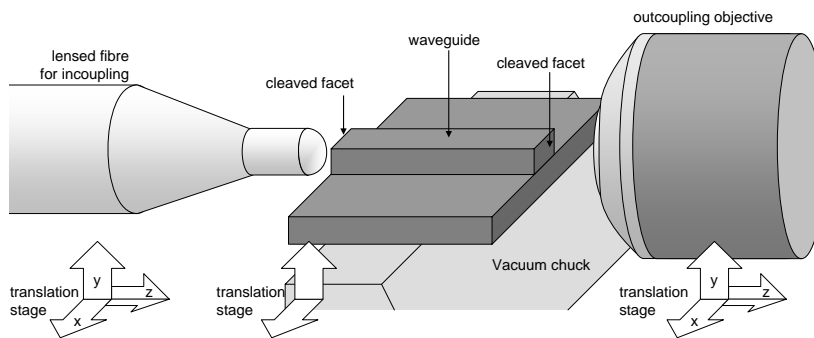


Figure 3.18: Setup for measuring gratings: light is coupled into waveguide through lensed fiber and lens is used for outcoupling

suring the light beam that is transmitted through or reflected by the grating. The quality of the fabricated gratings can be checked by comparing the measured values with the simulation results. The etched waveguides have defects causing power losses while the light propagates through the waveguide.

On the measurement setup (Fig. 3.17), the sample is placed on a stage and the light is coupled into the waveguide through a tapered fiber (Fig. 3.18). This fiber is connected with a laser source that is mechanically tunable between 1480nm and 1640nm. The light with an output power of at least 2mW is transmitted through the passive waveguide and out-coupled through an objective lens. To avoid stray light an adjustable aperture is placed between the lens and the photo detector.

By changing the wavelength the transmission spectrum of the grating can be detected. Fig. 3.19(a) shows the measured transmission spectrum of an overgrown sampled grating. The peaks spacing is in agreement with the simulated values. The envelope doesn't have a typical sinc function due to unwanted facet reflections. The single-layer AR coating doesn't eliminate the facet reflections to an acceptable level (lower than  $10^{-3} - 10^{-4}$ ) leading to Fabry-Pérot effects that cause an irregular behaviour of the peak heights in the transmission spectrum (see §3.7) and the typical sinc envelope can't be observed.

For reflection spectrum measurements, the reflected light from the grating is coupled back into the tapered fiber and through a 3dB fiber splitter half of it is detected by a photo detector. Once again by changing the wavelength of the tunable laser that is connected with the other arm of the 3dB splitter the wavelength dependent reflection of the created gratings can be characterised. Fig. 3.19(b) shows the reflection spectrum of a measured overgrown sampled grating. Due to unwanted facet reflections some peaks are split in two.

The transmission spectra of e-beam written gratings are shown in Fig. 3.20. The overgrown sampled gratings show a typical sinc-type envelope with a constant peak spacing. In comparison with Fig. 3.19 no irregularities can be detected indicating that the used reflection coating is much better than for the previously measured samples. For these samples an  $\text{HfO}_2$  coating was used instead of  $\text{AlO}_2$  indicating that its refractive index is closer to 1.8 (refractive index of an ideal coating). These sampled gratings are ready to be used in the fabrication of SG-TTGs.

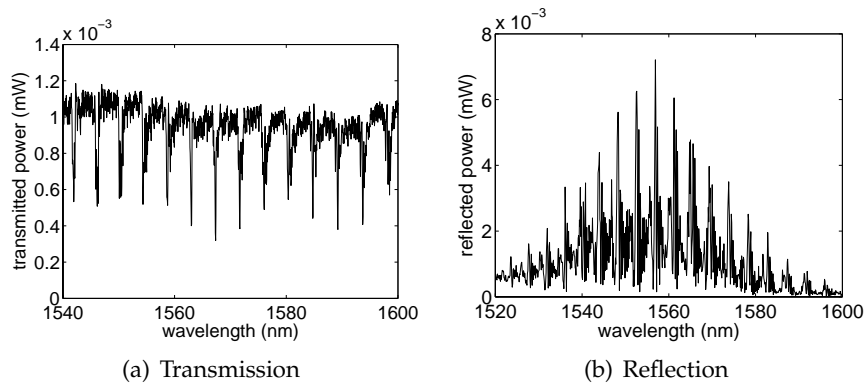


**Figure 3.19:** Measurements of Sampled Gratings fabricated through holography in transmission(a) and reflection(b) The sampled grating has a duty cycle of 7.5% and 30 superperiods with a length of 80 $\mu$ m each.

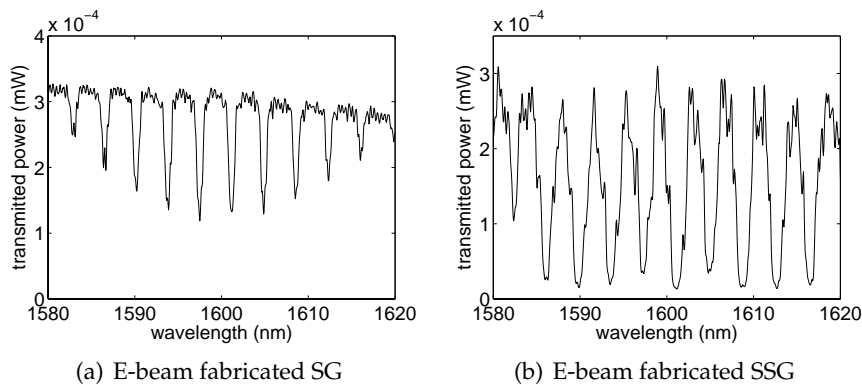


**Figure 3.20:** Transmission measurements of e-beam fabricated gratings: (a) Sampled Grating with a duty cycle of 12.64%, 97,3 $\mu$ m sampling period, 246nm grating period and 583.9 $\mu$ m grating length. (b) Superstructure Grating with a 95.9 $\mu$ m superperiod, and 575.64 $\mu$ m grating length. The grating period of the SSG has five discrete steps within a superperiod: 243nm, 244nm, 246nm, 248nm and 249nm.

The measured superstructure gratings (Fig. 3.20(b)) have a flatter envelope than the sampled gratings. Unfortunately the peak width of the superstructure grating is much bigger than originally anticipated by the simulations. The limited resolution of the e-beam lithography (only 9nm) is the cause of this peak broadening. So sampled gratings are preferred for the fabrication of the widely tunable twin-guide lasers due to the fabrication limits of the available e-beam facilities. Nevertheless both grating structures will be discussed in the design of the (S)SG-TTGs in chapter 4 because only a better e-beam facility with a higher writing resolution is needed to create SSGs that can be used in the fabrication of SSG-TTGs.

### 3.6 Influence of gain

Some recently proposed widely tunable laser diodes, such as the widely tunable twin-guide (TTG) laser (see chapter §4), have the grating above or below the active waveguide (i.e. in the gain section). The influence of the gain in these reflectors can change the reflection spectrum significantly.

#### 3.6.1 Effects on Reflection Spectra

The reflection spectra for sampled and superstructure gratings were calculated in an active and a passive waveguide structure using the transfer matrix method (see §3.1.3). Different values for the net gain and loss  $\Gamma g - \alpha_{int}$  have been considered:  $10\text{cm}^{-1}$ ,  $30\text{cm}^{-1}$  and  $-10\text{cm}^{-1}$ , which are typical gain and loss values for lasers with a length of 500 to  $1000\mu\text{m}$ . The resulting spectra are displayed in Figures 3.21 and 3.22.

As can be seen in Figure 3.21(a)-(b), the envelope, the peak width and the peak spacing of the reflection spectrum of a sampled grating doesn't change when gain is applied. In this grating concept the superperiod and the duty cycle play a more important role than the refractive index leading to a smaller influence of the gain on the reflection spectrum.

The influence of the gain in a superstructure grating is clearly visible in Figure 3.22(a)-(c), which gives the reflection spectrum for different gain values. If the influence of the gain has been neglected in the grating's design, the non-uniformity of the reflection peaks may cause problems for laser concepts like the SSG-TTG. For example in Fig. 4.10 quasi-continuous tuning can't be reached because some supermodes

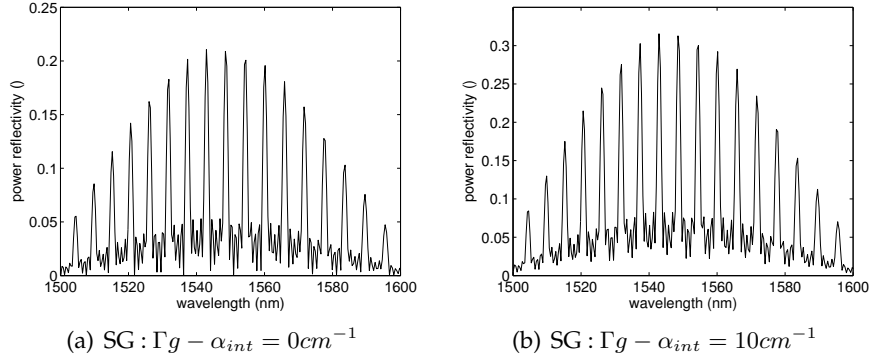


**Figure 3.21:** Influence of gain on the calculated reflection spectra of sampled gratings. Sampled Grating with a duty cycle of 10%,  $65.33\mu\text{m}$  sampling period,  $240\text{nm}$  grating period and  $326.7\mu\text{m}$  grating length.

are skipped due to the non-uniform peak envelope of the reflection spectrum caused by the gain. This happens when the partially overlapping neighbouring peaks are higher than the perfectly overlapping peaks.

Carrier-induced absorption losses are also present in passive grating sections and can be as high as  $-50\text{cm}^{-1}$  in SSG-DBRs [60]. The influence of a typical net loss of  $-10\text{cm}^{-1}$  is shown in Figure 3.22(d); it also leads to non uniformities in the envelope of the reflection peaks. This influence is very similar to that of a net gain, so only the optimisation of grating structures in a gain medium will be discussed further on.

### 3.6.2 Optimisation

In this section an optimisation algorithm will be presented that delivers an optimum grating with a flat reflection spectrum even in the presence of gain, such that a good tuning behaviour can be guaranteed.

Superstructure gratings were examined in which a superperiod consists of 6 segments with different pitches and different lengths. A superperiod of  $65\mu\text{m}$  was chosen, so only 11 parameters can be changed independently. The grating length was  $325\mu\text{m}$ .

The parameters were optimised numerically using a simulated annealing scheme combined with the downhill simplex method of Nelder and Mead [63]. The parameters of an optimised superstructure grating for zero net gain were used as initial values for this optimisation. The optimisation minimised the difference between the highest reflection

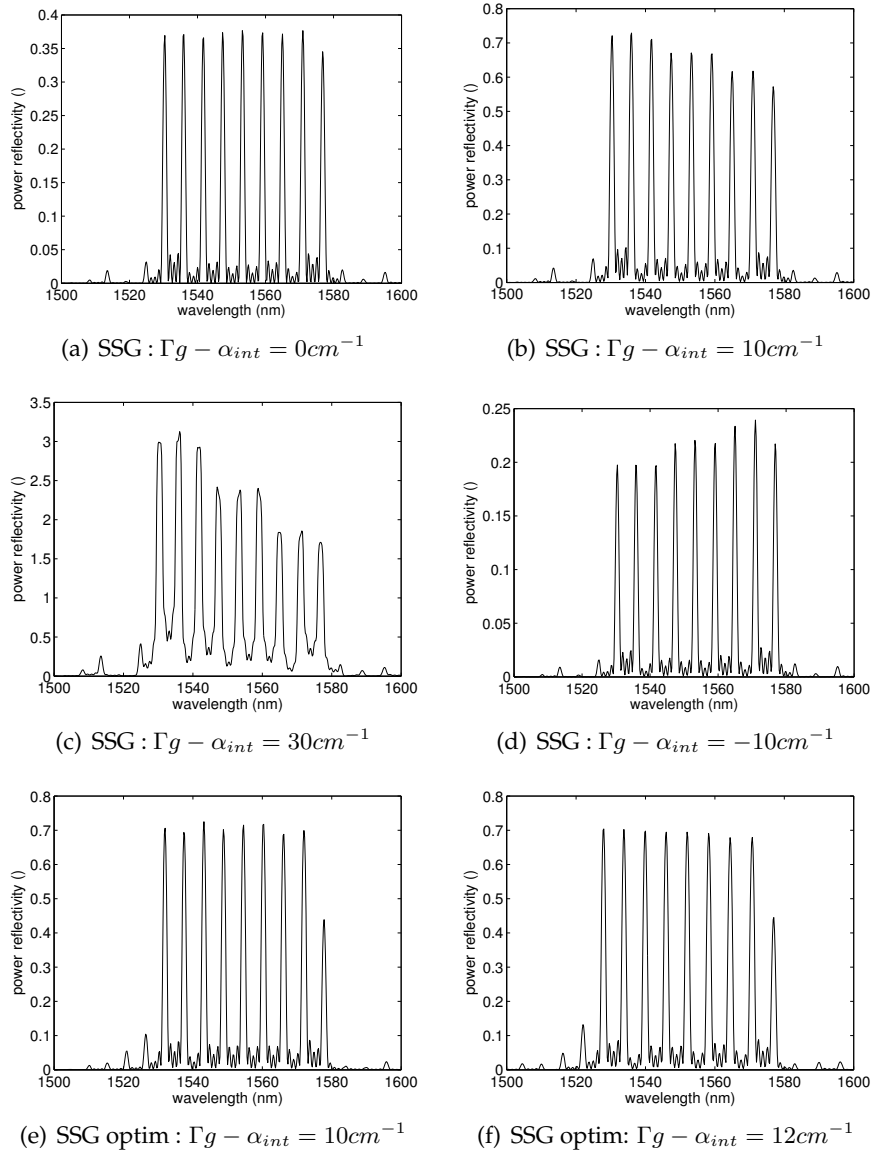


**Figure 3.22:** Influence of gain on the calculated reflection spectra of superstructure gratings. Parameters are shown in table 3.1

Optimised superstructure gratings without gain						
grating pitch (nm)	238.5	237.6	242.5	239.7	244	243.2
number of periods	52	44	35	42	56	38
Optimised superstructure gratings with gain						
grating pitch (nm)	237.9	238.9	242.1	240.1	243.6	244
number of periods	53	42	34	39	74	29

Table 3.1: Parameters for optimised SSG

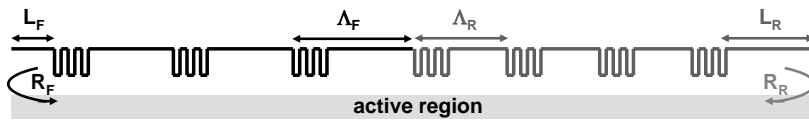


Figure 3.23: Schematic of a laser with reflecting facets

peak and the lowest peak, resulting in the reflection spectrum shown in Figure 3.22(e).

The optimised parameters are shown in table 3.1. It is clearly visible that the grating pitches do not increase monotonously within one superperiod. This is necessary to obtain a uniform envelope with the same amount of pitches in one superperiod. It is important to note that those optimised grating parameters can not be fabricated with the e-beam machine at the Technical University of Munich that has a limited writing resolution of 9nm (as mentioned in section §3.4.2). An e-beam with a better resolution is required to research the use of these optimised SSGs in SSG-TTG designs.

In practice the gain value can vary with 10% or more from the value used in the design phase, so the grating design should be able to work properly over a certain gain range. Figure 3.22(f) shows that the reflection spectrum stays optimal even if the gain varies with 20%.

### 3.7 Influence of facet reflections

The front and rear facet can cause unwanted reflections (Fig. 3.23) that can change the envelope of the reflection spectrum of the grating. These facet reflections are dependent on the position of the grating relative to the facet  $L_{R,L}$  and the power reflectivity of the facet itself  $R_{R,L}$ .

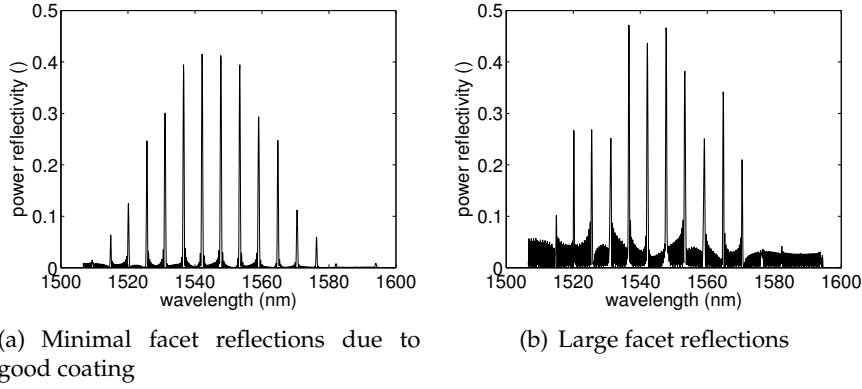


**Figure 3.24:** Simulated reflection spectrum showing the effects of the facet reflections: (a) minimal facet reflections due to a coating with 219nm thickness and 1.8 as effective refractive index (b) a coating with 219nm thickness and 1.9 as effective refractive index. In both cases the distance between the gratings and the facet was chosen to be 34 $\mu$ m.

Due to the facet reflections an extra Fabry-Pérot (FP) cavity is formed between the grating and the facet. This extra wavelength selective filter interferes with the wavelength dependent reflection from the grating. The peak spacing of the FP cavity can be given by

$$\Delta\lambda_{R,L} = \frac{\lambda^2}{2n_g L_{R,L}} \quad (3.28)$$

with  $L_{R,L}$  the length between the grating and the facet. Rear and front facet will have a different peak spacing. The FP filter will broaden, when the length  $L_{R,L}$  is minimised and all grating reflection peaks will get the same amount of suppression or enhancement. The interference is also decreased when the facet reflection  $R_{R,L}$  is minimised. Research from the Technical University of Munich [64] shows that a facet reflection of less than  $10^{-3} - 10^{-4}$  is needed to obtain a reflection spectrum with a sinc envelope for a sampled grating.

An anti-reflection coating is applied to the facet to minimize the power reflectivity  $R_{R,L}$ . The reflected beams interfere destructively when the coating is a quarter wavelength thick and when the refractive index of the coating is the square root of the effective refractive index of the laser. InP-based layers have an effective refractive index of about 3.2, so the ideal coating should have a refractive index around

1.8.  $\text{Al}_2\text{O}_3$  and  $\text{HfO}_2$  were both used as coating material for single-layer coatings.

The reflection spectra of uniform sampled gratings where a reflection coating is applied to the facets were simulated using the transfer matrix method (see §3.1.3). A grating with an ideal facet coating is shown in Figure 3.24(a), while the effect of a more realistic coating is shown in Figure 3.24(b)). The envelope of the reflection spectrum changes drastically by the unwanted facet reflections. Such an irregular envelope will change the tuning behaviour causing gaps in the tuning range [64].

A simple anti-reflection coating isn't good enough to minimize the reflection of the facet enough, so multilayer AR-coatings [65], tilted waveguides [66] or window structures [67] need to be introduced to decrease the reflection even further.

### 3.8 Conclusions

Diffraction gratings that can be used in widely tunable laser concepts were successfully designed, fabricated and characterised during this PhD research.

Sampled Gratings have the advantage that they are easy to fabricate through holography and that they are very robust against frequently occurring fabrication tolerances. The fabricated overgrown sampled gratings had characteristics that were in analogy with the simulated values.

Superstructure gratings have more design parameters and create a more uniform reflection spectrum which is more desirable in tunable laser concepts. They can only be fabricated through e-beam lithography. The fabricated gratings had a much broader peak than expected due to the limited resolution of the e-beam at the Technical University of Munich. Another disadvantage is their susceptibility for gain influences which can cause an unexpected tuning behavior in widely tunable lasers.

Sampled Gratings were preferred in the further fabrication of the widely tunable twin-guide lasers. Nevertheless the design for both grating types was examined.



## Chapter 4

# Widely Tunable Twin-Guide Lasers

In the past the development of monolithically widely tunable lasers has mainly focussed on integrated DBR-types lasers. They all need to go through a time-consuming calibration with three or four control currents to find the optimal operating points. Other disadvantages include low output power and limited modulation capabilities. DFB-type widely tunable lasers recently received more interest [1, 7, 24, 68], because they do not require a phase current and thus are easier to characterize and to control.

The concept of the widely tunable twin-guide laser [1, 2] is based on a distributed feedback tunable twin-guide (DFB-TTG), which was extensively researched during the nineties [7, 30, 31, 32]. Compared with other recently investigated DFB-types the widely tunable twin-guide laser has a less complex growth and fabrication process without alternating active and tuning sections [24, 68].

The device principle will be explained first and afterwards some design rules for wide tuning will be discussed and some simulation results will be given. The fabrication is briefly mentioned after which the characterisation of the fabricated samples is summarised. Finally, some alternative designs will be introduced.

### 4.1 Device Principle

The more basic distributed feedback tunable twin-guide laser was already introduced in section §2.3.2. The basic principle of a widely tun-

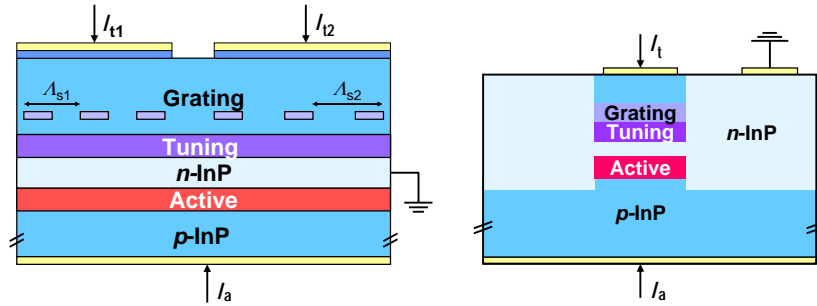


**Figure 4.1:** Sampled Grating Tunable Twin Guide (SG-TTG) Laser

able twin-guide laser is described in the next section and afterwards different layer structures for optical and electrical confinement will be discussed and compared.

#### 4.1.1 The widely tunable twin-guide laser

A widely tunable twin-guide lasers (Fig. 4.1) is a tunable twin-guide laser that consists of two sections with slightly different grating parameters [1]. Each section has a sampled grating (§3.2) or superstructure grating (§3.3) with different super periods. Each grating creates a comb-like reflection spectrum with several periodic maxima, whose spacing is determined by the super period as is illustrated in Figure 4.2 for two sampled gratings.

Lasing occurs at the wavelength where the reflection peaks of both gratings are perfectly aligned (indicated by the ellipse in Fig. 4.3). The frequency where reflection peaks of the two reflectors overlap the most, will reach the laser threshold first and this will be the wavelength of the out-coupled light. The overlapping of the reflector peaks from both reflectors is called a supermode.

A  $\pi$  phase shift between the two grating sections makes the TTG laser behave as a  $\lambda/4$  shifted DFB laser, guaranteeing stable monomodal behaviour.

A widely tunable twin-guide laser makes use of the Vernier effect to tune over a large wavelength range (Fig. 4.3). When current is injected in one of the reflectors, the refractive index will decrease and the reflector peaks of that reflector will move to lower wavelengths. Two other reflection peaks from both reflectors will start aligning, so the output

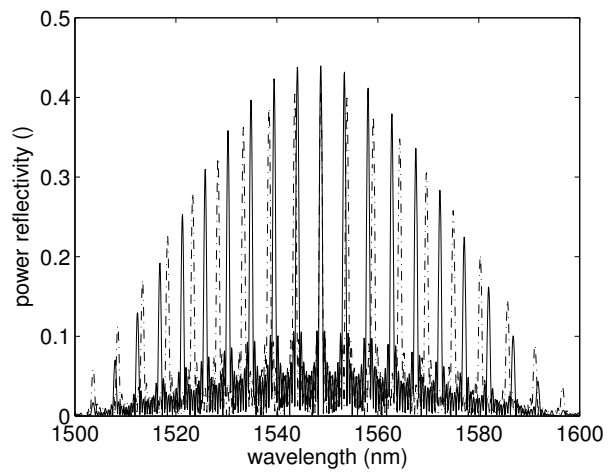


**Figure 4.2:** Simulated reflection spectra of sampled gratings with slightly different sampling period: 72 $\mu\text{m}$  and 80 $\mu\text{m}$

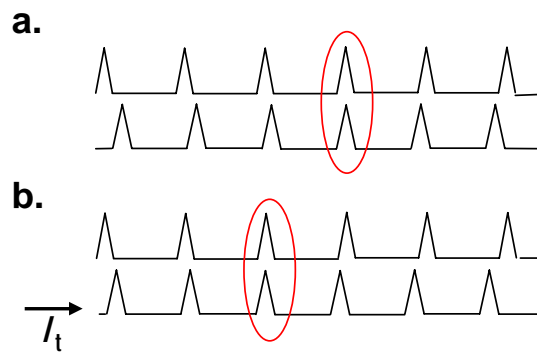


**Figure 4.3:** Definition of Vernier effect: lasing occurs first where peaks overlap perfectly. A small tuning current causes a large wavelength jump.

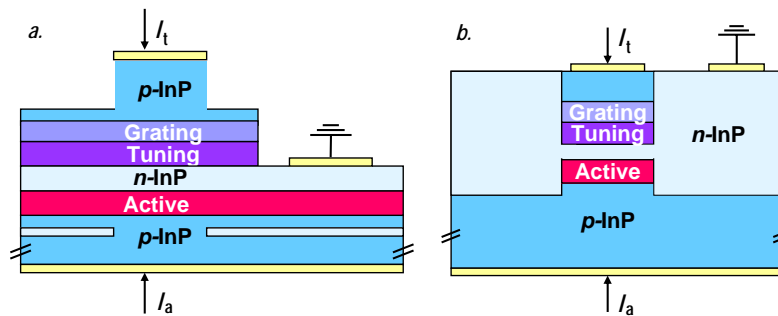


**Figure 4.4:** Two different layer structures: (a) Ridge Waveguide (b) Buried Heterostructure

wavelength will make a jump as large as the reflector peak spacing. This is called a super mode hop .

On the other hand, both reflectors can be tuned simultaneously in such a way that the same reflector peaks keep overlapping, while they are moved continuously to lower wavelengths and the wavelengths in between the jumps can be reached. This continuous tuning range is limited by the maximal refractive index change that is possible through current injection.

Only two currents are needed to change the wavelength of the laser diode, which leads to a faster characterisation. The (S)SG-TTG laser has, apart from its simpler tuning scheme, also the advantage that AR-coatings are allowed and even desired at both facets and that it can easily be integrated with semiconductor optical amplifiers to boost the output power. Another advantage is its shorter length.

#### 4.1.2 Layer Structure

The layer structure plays an important role in the optical and electrical properties. A well defined and stable laser beam can only be obtained when there's one transversal and one lateral mode during lasing. This is obtained by creating a waveguide in transversal and lateral directions. Two commonly used layer structures will be discussed in the next paragraphs.

A Ridge Waveguide (RW) creates electrical and optical carrier confinement by etching a ridge in the upper layers and adding a current injection window in the bottom layers (Fig. 4.4(a)). The lateral confinement is very low, so a very low continuous tuning range of around

2nm [31] can be obtained. A ridge waveguide layer structure has the advantage that it is easy to fabricate with only two regrowth steps. A high output power is possible thanks to a good current confinement of the gain current.

In a Buried Heterostructure (BH) layer structure [32], the tuning layer and active layer are surrounded by material with a lower refractive index (Fig. 4.4(b)). The enclosure by material with a higher band gap causes a better electrical confinement of the tuning currents than in the ridge waveguide structures (Fig.4.4(a)). A higher continuous tuning range of 7nm has been presented in the past for these BH devices [7] and within the Newton project 9nm was achieved [34]. A lower output power is obtained due to leakage currents across the forward biased p-n homojunction. Another disadvantage is the complex fabrication with three regrowth steps and selective area growth which may lower the fabrication yield.

Obtaining a large quasi-continuous tuning range (more than 40nm) was more important than a high output power, so for the widely tunable twin-guide laser a buried heterostructure layer structure was chosen.

### 4.1.3 Leakage Currents

The output power of a BH-TTG is typically limited by the leakage currents across the p-n homojunction [69]. The backside p-n homojunction is 20-25 $\mu\text{m}$  long, which is much larger compared to the 10 $\mu\text{m}$  for conventional BH laser diodes.

Underneath the n-contact the leakage current density is the largest, because there the series resistance of the n-InP channel is the lowest (Fig. 4.5). This series resistance decreases the voltage over the p-n homojunctions that are further away from the n-contact, so there the leakage currents decrease. This resistance also decreases the voltage over the active region.

At higher active currents the voltage over the n-InP channel increases, but the voltage over the homo-junction just underneath the n-contact barely changes, so an increasing part of the active current follows this route and does not contribute to stimulated emission in the active region leading to a saturation of the output power.

Even without the series resistance over the n-InP channel, the output power would saturate, because a p-n homojunction is used for the current confinement. When the voltage over the laser approaches the

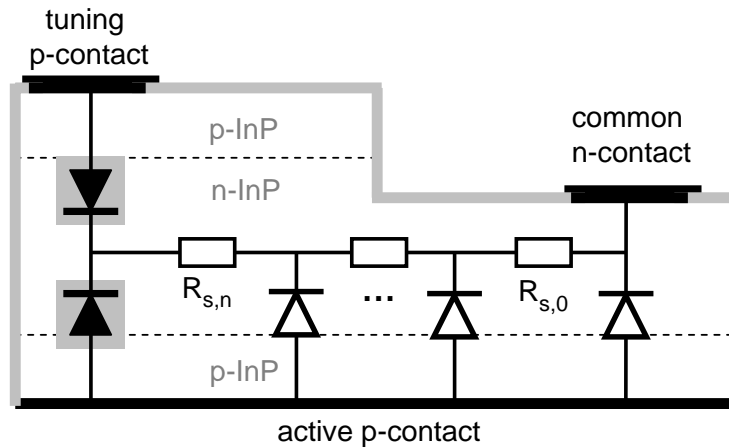


Figure 4.5: Series resistance in BH layer structures

built-in voltage of the homojunction, the current passing through the homo-junction will increase and becomes more important at higher voltages. The homojunction is dominated by the diffusion currents, while different recombination processes occur in the active heterojunction leading to a less efficient increase of the current density for the heterojunction.

An improvement of the output power is possible by increasing the doping of the n-InP channel surrounding the buried stripe. The leakage current density underneath the n-contact can be decreased by a factor 3-10 [70] leading to high output powers up to 24mW.

## 4.2 Design Rules for wide tuning

In the following paragraphs the different requirements for widely tunable twin-guide lasers are discussed and design rules are introduced to reach the specifications for telecom lasers that were described in section §1.2.

### 4.2.1 Quasi-continuous tuning

All wavelengths over the full tuning range are accessible when the peak spacing is smaller than the continuous tuning range of two overlapping

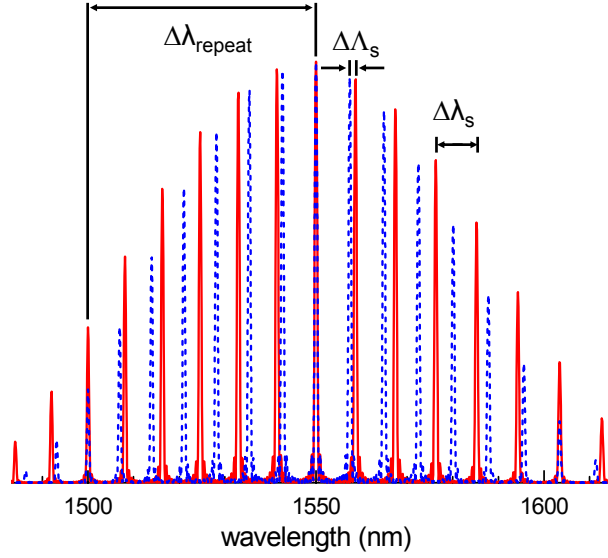


Figure 4.6: Definition of repeat-mode spacing.

reflector peaks. A limited continuous tuning range of 6nm [7] was chosen in the design phase. Using formula 3.23, the condition for the peak spacing can be written as:

$$\Delta\lambda_s = \frac{\lambda^2}{2n_g\Lambda_s} < 6nm \quad (4.1)$$

Out of this formula a minimal value for the sampling period or superperiod  $\Lambda_s$  can be extracted. A typical TTG layer structure has a group index  $n_g$  in the order of 3.3, so the superperiod  $\Lambda_s$  needs to be bigger than  $\pm 60\mu\text{m}$  to obtain quasi-continuous tuning.

#### 4.2.2 Large tuning range

The tuning range of the laser diodes is limited by the repeat mode spacing. This can be seen in Figure 4.6 where the reflector peaks perfectly overlap at 1550nm, but also at 1500nm and 1600nm. The repeat mode spacing is given by the following formula [22, 26]:

$$\Delta\lambda_{repeat} = \Delta\lambda_s \frac{\Lambda_s}{\Delta\Lambda_s} \quad (4.2)$$

In order to achieve a large tuning range, a large superperiod  $\Lambda_s$  and a small difference in superperiod  $\Delta\Lambda_s$  are desirable. Both of these pa-

rameters are, however, already somewhat limited by other constraints mentioned in this section.

### 4.2.3 High side-mode suppression

A good monomodal behaviour can be obtained when the peak spacing difference is sufficiently larger than the peak width, otherwise the neighboring peaks overlap too much, creating a low side-mode suppression. Additionally, the envelope of the reflection peaks needs to be high enough and flat enough over the full tuning range to obtain a high side-mode suppression. Finally, the length of each section is also important. If one section is much longer than the other, the  $\pi$  phase shift won't be in the middle of the laser cavity anymore and the SMSR will decrease. An asymmetry as large as 5% is acceptable [71].

### Sampled Gratings

For sampled gratings the full width at half maximum of the envelope [22, 26] depends on the duty cycle  $\delta$  (Fig. 3.5):

$$\Delta\lambda_{envelope} = \frac{\Delta\lambda_s}{\delta} \quad (4.3)$$

A duty cycle  $\delta$  of 10 to 15% is typically chosen for sampled gratings to obtain a sufficiently flat spectrum, because only the reflection peaks that have a power reflectivity that is more than the half of the highest reflection peak are usable. A lower duty cycle decreases the height of the reflection peaks (Fig. 3.5), because the effective grating length  $L_{g,eff}$  is proportional to the duty cycle:  $L_{g,eff} = L_{laser}\delta$ . A high selectivity combined with reasonable mirror losses can be obtained when

$$0.5 < \kappa L_{g,eff} < 1 \quad (4.4)$$

Hence, with the number of required reflection peaks, the sampling duty cycle and the coupling coefficient  $\kappa$  being more or less fixed, the only remaining parameter to achieve the required reflectivity is the grating length. Therefore, in the end this all comes down to a rather long SG-TTG device. This is not desirable due to the lower fabrication yield and the smaller cavity mode spacing. So a compromise needs to be made between tuning range and side-mode suppression.

### Superstructure Gratings

In superstructure gratings a large peak spacing (Fig. 3.7) and enough discrete steps (Fig. 3.8) are needed to obtain a large enough envelope width. Every reflection peak is only influenced by one grating pitch so the effective grating length is inversely dependent on the amount of discrete steps  $N$ :  $L_{g,eff} = L_{laser}/N$ . The grating length can't be increased with the writefield-limited e-beam at TU Munich to increase this decreased reflection, so a compromise needs to be made to satisfy constraint 4.4. Three discrete steps are a good compromise, because a large reflection peak and envelope width can be obtained. Additionally, three discrete steps are easier to fabricate with the resolution limited e-beam facilities.

## 4.3 Simulations

The static behaviour of widely tunable twin-guide lasers with sampled gratings (SG-TTGs) and superstructure gratings (SSG-TTGs) was examined with the threshold analysis tool of the simulation software CLADISS. This software was developed at INTEC [72] and a windows version was commercialised by Photon Design [73]. The TTG version of CLADISS is an adaptation of the original Unix version, where the special TTG structure and the SG and SSG grating structures are incorporated.

The wavelength and the normalised threshold gain difference were investigated as function of the tuning currents. The threshold gain difference  $\delta g$  (in  $\text{cm}^{-1}$ ) is the difference in required modal gain between the main mode and the most important side-mode. The side-mode suppression (SMSR) depends on the normalised threshold gain difference  $\delta g L$  with  $L$  the laser length [21]:

$$SMSR = \frac{2P_N \delta g L}{\hbar \nu v_g n_{sp} \alpha_{tot} \alpha_m} \propto \delta g L \quad (4.5)$$

with  $P_N$  the output power of the main mode,  $v_g$  the group velocity,  $n_{sp}$  spontaneous emission coefficient (the inversion factor),  $\alpha_{tot}$  and  $\alpha_m$  the total loss and mirror loss. A normalised threshold gain difference  $\delta g L = 0.05$  is typically enough to obtain a side-mode suppression of 30dB.

### 4.3.1 Limitations and Design choices

Before going into detail about the simulation results, a couple of limitations and design choices need to be clarified.

Gratings written with e-beam lithography facility at TU Munich are limited to a length of  $589\mu\text{m}$  and a resolution of  $9\text{nm}$ . Holography written sampled gratings don't have a length limitation. The sample can be placed further away from the light source so that the divergent coherent beam covers a larger area. In this case, the exposure time needs to be increased to compensate for the lower illumination intensity.

The TTGs fabricated are Buried Heterostructure devices with a continuous tuning range of about  $6\text{nm}$ , so both superperiods need to be between  $60\mu\text{m}$  and  $80\mu\text{m}$  to obtain quasi-continuous tuning. The coupling coefficient  $\kappa$  is limited to  $100\text{cm}^{-1}$ .

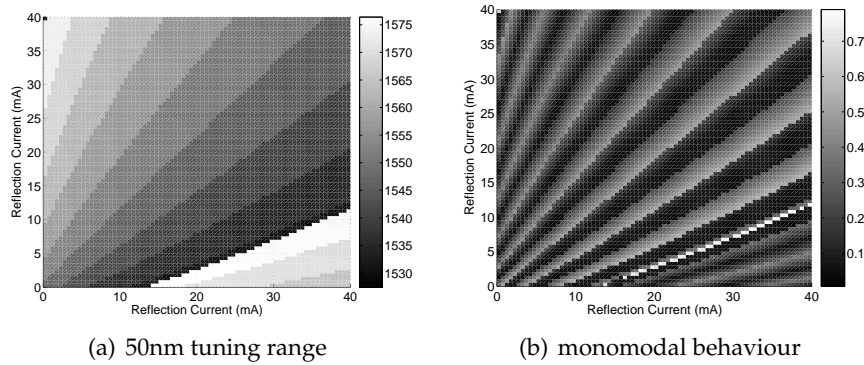
### 4.3.2 Threshold analysis of SG-TTGs

An SG-TTG has a limited amount of changeable parameters so it is more difficult to find a good combination of grating parameters that satisfies all the demands (e.g. large tuning range with complete wavelength coverage, high side-mode suppression, enough reflection of the grating, etc.). The design is straightforward and has high fabrication tolerances.

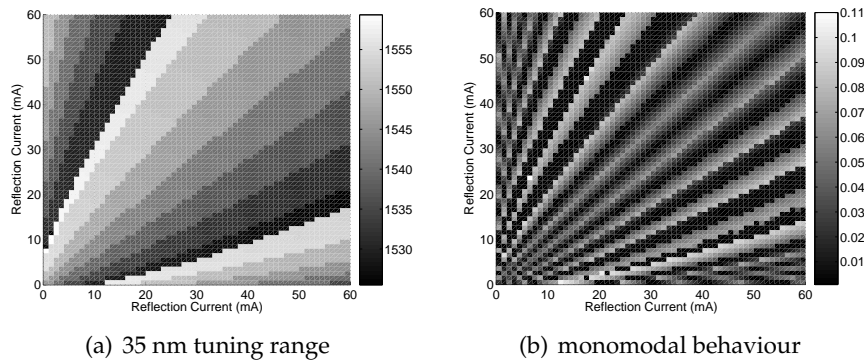
Some usable superperiod combinations were chosen that have more or less equally long sections, in order to put the phase shift in the middle of the laser.

Figure 4.7 and 4.8 show the wavelength and threshold gain difference (which is needed to determine the side-mode suppression) as a function of the reflector currents for two devices: a long SG-TTG with a laser length of  $1260\mu\text{m}$  and a shorter device with a length of  $583\mu\text{m}$ .

For long SG-TTG devices (Fig. 4.7) a large tuning range ( $45\text{nm}$ ) and a high side-mode suppression can be achieved by fine-tuning the design parameters. The shorter devices (Fig. 4.8) have a slightly smaller tuning range ( $35\text{nm}$ ) because it is more difficult to find a good combination of superperiods to obtain quasi-continuous tuning. The selectivity of the gratings is lower and the phase shift isn't in the middle of the device causing a lower side-mode suppression. So the  $590\text{nm}$  writing limitation of the available e-beam lithography at TU Munich is a disadvantage for fabricating SG-TTGs. The longer devices could only be fabricated through holography in this research.



**Figure 4.7:** Threshold Simulations of a long SG-TTG laser. Gratings with a pitch of 240nm and a coupling coefficient of  $100\text{cm}^{-1}$  were used. The sampled gratings have a duty cycle of 10% and a sampling period of  $63\mu\text{m}$  in the first grating section and  $70\mu\text{m}$  in the second section. The grating sections are each  $630\mu\text{m}$  long.



**Figure 4.8:** Threshold Simulations of a short SG-TTG laser. Gratings with a pitch of 240nm and a coupling coefficient of  $100\text{cm}^{-1}$  were used. The sampled gratings have a duty cycle of 10% and a sampling period of  $70\mu\text{m}$  in the first grating section and  $75.7\mu\text{m}$  in the second section. The grating sections are  $280\mu\text{m}$  and  $302.8\mu\text{m}$  long respectively.

### 4.3.3 Threshold analysis of SSG-TTGs

The SSG-TTG concept gives a larger freedom in choosing the design parameters. So there are more parameters to play with and the spectrum will resemble the ideal structure. The large parameter space makes the design phase more complex and the susceptibility to gain influences (§3.6) makes it even more complex. In the end a very complex set of parameters was obtained (table 3.1) resulting in a grating that can't be fabricated with the limited resolution of the e-beam lithography at TU Munich.

Only superstructure gratings with 3 to 6 discrete grating period steps within one superperiod were investigated. First the reflection spectra were simulated by the methods described in chapter 3. Only superstructure gratings with a flat reflection spectrum over a tuning range of 40nm or more were used in the simulations of SSG-TTGs.

In agreement with the SG-TTGs the simulations (Fig. 4.9) a lower tuning range (30nm) was obtained for shorter devices due to difficulty in finding a good set of grating parameters. The longer devices (Fig. 4.10) have a 44nm tuning range.

Not all wavelengths within the tuning range can be reached in the shorter device because some supermodes are skipped due to the non-uniform peak envelope of the reflection spectrum caused by the gain (see §3.6). This happens when the partially overlapping neighbouring peaks are higher than the perfectly overlapping peaks.

## 4.4 Fabrication

The widely tunable twin-guide lasers were fabricated at the Technical University of Munich. The TTG fabrication process has a lot of similarities with standard processing for Buried Heterostructure lasers. First the basic layer structure (Fig. 4.11(a)) containing a strained-layer multi quantum well active region with photoluminescence peak at around 1.55 $\mu\text{m}$  is grown using chemical beam epitaxy (CBE) and metal-organic vapor phase epitaxy (MOVPE). Afterwards the  $\sim 40\text{nm}$ -deep gratings are fabricated on a 180nm-thick InGaAsP tuning layer ( $\lambda_g=1.35\mu\text{m}$ ). The grating fabrication process is explained in section §3.4.

The gratings are overgrown with p-doped InP (Fig. 4.11(b)). The formation of blocking layers can occur due to exposure of the surface to air before regrowth. This can be prevented by doing an extra UV/ozone-cleaning before regrowth. Any surface damage or crystal damage leads

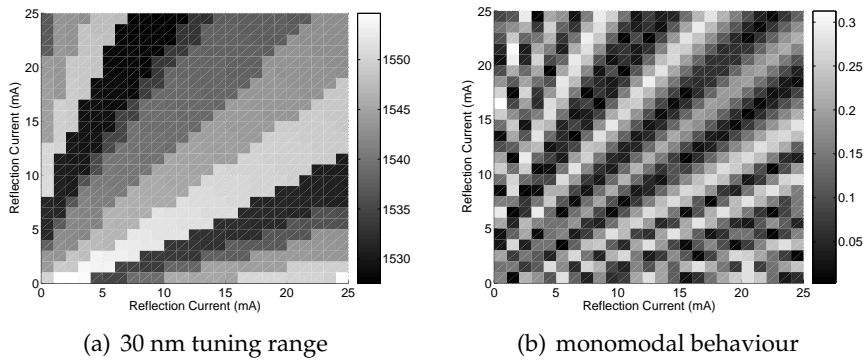


**Figure 4.9:** Threshold Simulations of a short SSG-TTG laser. Gratings with a pitch of 240nm and a coupling coefficient of  $100 \text{ cm}^{-1}$  were used. The superstructure gratings have a super period of  $60\mu\text{m}$  in the first grating section and  $72\mu\text{m}$  in the second section. The grating sections are  $300\mu\text{m}$  and  $290\mu\text{m}$  long respectively.

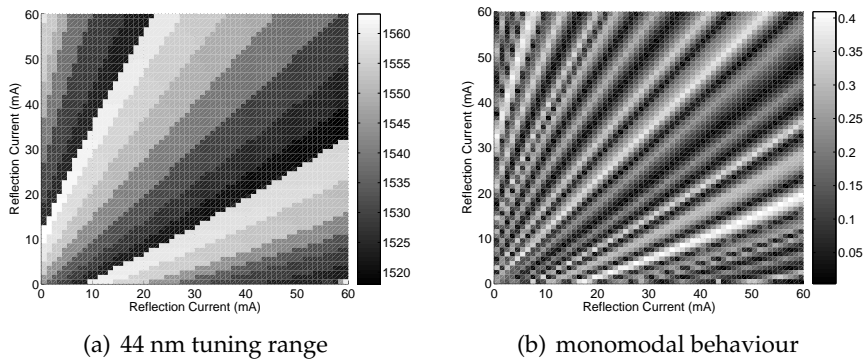


**Figure 4.10:** Threshold Simulations of a long SSG-TTG laser with missing supermodes, so no complete wavelength coverage over the full tuning range. Gratings with a pitch of 240nm and a coupling coefficient of  $100 \text{ cm}^{-1}$  were used. The superstructure gratings have a superperiod of  $70\mu\text{m}$  in the first grating section and  $76.4\mu\text{m}$  in the second section. The grating sections are  $770\mu\text{m}$  and  $764\mu\text{m}$  long respectively.

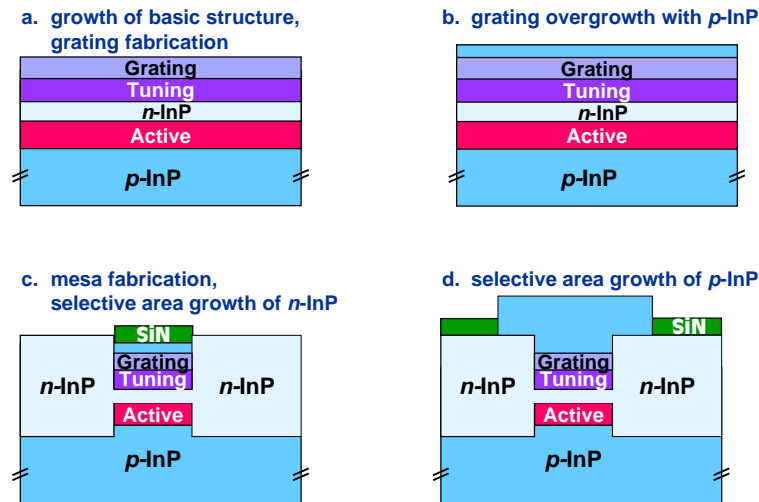


**Figure 4.11:** Fabrication steps of (S)SG-TTGs

to increased recombination and should be avoided at all costs. These effects reduce the efficiency of the carrier injection into the tuning region and cause an additional heat generation. This electrothermal heating causes a positive wavelength shift, counteracting the negative wavelength shift through carrier injection and limiting the achievable tuning range. MOVPE was used for the overgrowth steps to improve the interface quality.

A  $1.5\mu\text{m}$ -broad and  $0.7\mu\text{m}$ -deep mesa is etched in the next step through Reactive Ion Etching (RIE) creating lateral confinement. The next critical step is the selective area growth of n-doped InP to bury the mesa (Fig. 4.11(c)): cavities can occur causing increased recombination at the InP homojunction and a lower tuning range. The presence of superelevations can also complicate the following fabrication steps. Finally, a selective area overgrowth of p-InP is carried out and metallisation is used to add the contact layers (Fig. 4.11(d)). Figure 4.12 shows the top and side view of a fabricated SG-TTG laser.

The fabrication problems described above are all technology-specific and not device-specific. All the overgrowth steps that are necessary to create a twin-guide laser are the same as in the fabrication process of a Buried Heterostructure DFB laser.

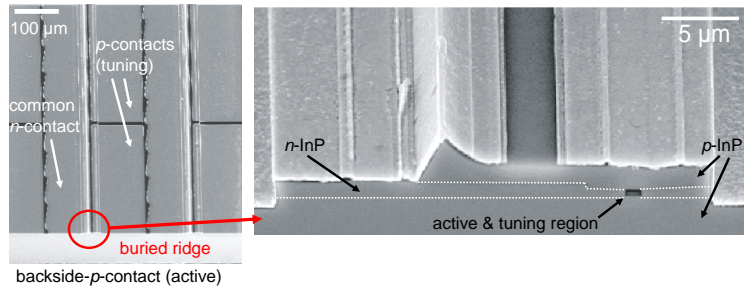


**Figure 4.12:** SEM picture of fabricated SG-TTGs: top view (left) and side view (right)

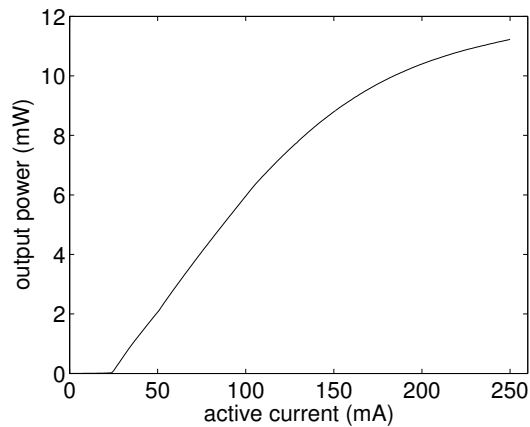


**Figure 4.13:** L-I characteristic of a SG-TTG

## 4.5 Measurements

The final batch of widely tunable SG-TTG lasers consisted of devices with a cavity length of around 1200 $\mu\text{m}$  and a grating pitch of 236nm. The sampled gratings had a duty cycle of 10% and a sampling period of 64.33 $\mu\text{m}$  in the first grating section and 56.52 $\mu\text{m}$  in the second section. The grating sections were 643.3 $\mu\text{m}$  and 621.72 $\mu\text{m}$  long respectively. The facets were AR-coated with a  $\lambda/4$ -thick  $\text{Al}_2\text{O}_3$  layer and a window structure were used to bring the facet reflection below  $10^{-3}$ . The devices were mounted on a copper heat sink, that was stabilised at a constant temperature of 25 degrees.

Figure 4.13 shows the output power versus the active current. Due to the longer cavity length the threshold current is increased to 30mA.

The power increases linearly after the laser threshold and saturates around 150mA due to leakage currents across the p-n homojunction. Output powers up to 25mW were measured by TU Munich [2].

A very regular tuning behaviour is obtained in Figure 4.14. From the plot of the emission wavelength versus tuning currents (Fig. 4.14(a)), one can easily recognize 7 supermodes covering a tuning range of almost 6THz (more than 40nm). The tuning currents are swept along 4 of those supermodes in Figure 4.16. The 5nm spacing between supermodes is in agreement with the SG design. The continuous tuning range of a supermode is larger than 5.7nm guaranteeing quasi-continuous tuning. As a comparison the simulation of an SG-TTG in Cladiss with the same grating parameters and an estimated coupling coefficient  $\kappa$  of  $100\text{cm}^{-1}$  is shown in Figure 4.15. Once again 7 supermodes are obtained with tuning over a 45nm wavelength range.

The measured supermodes aren't aligned around the central supermode (the Bragg wavelength). This asymmetry is caused by the non-flat gain characteristic (see Fig. 4.19). The supermodes on the long-wave side have higher threshold currents, so only two supermodes are reachable on this side, while 5 supermodes can be observed on the short-wave side. This deteriorates the reachable tuning range because more differential tuning is needed to access the supermodes that are further from the central supermode, so less tuning current is left to change the wavelength of this supermode. Furthermore a non-flat gain characteristic can have a deteriorating effect on the side-mode suppression if the partially overlapping peaks are at a wavelength with a higher gain than the perfectly overlapping peaks.

For each standardised ITU frequency within the tuning range the best point was extracted and characterised (Fig. 4.18). For most ITU frequencies the side-mode suppression ratio is above 40dB. So the laser remains monomodal over a large tuning range. A high side-mode suppression can also be observed when measuring the spectrum of the laser light coupled into an optical fiber (Fig. 4.17). The side-mode suppression is limited by neighboring supermodes that partially overlap.

The output power decreases at higher frequencies due to the tuning-induced losses (Fig. 4.18(b)). This contributes partly to the decrease in the side-mode suppression. The required tuning currents for each ITU frequency are portrayed in (Fig. 4.18(c)). Due to a high tuning efficiency only small tuning currents up to 40mA are needed to tune over the whole frequency range. Furthermore, the regular behaviour of the

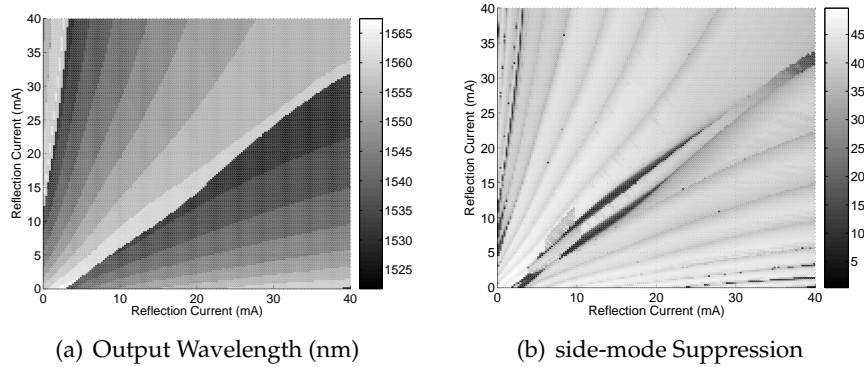


**Figure 4.14:** Frequency sweep of a fabricated SG-TTG laser. Gratings with a pitch of 236nm. The sampled gratings have a duty cycle of 10% and a sampling period of 64.33 $\mu\text{m}$  in the first grating section and 56.52 $\mu\text{m}$  in the second section. The grating sections are 643.3  $\mu\text{m}$  and 621.72 $\mu\text{m}$  long respectively.

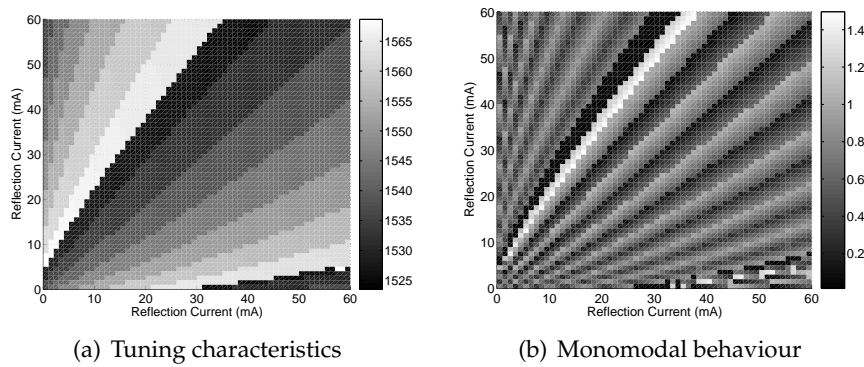


**Figure 4.15:** Threshold Simulations of a fabricated SG-TTG laser. Gratings with a pitch of 236nm and a coupling coefficient of 100  $\text{cm}^{-1}$  were used. The sampled gratings have a duty cycle of 10% and a sampling period of 64.33 $\mu\text{m}$  in the first grating section and 56.52 $\mu\text{m}$  in the second section. The grating sections are 643.3  $\mu\text{m}$  and 621.72 $\mu\text{m}$  long respectively.

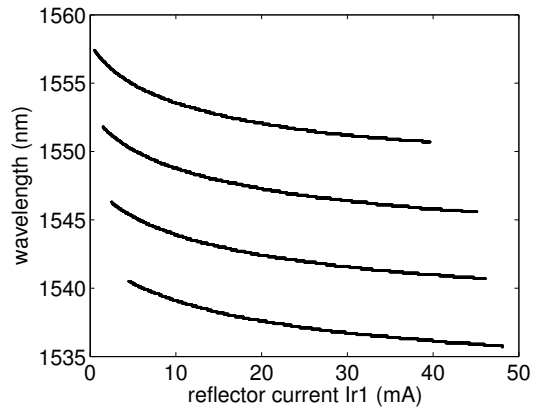


**Figure 4.16:** Diagonal Sweep of SG-TTG. Same SG-TTG parameters as Fig. 4.14

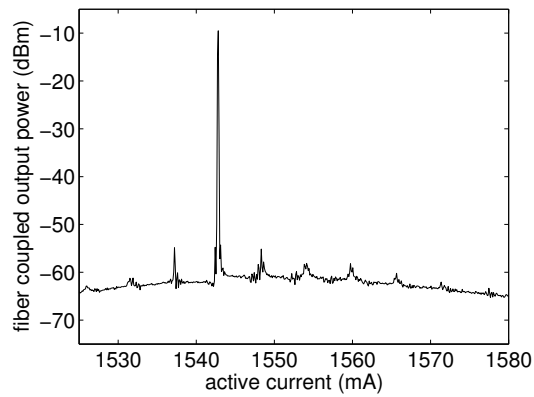
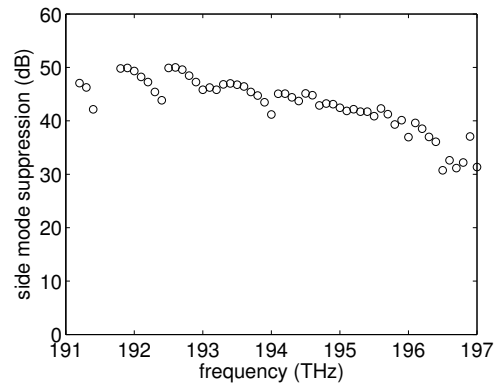
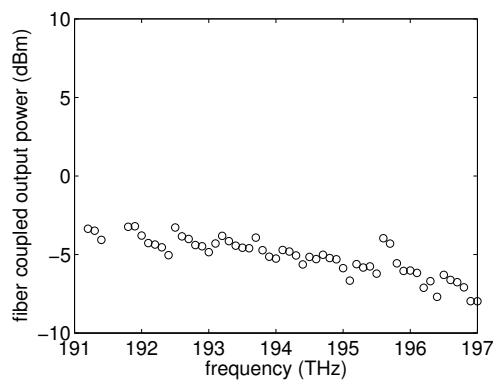


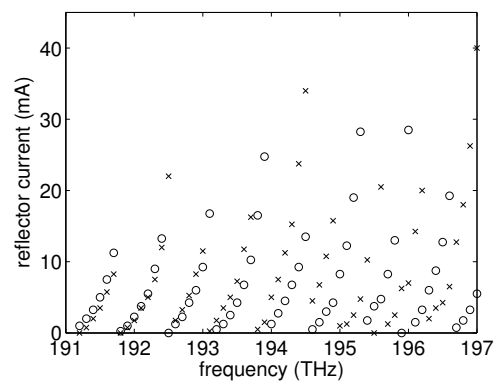
**Figure 4.17:** Spectrum of SG-TTG. Same SG-TTG parameters as Fig. 4.14



(a) Side-Mode Suppression (dB)



(b) Output Power (dBm)



(c) Variation of tuning currents (mA)

**Figure 4.18:** Characteristics of best points measured at each ITU frequency.

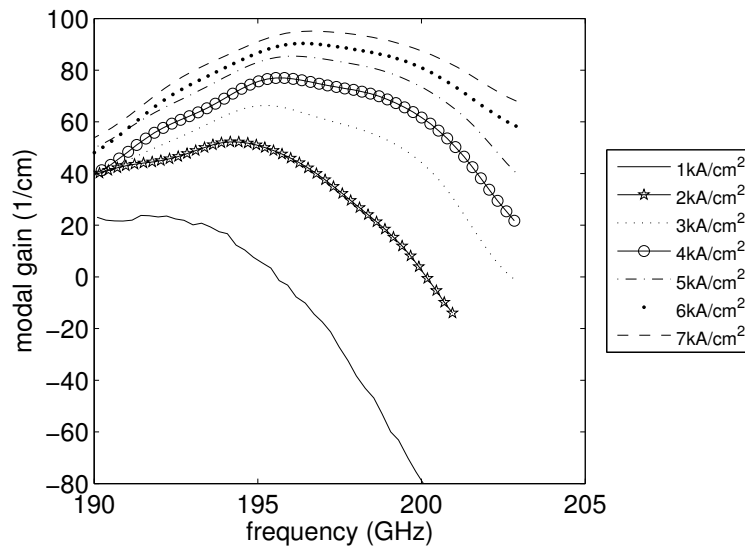


**Figure 4.19:** Modal gain changes due to frequency and current density variations. Measurement done by TU Munich using Hakki and Paoli method [74].

tuning currents indicates a very regular tuning behaviour for the SG-TTG laser.

A larger tuning range and side-mode suppression are possible after optimisation of the grating design. During the design a continuous tuning range of a supermode was estimated at 5.7nm, but DFB-TTG measurements show that this can go up to 9nm [34]. A larger peak spacing increases the tuning range and also the side-mode suppression is higher due to a better peak selectivity.

## 4.6 Alternative thermal designs

The widely tunable twin-guide laser has a very complicated layer structure with a lot of fabrication problems. This leads to leakage currents across the p-n homojunction that were counteracting the tuning behaviour. It took a long time for these problems to get fixed and in the meantime alternative designs were investigated and fabricated to prove the working principle of the TTG concept. A short overview of these alternative designs is given in this section.

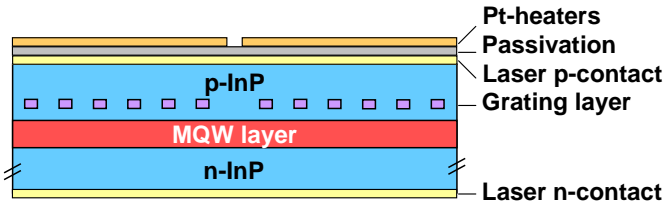


Figure 4.20: Thermally tunable sampled grating DFB laser

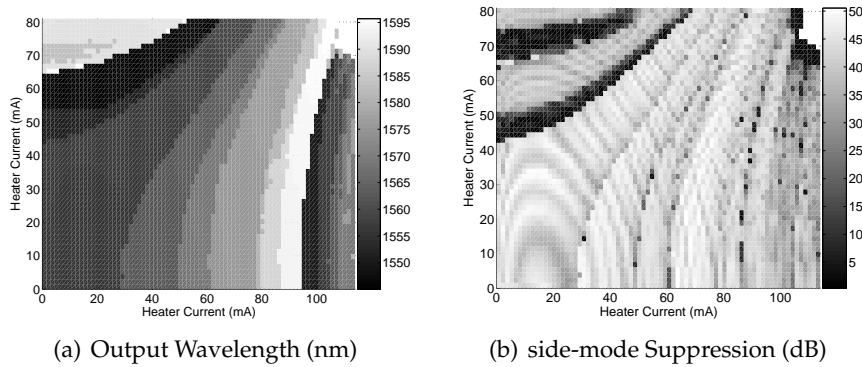


Figure 4.21: Frequency sweep of a fabricated thermal DFB laser with 60.6 and 54.7 $\mu\text{m}$  long sampling periods, 10% duty cycle and a laser length of around 1200 $\mu\text{m}$ .

#### 4.6.1 Thermally tunable sampled grating DFB laser

The new thermally tunable sampled grating DFB laser concept [75, 76] (Fig. 4.20) is very similar to the (S)SG-TTG, but the tuning sections are replaced by two Pt-stripe-headers on top of the device. This concept is easier to manufacture than the (S)SG-TTG lasers because it has a regular DFB-type layer structure, so the regular DFB laser fabrication techniques can be used.

By heating both sections separately the reflection spectra of both sampled gratings with different peak spacing will move independently and thanks to the Vernier effect wide tuning is once again obtained. Thermal cross-talk between the two sections can be prevented thanks to a 60 $\mu\text{m}$  long unheated spacing in between the Pt-stripe heaters.

Regular tuning behaviour is observed in the wavelength map and SMSR map (Fig. 4.21). The tuning range is around 50nm/6THz but not all the ITU channels within this tuning range can be accessed (only

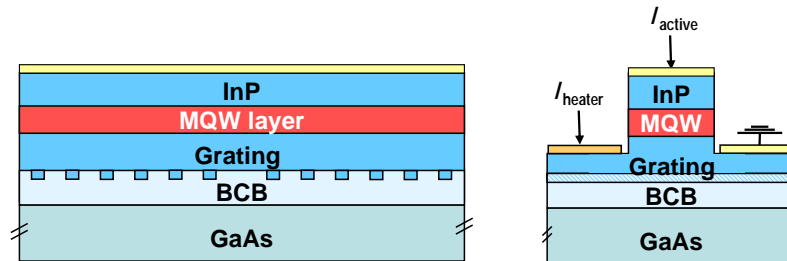


**Figure 4.22:** BCB bonded Thermally Tunable DFB laser

43nm). The side-mode suppression remains above 40dB for all these ITU channels. The output power is higher than 10mW and goes up to 29mW. Detailed tuning characteristics were measured by the Technical University of Munich and were published in literature [75, 76].

The small gaps in the tuning range are caused by supermodes that can't be tuned far enough to reach the neighboring supermode. This happens when a supermode can only be reached after a large temperature shift, so there's only a smaller potential temperature shift left to do the continuous tuning of this supermode.

#### 4.6.2 BCB-bonded thermally tunable SGDFB

Regrown layer structures can't be fabricated at INTEC, so an alternative design for thermally tunable sampled grating DFB laser was investigated in which BCB bonding [48] is used instead of regrowth (Fig. 4.22).

A sampled grating is fabricated in the layer structure and BCB is used afterwards to attach the grating layer to a GaAs carrier. The planarisation of the BCB is critical, because the presence of gas bubbles can deteriorate the laser characteristics.

Afterwards, the sample is turned upside down and a laser is fabricated in the top InP/InGaAsP material. Some Pt-heaters are included as well for thermal tuning. The Vernier effect can once again be used to obtain thermal tuning over a large wavelength range.

The laser contacts and the stripe heaters are all placed at the top of the device because the BCB has a bad electrical and thermal conductivity.

This design is at the moment investigated and developed by thesis students.

## 4.7 Conclusions and further research

The performance of the widely tunable twin-guide lasers is comparable with other monolithic widely tunable lasers. A tuning range of 6THz (over 40nm) while maintaining a side-mode suppression of more than 40dB for most ITU channels was demonstrated during this PhD research. A high output power was obtained as well.

The device can easily be manufactured with conventional DFB laser fabrication technology even though there are 3 regrowth steps required. This fabrication was carried out at TU Munich. My part in this research concentrated on the design and the characterisation of these devices.

Further improvements of the gratings design could increase the tuning range and the side-mode suppression even more. It would be interesting to see how gain compensated superperiod gratings behave in widely tunable twin-guide lasers. Therefore a better e-beam facility with a higher writing resolution is needed.

The integration of a semiconductor optical amplifier (SOA) could be investigated as well. By incorporating an SOA the tuning range can be increased. The confinement factor of the mode in the tuning region can then be increased at the expense of the confinement in the active layer. The obtained power decrease can then be compensated by the SOA.

Additionally, it would be interesting to investigate an asymmetric design with a short front mirror with a low duty cycle and a longer rear mirror with a higher duty cycle. This will create a higher output power, but probably deteriorates the side-mode suppression in the case of  $\lambda/4$ -shifted DFB lasers.

The use of only two tuning currents makes the characterisation quite simple. The control of the SG-TTG lasers will be discussed in chapter 6. A potentially high direct modulation bandwidth is also expected. This will be investigated in chapter 7.



## Chapter 5

# Modulated Grating Y-Branch Laser

The new widely tunable Modulated Grating Y-Branch (MG-Y) Laser has a very similar working principle as the existing widely tunable DBR-type lasers: two reflectors with slightly different peak spacing create tuning over a wide frequency range thanks to the Vernier effect.

The main difference is the use of a Y-splitter to combine the two reflections. Placing both reflectors at the back prevents a low output power and a large power variation because the light doesn't have to pass a lossy reflector before exiting the cavity.

Additionally, the MG-Y lasers have the same advantages as other widely tunable DBR lasers: a simpler fabrication, a good selectivity and an easy stabilisation.

This chapter will investigate if these interesting prospects for the MG-Y laser were realised. The first section introduces the device principle, while section 2 goes into more detail about the design. The fabrication is briefly mentioned in section 3, before presenting the characterisation results in section 4.

### 5.1 Device Principle

In the Modulated Grating Y laser concept [3, 4, 6] the different functions are separated into different sections (Figure 5.1). The gain section amplifies the light, the multi-mode interferometer (MMI) splits the light into 2 equal beams, the bends increase the separation between the two waveguides and the reflectors filter out certain frequencies. The differ-

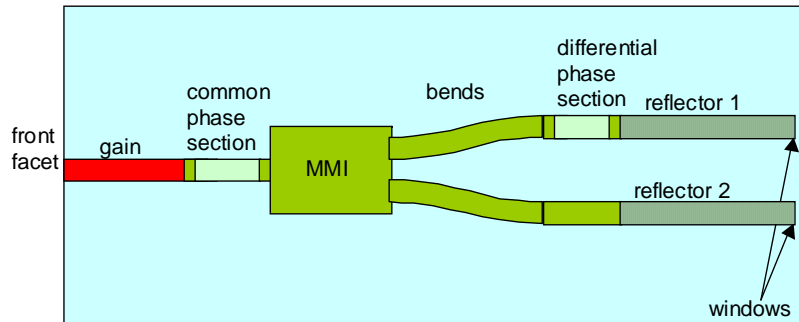


**Figure 5.1:** Schematic drawing of an MG-Y laser with 4 control currents

ential phase section guarantees that the reflected beams are added up in phase and the common phase section is responsible for the alignment between the cavity mode and the reflected peaks.

The additive Vernier effect is used to select one lasing frequency. Both reflectors have a slightly different peak spacing so the frequency where both peaks overlap will reach the laser threshold first. By injecting current into one reflector, the reflection spectrum will move to lower wavelengths and the overlapping peaks will occur at a higher frequency. By injecting current into both reflectors, both reflection spectra will move in the same direction and the same peaks will remain overlapping. Through this mechanism quasi-continuous tuning can be obtained.

The four independent tuning currents are a potential disadvantage, because the characterisation becomes time-consuming. In the next section some design details will be given that make it possible to reduce the number of control currents to only three.

## 5.2 Design

In this section the design of the Modulated Grating Y-Branch Laser will be discussed. Some design rules for wide tuning will be given and the reduction of the number of control currents will be discussed.

The basic design rules to obtain wide quasi-continuous tuning with the Vernier effect in widely tunable lasers were already discussed in section §4.2. So this section concentrates on the particularities of the additive Vernier effect. The design rules for quasi-continuous tuning

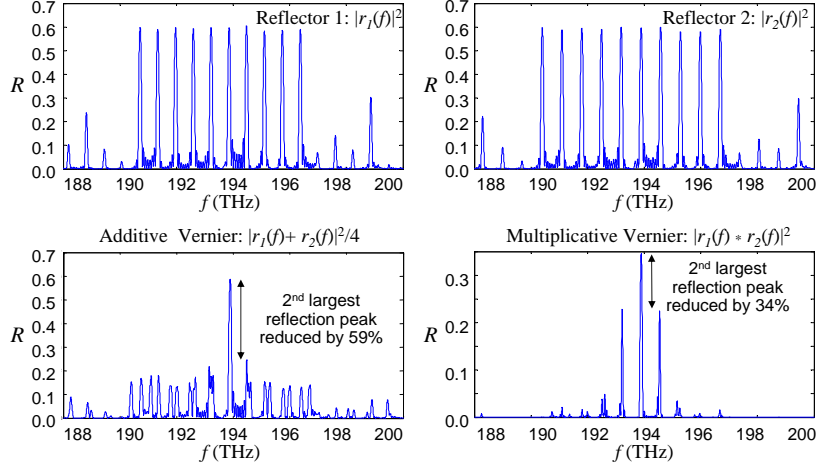


**Figure 5.2:** Reflection Spectra of the two reflectors (top figures) and the comparison between the additive (MGY) and multiplicative (SSG-DBR) Vernier effect (bottom figures). Simulations done by Syntune AB.

over a large frequency range remain the same and they can be found in §4.2.

### 5.2.1 High side-mode suppression

A higher side-mode suppression can be obtained than with the multiplicative Vernier effect (Fig. 5.2) where two reflectors are placed on a different side of the gain section (e.g. SG-DBR lasers), because in the MG-Y concept the neighboring peaks can be designed to add partly out of phase. This phase difference can be written as [3]:

$$\Psi = \frac{4\pi n_g}{c_0} \Delta f_s L_{eff} \quad (5.1)$$

So a large peak separation difference  $\Delta f_s$  or a long average effective reflector length  $L_{eff}$  is needed to obtain a high selectivity.

It should be noted that peaks that are further away from the main peak do not decrease in comparison with the multiplicative case (Fig. 5.2). This may cause problems when the peaks overlap far away from the gain peak. In that case a mode around the gain peak with a large enough remaining reflection can start lasing instead of the mode near the overlapping peaks.

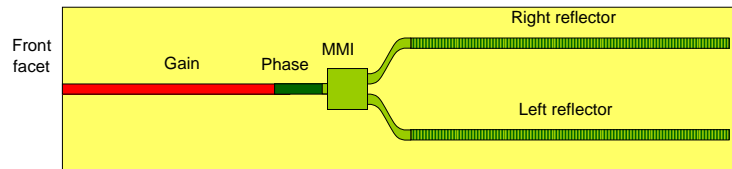


**Figure 5.3:** Schematic drawing of an MG-Y laser with 3 control currents

### 5.2.2 High output power and low power variation

Due to the MMI splitter the two reflectors can be placed at the back of the laser, so the photons do not have to pass a reflector section with tuning-induced losses before exiting the laser cavity. A higher output power and a lower power variation can be obtained in comparison with for example an (S)SG-DBR laser.

The output power and power variation can be further improved by minimizing the carrier-induced losses of the reflectors by decreasing the peak separation. A smaller tuning current is then needed to obtain quasi-continuous tuning leading to less carrier-induced losses.

### 5.2.3 Reducing the number of control currents

Two perfectly overlapping reflector peaks should add in phase. In order to obtain a constructive interference, the reflections from both reflectors should have the same phase at that frequency. Additionally, both reflectors should start at the same distance from the splitter to eliminate a potential phase difference between both cavities. The difference in the positioning of both gratings should be less than 35nm to keep the phase difference below the acceptable level of  $\pm 1$  radian.

With a careful design of the gratings and a careful processing of the branches, enough symmetry between the two branches is obtained and the differential phase section is no longer necessary so only 3 independent tuning currents remain (Fig. 5.3).

If there is asymmetry between the two branches the supermode boundaries will shift because an extra tuning difference is needed between the two reflectors to find an optimal overlap. The output power won't change because the transmission of each reflector remains the same, therefore the power maxima won't be any longer centered supermode wise. In figure 5.4 the output power of a widely tunable MG-Y laser without differential phase section is shown. The output

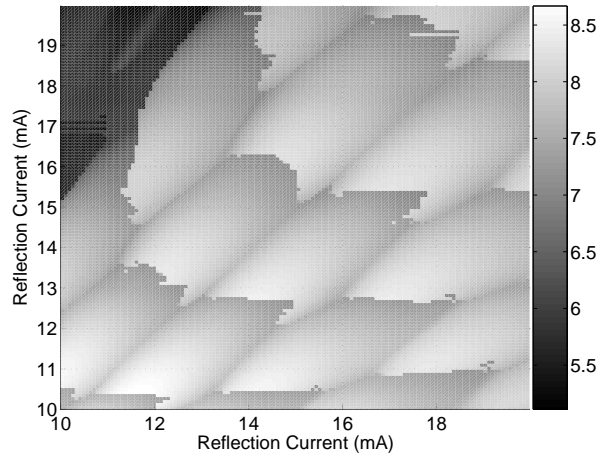


**Figure 5.4:** Output power in function of reflector currents

power remains centered supermode wise indicating that the removal of the differential phase current is justified in the MG-Y design. The non-linear gain is responsible for the non-centered output power cavity mode wise. It is also important to remark that inserting a differential phase section can create a certain asymmetry itself.

### 5.3 Fabrication

The MG-Y lasers were designed and fabricated by Swedish start-up Syntune AB. The fabrication of these InP/InGaAsP buried ridge Y-Branch lasers with multi-quantum well gain section is very similar to that of a widely tunable DBR laser and thus relatively simple. The front facet was coated to decrease the facet reflection to about 5% and a window structure was used to eliminate the unwanted backside facet reflections. A SEM picture of a fabricated MG-Y laser with 4 control currents is shown in Figure 5.5.

Some relevant parameters are summarised in the following table.

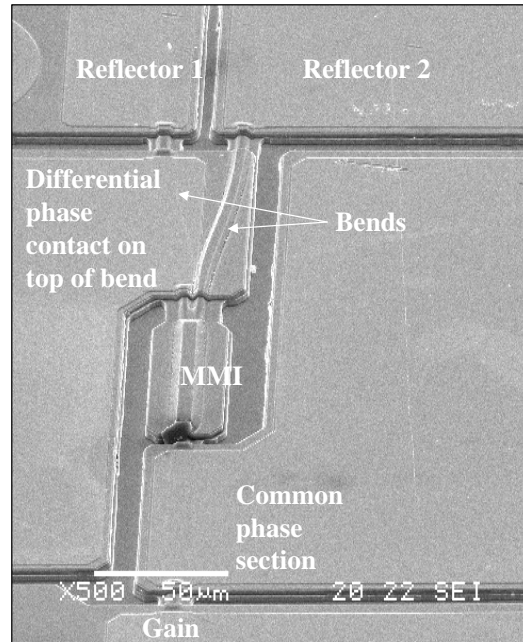
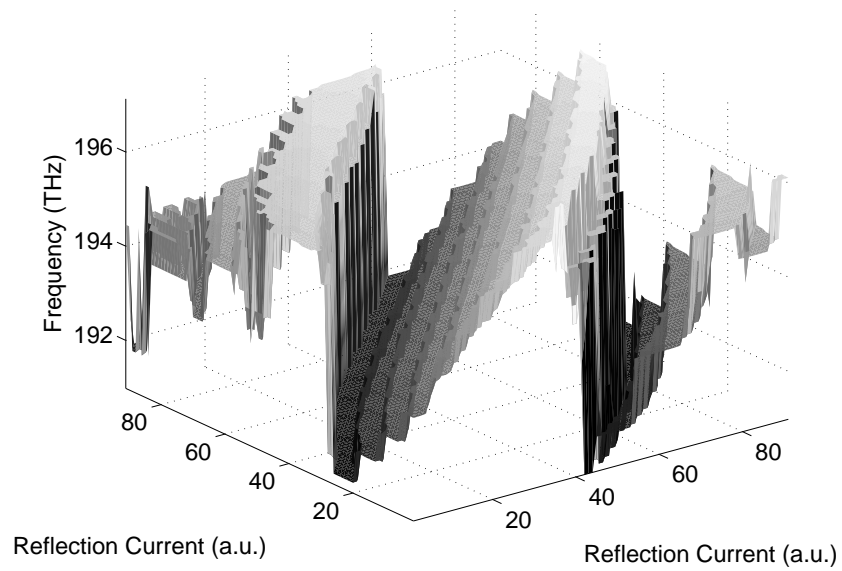


Figure 5.5: SEM picture of a fabricated MG-Y laser

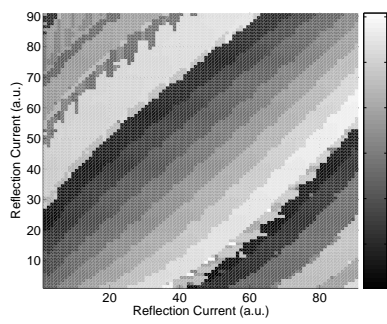
Gain section	length	400 $\mu\text{m}$
	width	1.6 $\mu\text{m}$
Common phase section	length	80 $\mu\text{m}$
	width	1.6 $\mu\text{m}$
MMI splitter	length	60 $\mu\text{m}$
	width	7 $\mu\text{m}$
Bends	radius	255 $\mu\text{m}$
	length	115 $\mu\text{m}$
	width	1.6 $\mu\text{m}$
Reflectors	length	700 $\mu\text{m}$
	coupling $\kappa$	30 $\text{cm}^{-1}$
	width	1.6 $\mu\text{m}$

## 5.4 Measurements

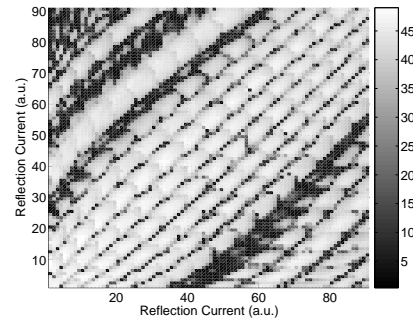
Figure 5.6 shows the output frequency and the side-mode suppression (SMSR) as a function of the reflector currents measured at a gain current of 100mA and a common phase current of 0.5mA.



(a) Frequency (THz)

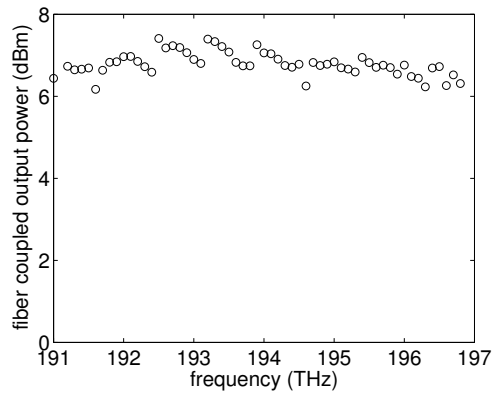


(b) Frequency (THz)

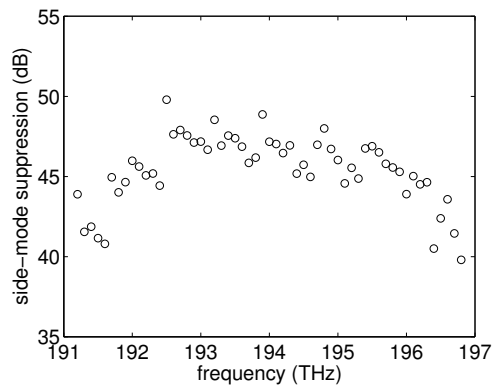


(c) Side-Mode Suppression (dB)

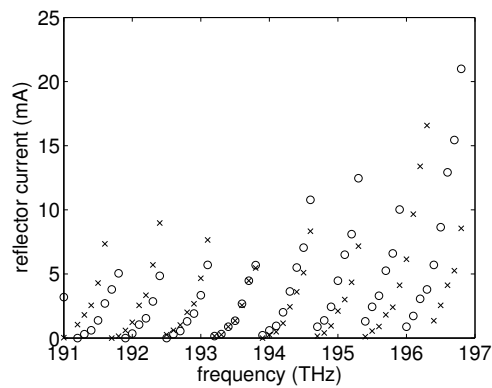
**Figure 5.6:** Frequency and side-mode suppression of a fabricated MG-Y laser.



(a) Output Power (dBm)



(b) Side-Mode Suppression (dB)



(c) Variation of tuning currents (mA)

**Figure 5.7:** Characteristics of best points measured at each ITU frequency.

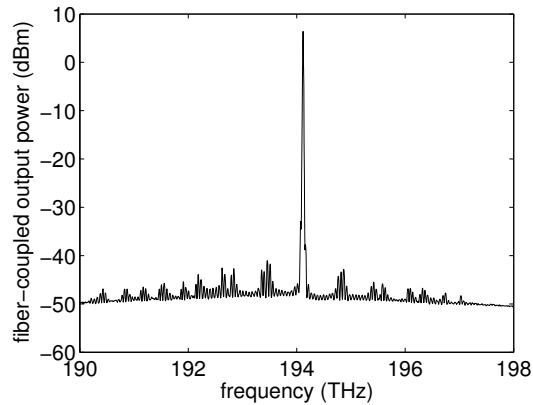


Figure 5.8: Optical spectrum of an MG-Y laser

A very regular tuning behaviour of more than 5.5THz (45nm) can be reached. For each standardised ITU frequency within this tuning range the best operating point was extracted and characterised. The properties are shown in Figure 5.7. The fiber coupled output power varies only 1.2dB over the full tuning range (Fig. 5.7(a)). The facet output power is around 14dBm or 25mW.

For each ITU frequency between 191.2THz and 196.8THz a side-mode suppression of more than 40dB is measured (Fig. 5.7(b)). The good monomodal behaviour can also be noticed when observing the optical spectrum (Fig. 5.8). The side-modes decrease more than was initially expected from the additive Vernier effect (Fig. 5.2) thanks to a better (proprietary) grating design that causes a better destructive interference of partially overlapping peaks.

Most tuning currents are below 15mA (Fig. 5.7(c)) so switching between channels can happen faster due to the lower thermal transients when changing currents. Only low tuning currents are necessary due to the small peak separation of the reflection peaks.

The researchers at Syntune obtained even better measurement results [77]: a tuning range of 6.4THz was observed with a maximum output power of up to 45mW. This is the highest output power for monolithic tunable laser (without integrated amplifier) ever measured.

## 5.5 Conclusions

The modulated grating Y-branch (MG-Y) concept yields state-of-the-art widely tunable lasers with full C or L-band frequency coverage while maintaining a high side-mode suppression and a low output power variation.

The output power was the highest measured and reported for a monolithic tunable laser (without integrated amplifier). The output power can be further increased by incorporating an SOA.

The lasers satisfy all the telecom specifications (see section §1.2) so they are worthy competitors for other transmitters for optical telecom networks. They are commercialised by the Swedish start-up Syntune AB who will further optimize the design and investigate the monolithic integration of an SOA and a modulator.

With three control currents it has the same control complexity as SG-DBR or GCSR lasers. A control method will be introduced in chapter 6. The modulation properties will be briefly discussed in chapter 7.

## Chapter 6

# Control and Stabilisation

Several widely tunable laser concepts have been investigated in the past (see chapter 2) and all of them require the adjustment of two or more control currents to obtain a certain frequency, which makes the control of widely tunable lasers rather complex. Without control and stabilisation algorithms widely tunable lasers are of limited commercial interest to telecom operators who require an easy control and a very stable output.

To overcome the control difficulties, the lasers are sold with an easy user interface in which the wanted frequency is set by sending a simple digital command to a microprocessor. A tuning table is then used to convert the requested frequency into the required control current values. Creating such a tuning table is very time-consuming due to the many variables. Additionally fabrication tolerances cause a different tuning behaviour in each laser, so this characterisation needs to be done for each laser separately. So a fast characterisation algorithm is needed to speed up this process and minimize the cost.

Tunable lasers degrade over time, due to the development of defects at overgrown interfaces within the semiconductor material [78, 79, 80, 81] that cause a larger non-radiative recombination and a reduced carrier life time. These degradation effects together with environmental changes lead to a frequency drift and a decrease of the tuning efficiency, so feedback control strategies are needed to guarantee a reliable operation over time. Without a high frequency accuracy and high side-mode suppression the optical signals will be intermixed and fluctuating, leading to irrecoverable communication errors. A feedback mechanism that can counter the environmental influences and that postpones the re-

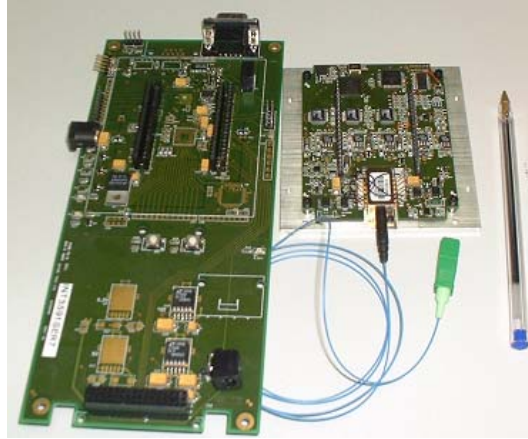


**Figure 6.1:** Picture of a control board for a widely tunable MG-Y laser

calibration of the device as long as possible is needed to make these devices commercially interesting.

This chapter discusses the control and stabilisation possibilities of the widely tunable modulated grating Y-branch (MG-Y) laser that was introduced in chapter 5. Existing methods for frequency and mode stabilisation of other types of widely tunable lasers will be explained in the next section. The control and stabilisation of the MG-Y laser will be theoretically discussed and experimentally demonstrated in sections 2 and 3. The control of the widely tunable twin-guide laser will be briefly discussed in section 4.

## 6.1 Existing Methods

In this section an overview is given of existing control and stabilisation methods for widely tunable lasers. These existing methods were investigated to find a good control and stabilisation scheme for the new widely tunable laser concepts.

### 6.1.1 Frequency stabilisation

Degradation and environmental changes cause a frequency drift of the output signal. Different possibilities to correct this drift will be introduced in the next paragraphs.

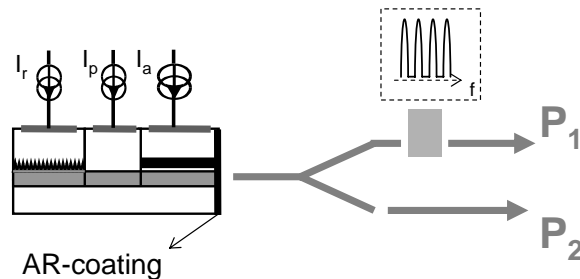


**Figure 6.2:** Principle of Frequency Stabilisation through a Wavelength Locker

### Optical filter

For most widely tunable lasers a wavelength locker is used to stabilize the frequency (wavelength): an optical filter with peaks corresponding to frequencies on the standardised ITU grid translates the frequency variations into power intensity variations (Fig. 6.2). A Fabry-Pérot etalon [82], an arrayed waveguide grating [83, 84] and a fiber Bragg grating [85, 86] are mostly used as the reference optical filter.

In some designs [82, 84] the laser is locked by using the edge of the filter transfer characteristic and a reference intensity: an error signal can be generated by comparing the measured power ratio (between the filtered and the unfiltered signal) with a reference power ratio (corresponding to the position of the ITU frequency). This error signal is minimised by adjusting the temperature or the phase current.

A small modulation signal can also be sent through one of the reflectors to detect and to lock on to the transmission peak of the optical filter [84].

Frequency stabilisation is only possible over a limited temperature range because a mode hop occurs when the temperature changes too much and the laser will then stabilize at the wrong ITU frequency. So a wavelength locker should be used in combination with a mode stabilisation system.

### Integrated Detectors

Other more complicated control techniques based on integrated detectors have also been studied in the past. In a design from UCSB [87] an SG-DBR laser is coupled to a wavelength dependent integrated splitter and a pair of integrated detectors. Due to the wavelength depen-

dent splitter the normalised detector response varies sinusoidal with the wavelength creating a waveguide monitor over a range of 30nm that can be used to stabilize the wavelength.

### 6.1.2 Mode stabilisation

A mode stabilisation scheme is used in cooperation with a frequency stabilisation scheme otherwise mode hops can occur when the laser degrades too much and the frequency stabilizes at the wrong ITU frequency.

#### Output power and Voltage

For DBR-type lasers, the fluctuations of the output power with changing tuning currents are often used for mode stabilisation: the alignment of the reflector peak with a cavity mode can be detected as a power extremum because sufficiently far above threshold the variations in output power are determined by differential efficiency variations [83].

This control method can also be implemented by integrating detectors in the laser design: in a 2 or 3 section DBR laser [88] such a detector is placed after the DBR section to measure the light transmitted through the Bragg reflector. In these devices a high side-mode suppression is obtained when the cavity mode overlaps with the reflection peak of the Bragg section. This maximum reflection is equal to a minimal detector current, so the reflector current needs to be adjusted to minimize the detector current. A phase section is present in a 3 section device where both the reflector and phase currents need to be tuned to guarantee an overlap of the cavity mode and the reflection peak while continuously tuning the wavelength of this laser.

The stabilisation method based on the output power can't be used when the output power decreases too much during tuning due to the carrier-induced losses in the reflector sections. The voltage over the active section is a possible alternative: the carrier density increases when the reflector peaks are detuned from the cavity mode to obtain enough cavity gain. This increase in carrier density creates a higher voltage over the active section so a high side-mode suppression can be obtained when this voltage is minimised [82].

Some laser devices like the grating-assisted coupler with rear SG or SSG reflector laser (GCSR) or 3-section DBR lasers can't be controlled by the output power or active voltage mode stabilisation methods. This is in general the case when the round-trip gain (or optical feedback) in the

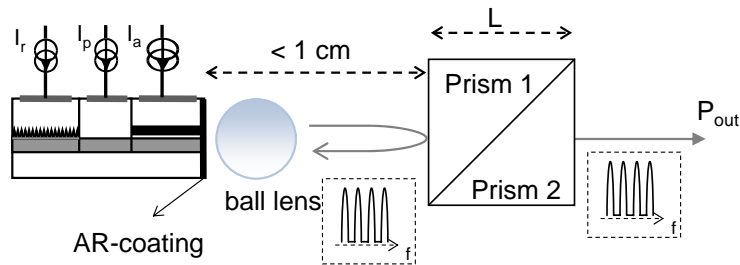


Figure 6.3: Principle of Injection Locking (Picture from Bart Moeyersoon)

laser is less wavelength selective or when non-linear effects dominate, such that an extremum in voltage or optical power can no longer be observed away from the mode boundaries.

### Injection locking

Injection locking can also be used to control the frequency and to stabilize the device: by injecting multi-wavelength light into the laser cavity, the laser will reach threshold first at one of the injected wavelengths [89] so the laser will always stabilize at one of the injected wavelengths reducing the effects of ageing and tuning table inaccuracies.

It has also been proposed [41, 90] to inject the light from the tunable lasers back into the cavity through an optical feedback loop (Fig. 6.3) containing a comb filter in order to speed up the wavelength switching and improve the wavelength accuracy.

The external filter or light source used to stabilize the laser, should be less sensitive to temperature changes, degradation and environmental changes.

## 6.2 Calibration of an MG-Y laser

A tuning table is used to convert a wanted frequency into the control current values. The many variables make the creation of such a tuning table very time-consuming. Additionally fabrication tolerances cause a different tuning behaviour in each laser, so this characterisation needs to be done for each laser separately. So a fast characterisation algorithm is needed to speed up this process and minimize the cost. The tuning table needs recalibration from time to time, when the frequency

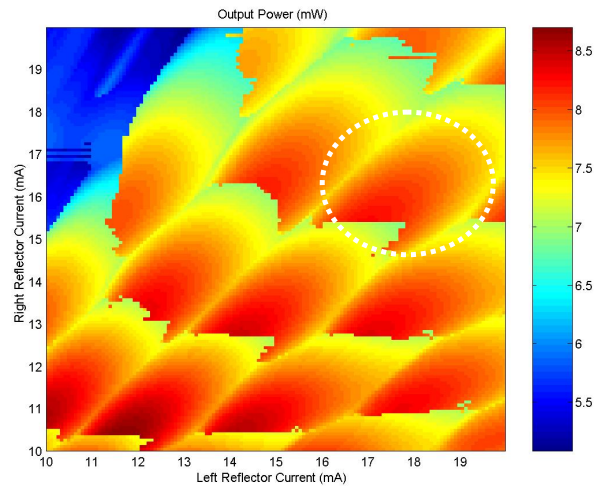


**Figure 6.4:** Output power in function of reflector currents

shifts too far from its initial point due to degradation and environmental changes.

Creating a look-up table comes down to finding reliable operating points that guarantee continuous tuning at a constant power level. The presence of three control currents makes this calibration quite complex and time-consuming. Due to hysteresis the characteristics of the measured point change depending on the previously measured point, so it is difficult to find reliable operating points. Hysteresis occurs in all DBR-type lasers, but the hysteresis in MG-Y lasers is substantial and covers up to 50% of the cell area. This is slightly more than that of a commercially available DBR and GCSR laser. It's expected that hysteresis will be further decreased as the new MGY-design is further optimised. In this section an algorithm will be presented that is capable of automatically finding reliable operating points and producing a look-up table. This work was done in collaboration with Intune Technologies.

In a first step, a coarse power plane measurement (Fig. 6.4) is carried out in which the power is measured as a function of the two reflector currents while the gain current is increased during tuning to compensate for the tuning losses in the reflectors. A very coarse quick power plane measurement is done beforehand to estimate roughly how much the power drops off so that the gain current can be corrected while tuning. From the power plane measurement data, reliable oper-

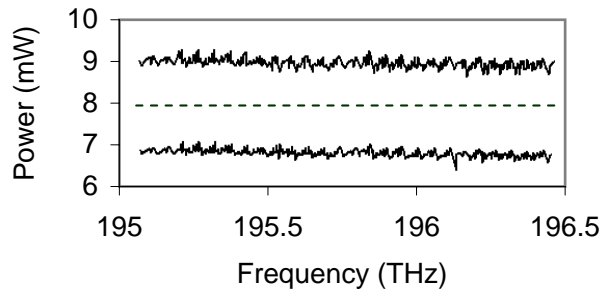


**Figure 6.5:** Extracting set of operating points: Output power of operating points in both the low power (plot at  $\sim 7\text{mW}$ ) and high power (plot at  $\sim 9\text{mW}$ ) coarse characterisations. The dashed line in between is the target power ( $8\text{mW}$ )

ating points can be extracted (e.g. by using an image processing technique) where the overlap between the reflector peaks and the cavity mode is optimal causing a high side-mode suppression and a high output power.

Secondly, the influence of the phase current is investigated by repeating the power plane measurements for different phase currents. With increasing phase current, the power plane cells (shaped by the mode boundaries) move to higher reflector currents and the extracted operating points are at higher frequencies. By only changing the phase current, tuning of approximately  $100\text{GHz}$  is possible before a mode jump occurs. Through interpolation any frequency within these tuning limits can be located.

For every frequency on the ITU grid (with a  $50\text{GHz}$  spacing) within the tuning range two optimal operating points are extracted for a power above and below the target power level (Figure 6.5). Out of those two sets of operating points the ultimate set at the wanted power level can be extracted through interpolation.

90 channels between  $192.35\text{THz}$  and  $196.8\text{THz}$  were extracted using the algorithm described in the previous paragraph. All channels (Fig. 6.6) were within  $\pm 2\text{GHz}$  in frequency of the desired ITU point and  $\pm 0.2\text{dB}$  in power of the target value. The side-mode suppression was measured to be greater than  $35\text{dB}$  for all channels.

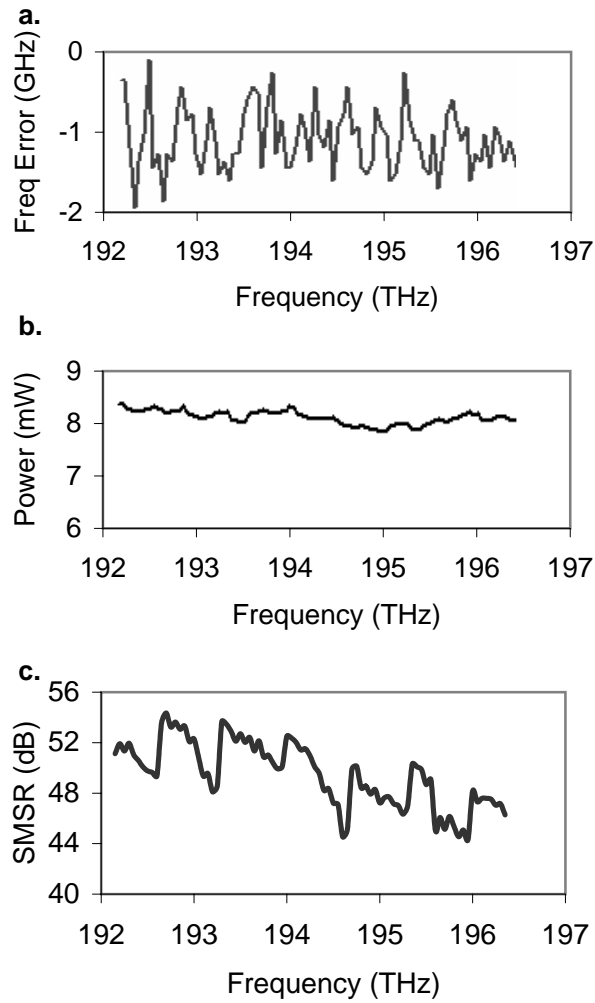


**Figure 6.6:** Final set of operating points at different ITU frequencies: (a) Frequency error (b) output power (c) side-mode suppression (Measurements by Intune Technologies)

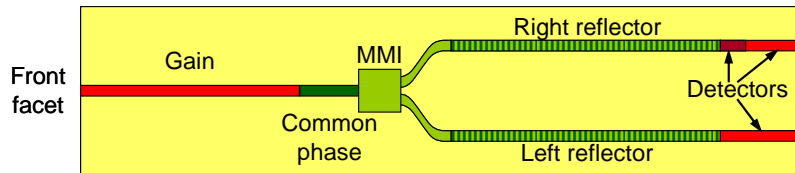


**Figure 6.7:** Schematic drawing of an MG-Y laser diode with integrated photodetectors

### 6.3 Stabilisation of an MG-Y laser

In this section the control and stabilisation of an MG-Y laser (Fig. 6.7) will be discussed. A control scheme based on integrated photo detectors will be presented that is capable of locking the operating point to the middle of a cell. This guarantees that the laser can continue operating even when the environmental conditions change or when the tuning sections of the laser diode degrade. For frequency stabilisation a standard wavelength locker was used that changes the phase section current.

#### 6.3.1 Mode Stabilisation Scheme

Integrated photodiodes (Fig. 6.7) are used for the mode stabilisation. In this tunable laser concept a high side-mode suppression and high output power is obtained when the cavity mode overlaps with a reflection peak of both reflectors. At each reflection peak the light transmitted through the reflector and detected by the integrated photodiode is then minimal. So an optimal operating point coincides with a minimum in both detector currents (Fig. 6.8). The small deviation between both extrema is caused by the tuning-induced losses in the reflectors.

The cell indicated by the dashed oval line in Figure 6.4 was examined by sweeping the reflector current along a horizontal and a vertical line. Figure 6.9 shows for both sweeps the measured output power and the measured detector current corresponding with the changed reflector current. The measurements in Figure 6.9 show that within a cell there's a clearly defined detector minimum or output power maximum to lock to. Locking can be easily implemented because the extremum can be detected by dithering the reflector currents. This way the reflector currents can be adjusted to stabilize the laser operation in the mid-

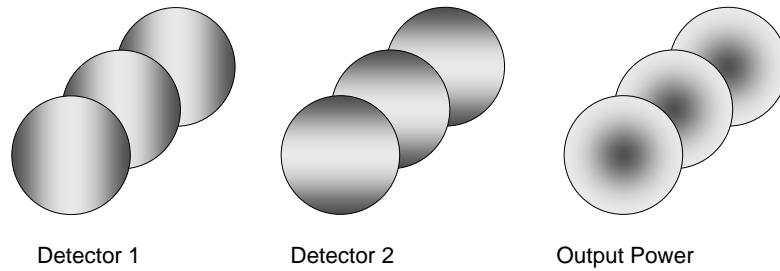


**Figure 6.8:** Variation of detector current and output power as the reflector current is varied vertically and horizontally through the cell. The horizontal (vertical) axis in the intensity plot corresponds with a variation of the current in the left (right) reflector. An optimal operating point with high SMSR and output power coincides with a minimum in both detector currents.

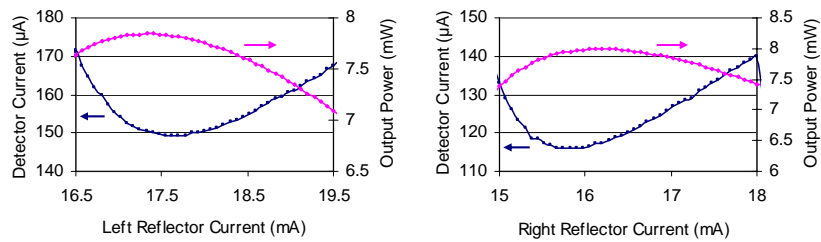


**Figure 6.9:** Variation of detector current and output power as the reflector current is varied vertically and horizontally through the cell which is indicated by the white dashed oval in Fig. 6.4

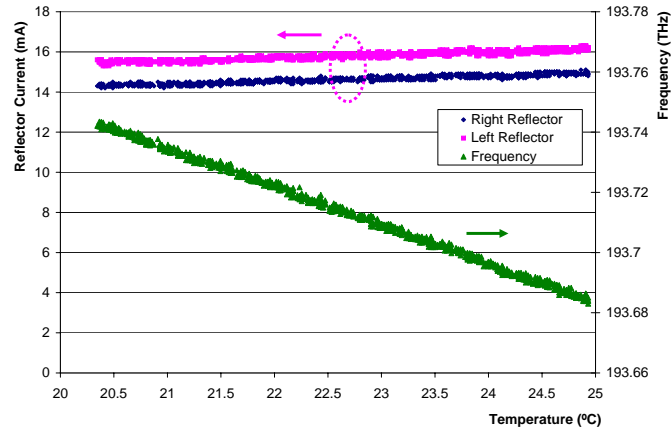


**Figure 6.10:** Variation of right and left reflector currents and frequency while the temperature is swept between 20 and 25 degrees: thanks to the stabilisation scheme a mode hop is prevented

dle of the cell and prevent a mode hop. The dithering of the reflector currents was done with a 0.01mA amplitude and a 4Hz frequency resulting in a fairly small output frequency error of 100 to 200MHz which is corrected by the wavelength locking loop.

In the feedback scheme the light coming from the laser diode is coupled into a fibre. A small part of this light is sent through an etalon to create a frequency error signal that corrects the phase current. This way the output frequency is locked to a point on the ITU grid. At the same time the detector currents are used to lock the mode into the middle of the cell compensating frequency drifts and expanding the lifetime of the device.

### 6.3.2 Control experiments

Through a series of tests the frequency and mode stabilisation algorithms described in the previous section were experimentally examined. The stability of the MG-Y laser diodes is too good to detect the effects of ageing during operation. To reproduce the effects of degradation in the tuning sections over a longer time period, the temperature of the laser sample was slowly swept.

In a first series of tests the laser was set up at a certain ITU frequency and the temperature was increased to check the degradation effects. Figure 6.10 shows what happens to the frequency when only

the mode stabilisation is used. The algorithm compensates the temperature effects so that the laser keeps lasing in the same mode over a large temperature range. This way the same position within a cell can be maintained over more than one longitudinal mode. A mode hop can be prevented, which would not be the case if only the frequency was stabilised through the phase current.

In a second series of tests that were done by Intune Technologies, the previously tested stabilisation scheme is used in combination with a wavelength locker while the temperature is swept from 19°C to 28°C in steps of 0.5°C. At each step, the phase current decreases to maintain the target frequency. At the same time, the reflector currents are changed to maintain a constant position of the operating point within the cell. The movement of this cell is not only caused by the temperature change but also due to changes in the phase section current induced by the frequency stabilisation loop.

These feedback tests are shown in Figure 6.11 for five different temperatures. The output power cells move over a considerable range as the temperature is increased. The tuning currents are decreased by the stabilisation algorithm to compensate for the temperature change. There's no mode hop though, since the cell shifts in the same direction as the operating point so that a constant position within the cell can be sustained. For each temperature the operating point is stabilised around the highest output power within the cell.

Figure 6.12 shows what happens to the operating point when the temperature is swept from 19 to 27 degrees with the power plane of the starting temperature as background image. The operating points move over a considerable range as the temperature is increased to sustain a constant position within the cell.

The above experiments prove that feedback mechanisms for frequency and mode stabilisation are able to endure a considerable amount of degradation in the tuning sections of the laser diode. The lifetime of the device is greatly expanded because the stabilisation algorithm compensates for the early degradation and postponing recalibrations.

The locking based on detector currents is much more accurate than the voltage locking or the output power locking where non-linear cavity effects and tuning-induced losses deteriorate the stabilisation. Additionally, the detector currents have a much smaller range than the active voltage values, which makes it easier to obtain a higher sensitivity. So the proposed scheme has advantages over previously published mode stabilisation concepts.

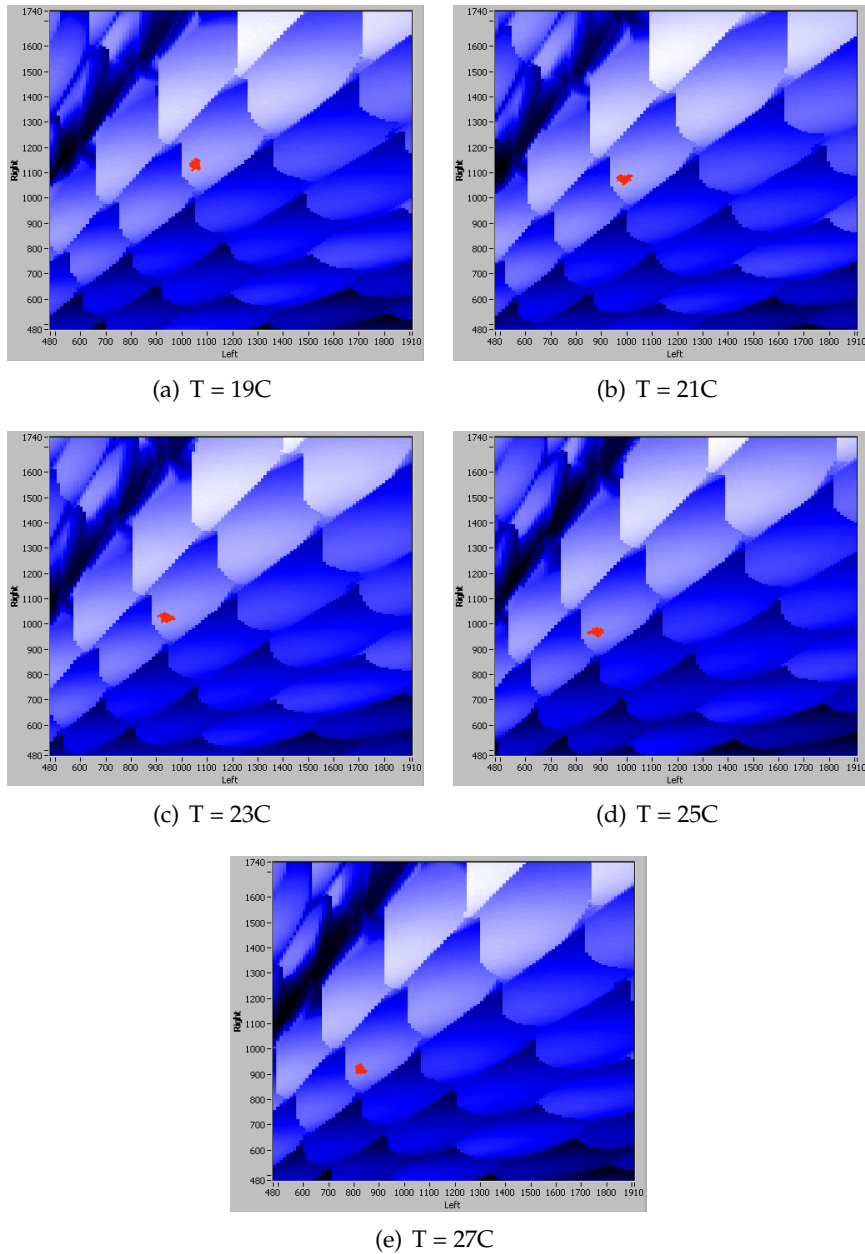


**Figure 6.11:** Stabilisation of the operating point around the highest output power within the cell while the temperature is swept between 19 and 27 degrees. (Measurements by Intune Technologies)

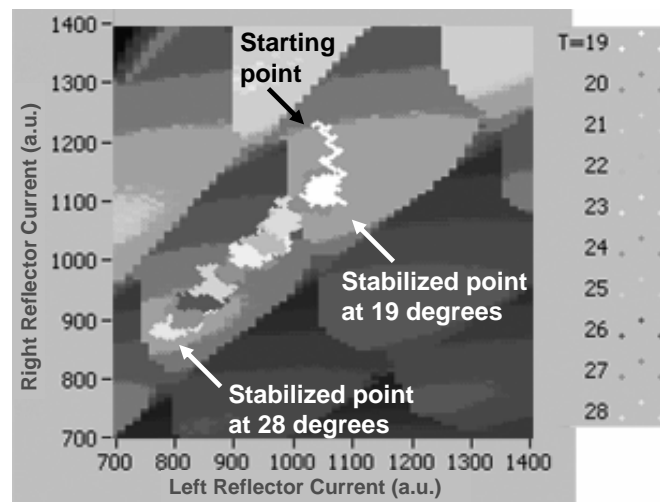


**Figure 6.12:** Variation of the operating point during mode and frequency locking, while the temperature is swept between 19 and 28 degrees. Each temperature is indicated by different shades of gray. The power plane was taken at the initial temperature of 19 degrees with the reflector currents in arbitrary units. There's no mode hop though, since the cell shifts in the same direction of the operating point so that a constant position within the cell can be sustained (Measurements by Intune Technologies)

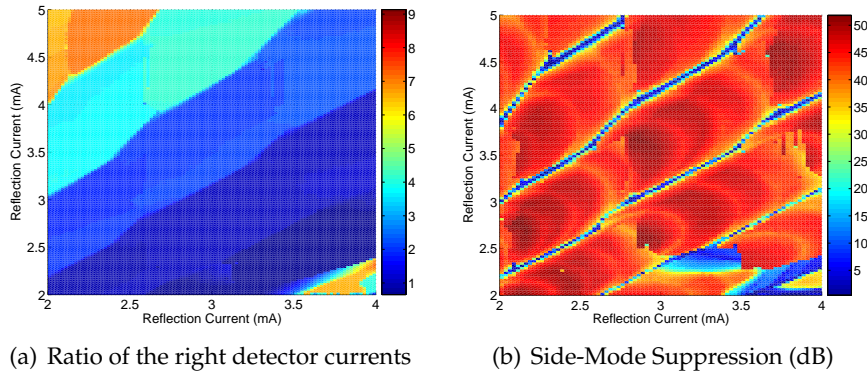


**Figure 6.13:** The ratio of the two right detector compared with the side-mode suppression.

### 6.3.3 Ratio of right detector currents

Figure 6.7 shows that the right detector is split in two. In the previous section they were used as one detector. However by measuring them separately some useful information for the characterisation and stabilisation of the MG-Y lasers can be obtained.

The ratio of the two right detector currents remains almost constant within one supermode (Fig. 6.13(a)), but changes drastically between supermodes due to the frequency dependence of the absorption of the detectors. Comparing the ratio with the side-mode suppression (Fig. 6.13(b)), it is obvious that the ratio values change around the supermode boundaries.

The ratio of the right detector currents can be used to define the supermode boundaries quickly, after which the characteristics of the device only need to be measured along the supermodes speeding up the characterisation process.

The ratio can also be used as extra check during stabilisation to guarantee that the laser is still lasing at the same (super)mode.

## 6.4 The widely tunable twin-guide lasers

This section will briefly discuss the issues involved with characterizing and controlling a widely tunable twin-guide laser (chapter 4).

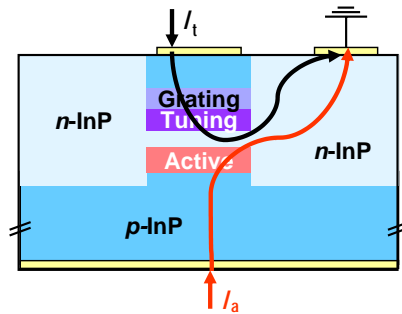


Figure 6.14: Currents Flow in TTAG layer structure

### 6.4.1 Characterisation

The characterisation of the widely tunable twin-guide lasers is easier due to its operation as a  $\lambda/4$ -shifted DFB laser, which automatically ensures that the lasing cavity mode coincides with the overlapping filter peaks. So a phase section is redundant and only two tuning currents are needed to tune over a large wavelength range.

The development of a look-up table for the (S)SG-TTG laser can be based on the detection of a number of supermode boundaries and the determination of a number of one-dimensional wavelength vs. current characteristics. An efficient characterisation is possible if the detection of the supermode boundaries can be done fast e.g. using power measurements in combination with the use of coarse filters.

### 6.4.2 Control

Three different control possibilities were investigated during this PhD but none of them delivered a useful stabilisation algorithm.

#### Active Voltage

The optical feedback in the SG-TTG laser consists of the product of the reflections from both sampled gratings and thus has a sharply peaked wavelength dependence. Therefore one could expect that points of maximum side-mode rejection would correspond with points of minimum threshold gain and thus minimum voltage.

The tuning currents and the active current both run through the same n-InP channel (Fig. 6.14) contributing to the voltage drop along the InP-channel. So the voltage measured between the active p-contact

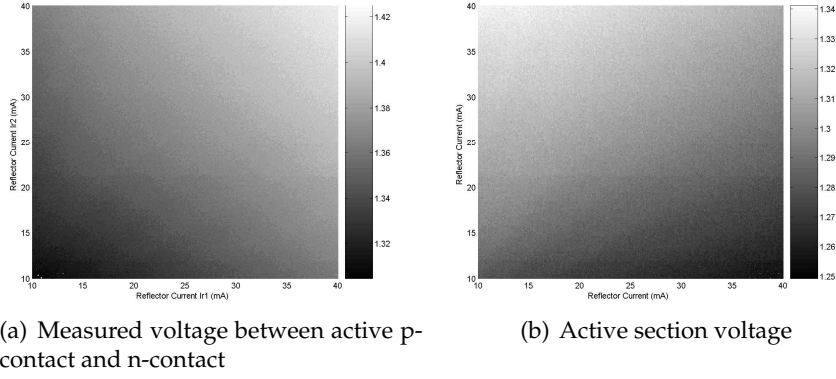


**Figure 6.15:** Variation of the active voltage of an SG-TTG laser while sweeping the reflector currents.

at the bottom and the n-contact at the top of the device (Fig. 6.15(a)) includes a voltage drop along the InP-channel caused by the tuning currents:

$$\begin{aligned} V_{measured} &= R_a I_a + R_{InP-channel}(I_a + I_{t1} + I_{t2}) \\ V_{measured} &= V_{active} + R_{InP-channel}(I_{t1} + I_{t2}) \end{aligned} \quad (6.1)$$

In order to obtain the wanted active section voltage  $V_{active}$ , one needs to find a value for the resistance of the InP-channel  $R_{InP-channel}$  and correct the measured voltage values. The term in formula 6.1 due to the tuning currents is clearly the dominant term as can be seen in Figure 6.15(a). So one can extract a value for  $R_{InP-channel}$  out of these voltage measurements. The obtained values for the active section voltage are shown in Figure 6.15(b).

However, this method is only usable if the influence of tuning-induced losses remains small over the whole tuning range. High losses will create a quickly increasing threshold gain making the minimum gradient in active voltage undetectable as can be seen in Figure 6.15(b).

### Output Power

Another control idea is based on the following formula for the output power [91]:

$$P = \frac{2\alpha_{end}}{2\alpha_{end} + \alpha_{int}} \frac{I - I_{th}}{qV} \quad (6.2)$$

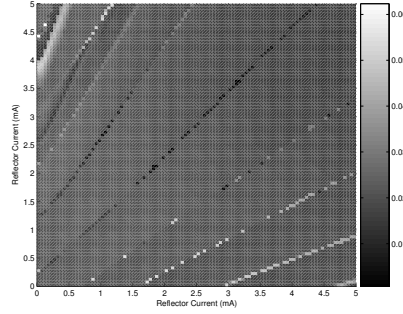


**Figure 6.16:** Variation of the output power gradient of an SG-TTG laser while sweeping the reflector currents.

with  $\alpha_{end}$  the mirror loss,  $\alpha_{int}$  the internal loss,  $I_{th}$  the threshold current and  $V$  the active region volume occupied by photons. From this formula one can derive the following equation

$$\frac{\Delta P}{\Delta I/qV} = \frac{2\alpha_{end}}{2\alpha_{end} + \alpha_{int}} \quad (6.3)$$

The mirror losses  $\alpha_{end}$  are minimal when reflection peaks of the two gratings perfectly overlap. So the side-mode suppression will be maximal where a minimum in the  $\Delta P/\Delta I$  characteristic is distinguished.

The values for  $\Delta P/\Delta I$  in Figure 6.16 were obtained through a static measurement at two active currents (100mA and 110mA). A dynamic measurement around 1MHz would be even better due to their lower temperature dependence. The obtained values do not clearly show a minimum, so they can't be used for stabilisation purposes. However the supermode boundaries can clearly distinguished, so these measurements might be useful in speeding up the characterisation process.

### Integrated Detectors

In the last batch of SG-TTG laser fabricated by the Technical University of Munich, integrated detectors were added in front and at the back of an SG-TTG laser for control purposes.

Apparently there is some cross-talk between the monitor diodes and the laser. Fig. 6.17 shows that the probing of the integrated detectors has a negative effect on the lasing characteristics. The resistance between the n-contact of the laser and the first detector is only 60 Ohm.

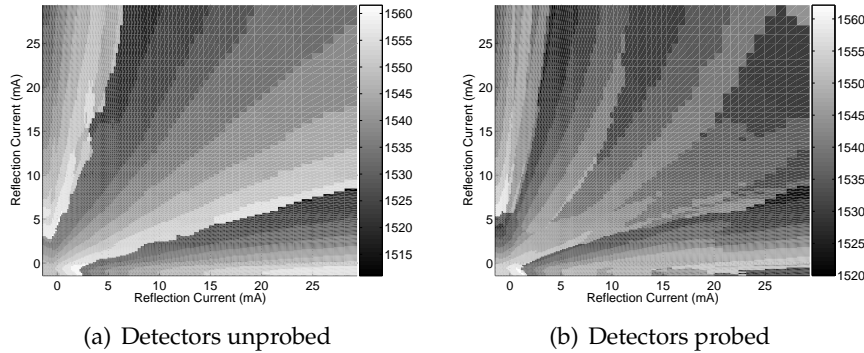


**Figure 6.17:** Effect of the probing of the integrated detectors on tuning behaviour of a SG-TTG laser.

That's not enough, so future tests with integrated detectors should include some process modifications to prevent this.

The measured detector values weren't usable. The detector currents do not change much because the absorption characteristic of the detectors is fairly flat.

## 6.5 Conclusions

In this chapter an algorithm for the characterisation of MG-Y lasers has been presented that can find good operating points at standardised frequencies over a large frequency range of more than 5THz. All these points exhibit only a very small deviation from the target output frequency ( $\pm 2\text{GHz}$ ) and target output power ( $\pm 0.2\text{dB}$ ) and a side-mode suppression of over 35dB.

A stabilisation algorithm for MG-Y lasers was demonstrated. A wavelength locker is used to stabilize the optical frequency by correcting the phase current. The output currents of the photo detectors that were integrated after each reflector were used to stabilize the mode. The reflector currents are adjusted to minimize the output of the photo detectors.

This stabilisation scheme guarantees that the operating point of an MG-Y remains in the center of the cell preventing a mode hop. So the laser continues operating at the wanted frequency even when the tuning sections degrade or when environmental conditions change. Thanks

to the algorithm re-calibrations can be postponed decreasing operating cost.

The control of the widely tunable twin-guide lasers is much more complex than originally anticipated. Several stabilisation methods were investigated but none were successful. Further research in the control possibilities of SG-TTGs needs to be done in the future. Certainly the integration of detectors should be further investigated.

# Chapter 7

## Modulation

In the previous chapters the static properties of the new widely tunable lasers were examined. This chapter investigates the dynamic properties of these lasers. These are very important in telecom applications where the laser signals are modulated to broadcast data over optical fiber. Today a data bit rate of 2.5 or 10 Gbit/s per ITU channel is typical, but a move to 40Gbit/s is expected in the near future.

High speed modulation can be achieved by either directly modulating the active current or by using an external modulator. Better modulation properties are obtained through an external modulator but the device design and fabrication becomes more complex and more expensive. The output power is also decreased due to coupling losses between the modulator and the laser diode.

The noise characteristics and the direct modulation properties of the widely tunable twin-guide laser will be extensively examined in this chapter. The properties of the Modulated Grating Y-Branch laser will also be discussed shortly and afterwards the dynamic behaviour of both designs will be compared with other widely tunable laser concepts.

### 7.1 Noise characteristics of an SG-TTG laser

From the measurements of the relative intensity noise, the K-factor and the theoretical maximum modulation bandwidth under small signal modulation can be derived.

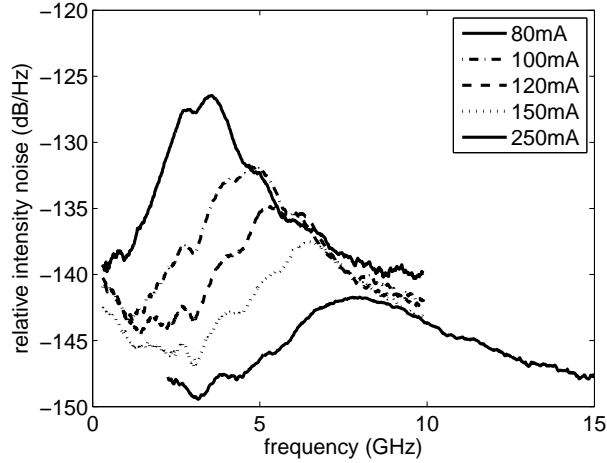


**Figure 7.1:** RIN measurements of an SG-TTG laser for different active current values. The tuning currents were set to an output frequency of 193.2THz.

### 7.1.1 Relative intensity noise

The relative intensity noise (RIN) describes the amplitude fluctuations in the optical field due to spontaneous emission. The spontaneous emission is random and omnidirectional so some photons are emitted in the direction of the laser cavity leading to amplitude fluctuations. This noise is defined as the ratio of the spectral density of the photon density fluctuations and the square of the average photon density [27]:

$$RIN(f) = A \frac{f^2 + \left(\frac{\gamma}{2\pi}\right)^2}{(f_r^2 - f^2)^2 + \left(\frac{\gamma}{2\pi}\right)^2 f^2} \quad (7.1)$$

with  $f_r$  the resonance frequency and  $\gamma$  the damping. The RIN is expressed in dB/Hz.

A high speed photo detector with a bandwidth higher than 10GHz is used to measure the laser emission. The noise spectrum is extracted using a highly sensitive electrical spectrum analyzer. The measured RIN results of an SG-TTG laser with a total length of 1200 $\mu$ m for different values of the active current are shown in Figure 7.1. The tuning currents were set to an output frequency of 193.2THz.

At low bias currents the RIN is dominated by the laser source noise, while at higher powers the photodiode shot noise becomes the important factor. The resonance frequency increases at higher active currents

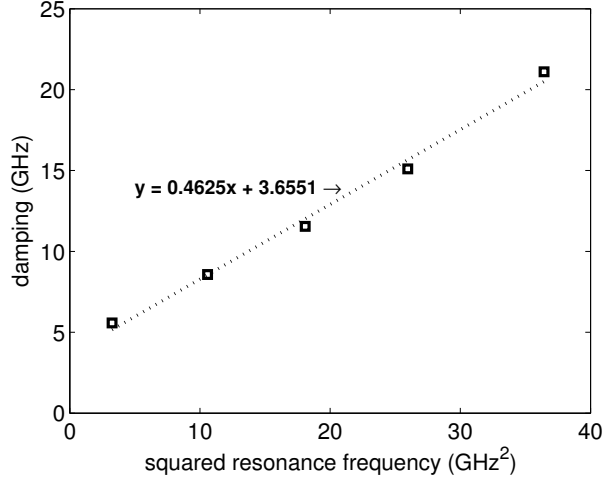


**Figure 7.2:** Linear relationship between damping factor and squared resonance frequency

while the maximum RIN decreases at higher output powers (for high enough output powers).

### 7.1.2 Extracting the modulation bandwidth

Out of the measurements of the RIN for different active current values a theoretical value for the intrinsic modulation bandwidth can be extracted. The method is described below.

A value for the resonance frequency  $f_r$  and damping factor  $\gamma$  can be extracted from fitting the RIN formula 7.1 on each RIN measurement.

Far above threshold there's a linear relationship (Fig. 7.2) between the damping and the squared resonance frequency [91, 92]:

$$\gamma = \gamma_0 + K f_r^2 \quad (7.2)$$

The K-factor describing the damping of the laser response at high frequencies can be extracted from these fitted parameters. The K-factor is determined by the photon lifetime of the laser cavity and is inversely proportional to the maximum intrinsic modulation bandwidth [91, 92]:

$$f_{max,damping} = \frac{2\pi\sqrt{2}}{K} \quad (7.3)$$

The extracted theoretical values for the maximum intrinsic modulation bandwidth over the tuning range of an SG-TTG laser are given for

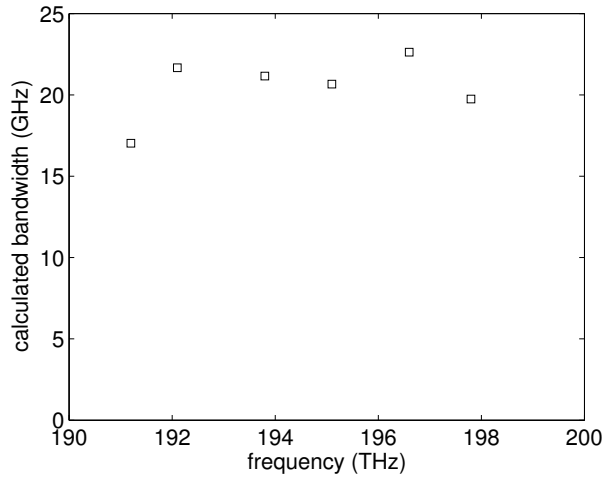


**Figure 7.3:** Extracted theoretical values for maximum intrinsic modulation bandwidth over tuning range of SG-TTG laser

several ITU frequencies in Figure 7.3. The limit varies over the tuning range due to the wavelength dependence of the material and optical cavity parameters.

This extracted bandwidth maximum (Fig. 7.3) is for an ideal laser diode. In practice the performance of the device will be worse than predicted due to the presence of parasitics like stray capacitances parallel to the active region, the resistance of the semiconductor layers (around  $5\Omega$  according to Fig. 7.4), the inductance of bond wires, contact capacitance, ...

Thermal effects can deteriorate the obtained maximum bandwidth value even more. Heat generated by injecting current into the device can cause a saturation of the resonance frequency to a value  $f_{r,max}$ . The maximum bandwidth is then given by [91, 92]

$$f_{max,thermal} = \sqrt{1 + \sqrt{2}} f_{r,max} \quad (7.4)$$

Better cooling can improve the thermal effects, while a high speed design of the laser minimizes the parasitic effects.

### 7.1.3 Indication of actual bandwidth

Not only the theoretical maximum can be extracted out of the RIN measurements, but also an indication of the actual bandwidth of the modu-

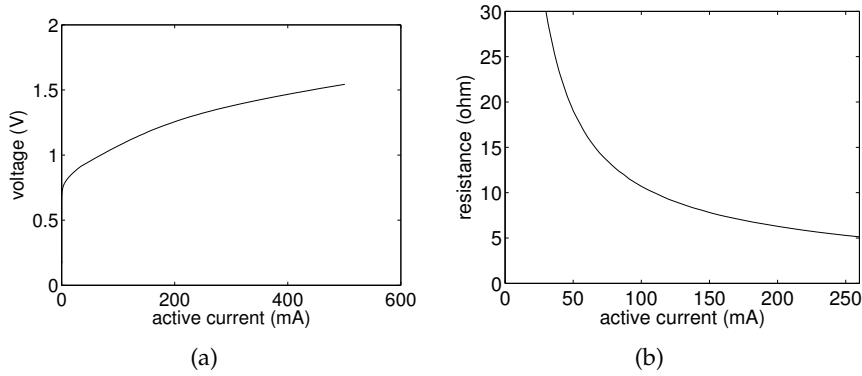


**Figure 7.4:** Voltage vs. active current measurement and the extracted value for the series resistance

lation response can be obtained. The modulation response can be written as:

$$|M(f)|^2 = \frac{1}{1 + \left(\frac{f}{f_p}\right)^2} \frac{f_r^4}{(f_r^2 - f^2)^2 + \left(\frac{\gamma}{2\pi}\right)^2 f^2} \quad (7.5)$$

The first factor is due to the parasitic effects. The parasitic cut-off frequency  $f_p$  characterizes the extrinsic limitations due to carrier transport and parasitic elements of the laser structure. The other parameters of this modulation response formula are the same as in formula (7.1). So an indication of the actual 3dB bandwidth without parasitic effects can be obtained by inserting the extracted parameters from the RIN fitting (at an active current of 250mA) in this modulation response and neglecting the first factor. This leads to the 3dB bandwidth values shown in Figure 7.5. For all measured ITU frequencies a bandwidth higher than 8GHz and up to 12GHz is obtained.

The extracted bandwidth is quite uniform over the whole tuning range. This is due to two counteracting effects. The tuning increases the threshold current considerably and this has a decreasing effect on the resonance frequency. On the other hand, the spectral variation of  $dg/dN$  (Fig. 4.19) compensates this because tuning is towards the high-frequency side where  $dg/dN$  is larger [93].

These two counteracting effects result in a more or less uniform bandwidth throughout most of the tuning range and simultaneously explain for the decrease of the bandwidth at the edges of the tuning range where the  $I - I_{th}$  decrease is the largest and the  $dg/dN$  variations

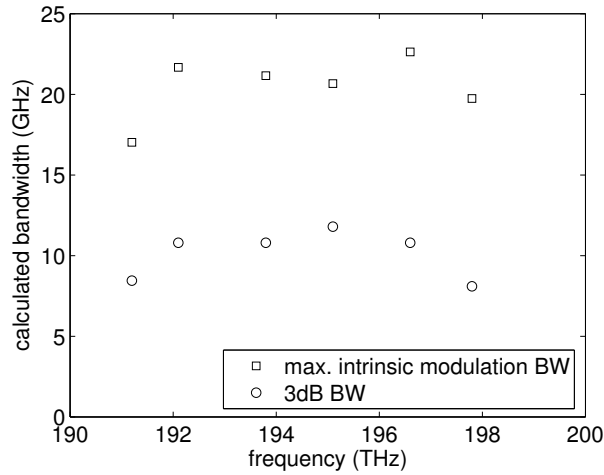


**Figure 7.5:** Theoretical indication of actual bandwidth of an SG-TTG laser through modulation response formula.

are not strong enough anymore to compensate this. By adjusting the detuning of the gain peak and moving the grating center wavelength to lower frequencies, the average  $dg/dN$  value can be increased without decreasing  $I - I_{th}$  and, therefore, the bandwidth can on average be increased.

## 7.2 Small-Signal Modulation of an SG-TTG laser

The SG-TTG laser sample has been probed with Picoprobe 40A, a high frequency needle for small-signal modulation up to 40GHz. A bias-T combines the DC and AC signal and isolates the sources from each other. The small sinusoidal AC signal is generated by a signal generator (Rhode & Schwarz) that is capable of reaching frequencies up to 3GHz. Using Labview the modulation frequency is swept over the full frequency range and the output signal is detected by a high speed photo diode and processed by an HP71400 light wave signal analyzer to extract the amplitude of the optical power modulation (Fig. 7.6(a)). A digital spectrum analyzer that digitally analyzes the output power can also be used to measure the amplitude (Fig. 7.6(b)). The difference in output power between both methods can be explained by a difference in coupling losses.

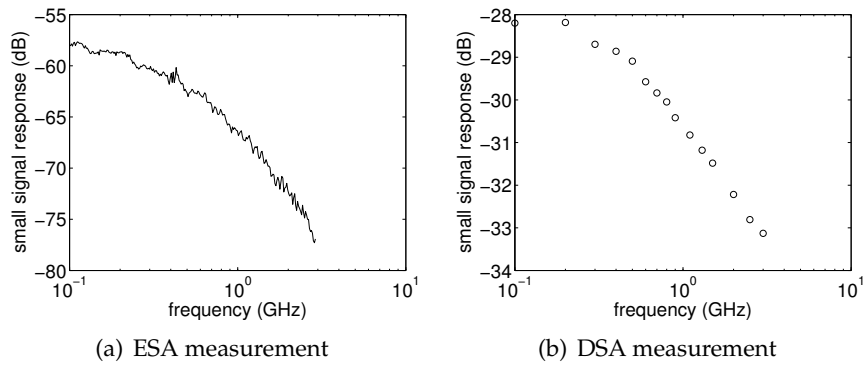


**Figure 7.6:** Small signal modulation response measured by an electrical spectrum analyzer and a digital spectrum analyzer

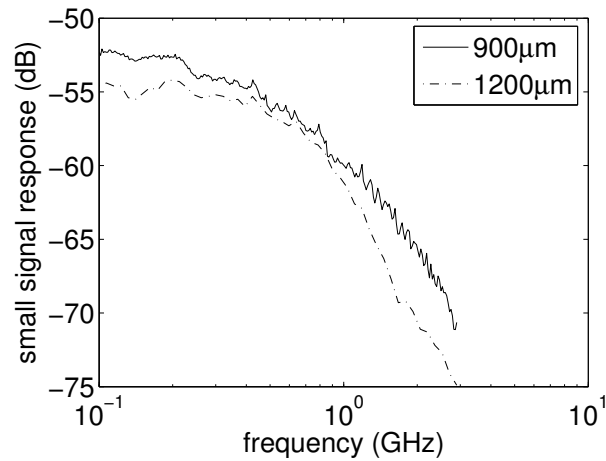


**Figure 7.7:** Small-signal intensity modulation of a 900 μm and 1200 μm long SG-TTG laser

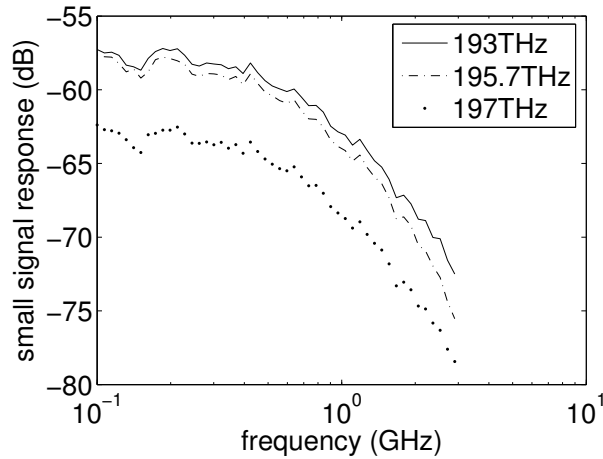


**Figure 7.8:** Small-signal intensity modulation of 1200µm long TTG laser at different ITU frequencies

The small-signal behaviour of two SG-TTG lasers with a different laser length is shown in Figure 7.7. A 3dB cut-off frequency is reached around 1GHz. The bandwidth for the 900µm long device is better than for the longer 1200µm device indicating that the parasitic effects play an important role.

By injecting tuning current, the carrier density in active layer increases and the carrier lifetime in the active layer shortens so an increase of the 3dB cut-off frequency is expected. This tuning-effect was observed with the original DFB-TTG lasers [94] where the FM modulation bandwidth increased from 150MHz at  $I_t = 2mA$  to 470MHz at  $I_t = 50mA$ . The effect of a frequency tuning on the small-signal modulation is shown in Figure 7.8. The 3dB cut-off frequency does not change during tuning due to parasitic effects.

The dynamic properties does not change either when the active current is increased (Fig. 7.9). It is another indication that the parasitic effects dominate the dynamic behaviour.

The low modulation bandwidth isn't a surprise because the laser wasn't designed for high frequency operation. Better bandwidth values should be reachable when the contact pads are smaller and when the laser is packaged for high speed operation.

The parasitic series resistance is around  $5\Omega$ , so the parasitic capacitance is around 32pF for a 1GHz 3dB cut-off frequency. The huge contact pad ( $1200 \times 110\mu m^2$ ) contributes to 8pF of this 32pF capacitance and

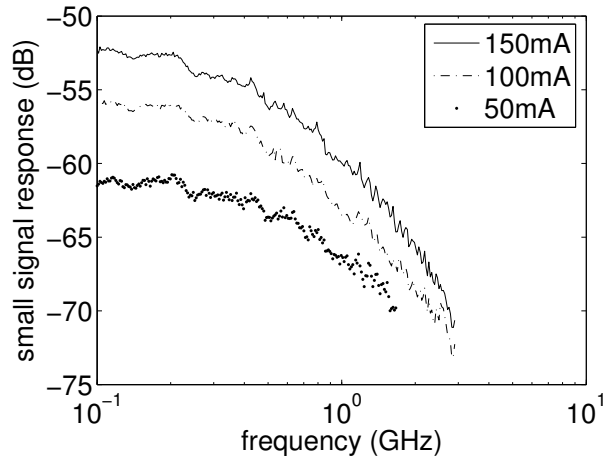


**Figure 7.9:** Small-signal intensity modulation of 900 $\mu\text{m}$  long TTG laser at different active currents

can be almost completely eliminated simply by reducing its size and using a more suitable passivation like BCB. The remaining 24pF capacity is most likely caused by the large p-n-junction width of 25 $\mu\text{m}$ . To get close to the magical 10GHz a capacity of 3.2pF is needed (assuming again a 5 $\Omega$  series resistance). This can be obtained with a p-n-homojunction width of about 5 $\mu\text{m}$ . This is feasible with some design optimisations.

Additionally, modified concepts have been presented [32, 70] to increase the output power or the pumping efficiency of the TTG lasers considerably and thereby also the modulation bandwidth.

### 7.3 The Modulated Grating Y-branch laser

The direct modulation properties of the modulated grating Y-branch laser were intensively investigated by a group from KTH Stockholm. The results are described in two papers [5, 6] and are summarised in the table below.

Wavelength (nm)	Damping (GHz)	Thermal (GHz)	Parasitic (GHz)	Measured @80mA (GHz)
1535	20.3	13.6	20.7	8.44
1555	14.9	13.7	19.0	8.57
1574	14.7	11.5	15.0	7.66

Theoretical maximum intrinsic modulation bandwidth values up to 20GHz were extracted from the RIN measurements. Direct modulation experiments were also carried out using an impedance matched coplanar probe and a precision current source. An 8GHz modulation bandwidth was measured at an active current of 80mA. The active current couldn't be further increased due to the heating in the probe resistor. With an improved driving circuit that can handle a higher active current and a high frequency mounting an actual bandwidth of 15GHz seems feasible.

## 7.4 Comparison with other widely tunable lasers

In this section the modulation properties of the widely tunable twin-guide laser and the modulated grating Y-branch laser will be compared to other widely tunable laser concepts.

For the grating assisted coupler sampled reflector laser (§2.4.4) a maximum intrinsic modulation bandwidth of 12GHz [95] was reported. A 7GHz bandwidth was reached during modulation experiments due to low parasitic contacts. Better cooling could decrease the thermal effects and increase the actual bandwidth.

For the sampled grating DBR laser (§2.4.2) a maximum intrinsic modulation bandwidth of 14.8GHz was reported [96]. The bandwidth measured is only 4.8GHz due to RC parasitics. 10GHz seems feasible if the parasitics can be decreased.

The widely tunable twin-guide laser has promising prospects. It has a maximum theoretical bandwidth above 20GHz and the 3dB bandwidth at 250mA indicates that an actual bandwidth of 12GHz should be possible. This is the highest maximum theoretical bandwidth reported so far. The current lasers are at the moment not designed for high-speed modulation, so only 1GHz modulation can be reached at the moment.

The modulated grating Y-branch laser has better track records. An 8GHz bandwidth was measured at 80mA active current. One of the highest reported so far, while the intrinsic modulation bandwidth indicates that that number can be doubled through a better high frequency design.

Nevertheless the two new laser concepts look like worthy competitors in the widely tunable laser market when it comes down to dynamic behaviour.

## Chapter 8

# Conclusions and Perspectives

### 8.1 Conclusions

The primary goal of this doctoral research was to develop and experimentally investigate new types of widely tunable laser diodes that have the same qualities as (non-tunable) DFB lasers, i.e. high output power and high side-mode suppression, and are widely tunable, easily controllable and easily manufacturable.

The performance of the widely tunable twin-guide lasers is comparable with other monolithic widely tunable lasers. A tuning range of 6THz (over 40nm) while maintaining a high output power and a side-mode suppression of more than 40dB was observed for most ITU channels.

Diffraction gratings that can be used in widely tunable laser concepts were successfully designed, fabricated and characterised during this PhD research. Sampled Gratings were preferred in widely-tunable twin-guide lasers because they are easy to fabricate and they are very robust against frequently occurring fabrication tolerances.

The modulated grating Y-branch (MG-Y) concept has full C-band frequency coverage while maintaining a high side-mode suppression and a low output power variation. The output power was the highest measured and reported for a monolithic tunable laser (without integrated amplifier).

Algorithms for the control and the stabilisation of the MG-Y lasers were developed and successfully tested speeding up the calibration process guaranteeing that the laser continues operating at the wanted

frequency even when the tuning sections degrade or when environmental conditions change.

The dynamic behavior of both designs showed promising prospects. The widely tunable twin-guide laser has the highest maximum theoretical bandwidth reported so far. The current design wasn't adapted for high-speed modulation, so only a 1GHz modulation could be reached. 8GHz modulation was demonstrated for the modulated grating Y laser, while the intrinsic modulation bandwidth indicates that this number can be doubled through a better high frequency design.

Both laser concepts satisfy all the telecom specifications (see section §1.2) and show promising dynamic behavior so they are worthy competitors with other transmitters for optical telecom networks.

## 8.2 Perspectives and Future Directions

Widely tunable semiconductor laser diodes with tuning ranges of several tens of nanometers will become key components in optical telecommunication networks, because they can help telecom operators respond to the increasing bandwidth demand at a low price, while introducing new functionality and higher flexibility in the network.

Miniaturisation and integration will be driving forces for future research because they reduce the packaging cost and add extra functionality to widely tunable lasers. A semiconductor optical amplifier (SOA) can be integrated with both laser concepts to improve the output power and to decouple the power and wavelength control. Integrating a modulator to improve the dynamic behavior is also a logic next step for both laser concepts. Additionally tapers can be added at the front of the device to obtain a higher coupling efficiency to optical fiber.

Both designs can be further optimised for high speed operation as well. Smaller contacts and packaging of the devices can have positive effects on the maximum modulation bandwidth. The move of the Bragg peak to higher frequencies in order to improve the dynamic behavior will also be an interesting research area for SG-TTG lasers, because it might deteriorate the static properties.

Additionally, it would be interesting to see how other superperiod gratings behave in widely tunable twin-guide lasers. Therefore a better e-beam facility with a higher writing resolution is needed. The influence of the gain could then be further investigated and we should be able to check the gain compensated superstructure gratings designs that were developed during this PhD.

An asymmetric SG-TTG design could be investigated as well with a short front mirror that has a low duty cycle and a longer rear mirror that has a higher duty cycle. This design will create a higher output power, but probably deteriorates the side-mode suppression in the case of  $\lambda/4$ -shifted DFB lasers.

The control of the widely tunable twin-guide lasers is complex, so further research in the control possibilities of SG-TTGs needs to be done in the future. Integrating detectors seems the most logical next step in trying to control these devices.



# Appendix A

## Acronyms

ARC	Anti-reflection coating
BH	Buried heterostructure
CBE	Chemical beam epitaxy
DBR	Distributed Bragg reflector
DFB	Distributed feedback
DS	Digital supermode
FP	Fabry-Pérot
GCSR	Grating-assisted coupler with rear sampled reflector
ICP	Inductively coupled plasma etching
ITU	International telecommunication union
MG-Y	Modulated grating Y-branch
MMI	Multimode interferometer
MOVPE	Metallic-organic vapor phase epitaxy
MQW	Multi-quantum well
RIE	Reactive ion etching
RIN	Relative intensity noise
RW	Ridge waveguide
SG	Sampled grating
SMSR	Side-mode suppression
SOA	Semiconductor optical amplifier
SSG	Superstructure grating
TTG	Tunable twin-guide
VCSEL	Vertical cavity surface emitting laser
WDM	Wavelength division multiplexing



# List of figures

1.1	Principle of wavelength division multiplexing . . . . .	1
1.2	Example of a telecom network . . . . .	2
1.3	Optical sensor incorporated in pressure vessel . . . . .	5
1.4	Optical sensor incorporated in a plate . . . . .	6
1.5	Definition of side-mode-suppression . . . . .	7
1.6	Definition of linewidth . . . . .	7
2.1	Lasing condition . . . . .	14
2.2	Distributed Feedback Laser . . . . .	16
2.3	Mechanically tuned External Cavity Laser . . . . .	18
2.4	Distributed Bragg Reflector Laser . . . . .	19
2.5	Tunable Twin Guide Laser . . . . .	20
2.6	Tuning characteristic of a DFB-TTG . . . . .	20
2.7	Vertical Cavity Surface Emitting Lasers . . . . .	21
2.8	SG-DBR laser integrated with amplifier and modulator . . . . .	22
2.9	Widely tunable DFB laser array . . . . .	23
2.10	Widely tunable DFB laser array . . . . .	23
2.11	External Cavity Wavelength Tunable Lasers . . . . .	24
2.12	Double-Ring Resonator Coupled Laser . . . . .	24
2.13	SG-DBR laser . . . . .	25
2.14	Digital-Supermode Distributed Bragg Reflector . . . . .	26
2.15	Grating-assisted coupler with rear sampled reflector . . . . .	26
2.16	Sampled Grating Tunable Twin Guide Laser . . . . .	27
2.17	Modulated Grating Y-Branch lasers . . . . .	28
3.1	Uniform Grating . . . . .	32
3.2	Reflection Spectrum of a uniform grating . . . . .	33
3.3	Reflection matrix . . . . .	35
3.4	Sampled Grating . . . . .	37
3.5	Reflection Spectrum of Sampled Gratings . . . . .	38

3.6	Superstructure Grating . . . . .	39
3.7	Effect of SSG superperiod . . . . .	40
3.8	Effect of discreet SSG steps . . . . .	40
3.9	Effect of adding a phase shift . . . . .	41
3.10	SG Fabrication Process . . . . .	43
3.11	Overgrown grating . . . . .	44
3.12	Phase shift etched between two grating sections . . . . .	45
3.13	Top view of phase shift etched between two grating sections . . . . .	45
3.14	Effect of adding a phase shift . . . . .	46
3.15	Phase shift between two grating sections through width changes . . . . .	46
3.16	Measuring gratings . . . . .	47
3.17	Setup for measuring gratings . . . . .	47
3.18	Setup for measuring gratings . . . . .	47
3.19	Measurements of Sampled Gratings . . . . .	49
3.20	Transmission measurements of e-beam fabricated gratings . . . . .	49
3.21	Influence of gain on sampled grating . . . . .	51
3.22	Influence of gain on reflection spectrum . . . . .	52
3.23	Schematic of reflecting facets . . . . .	53
3.24	Influence of facet reflections . . . . .	54
4.1	Sampled Grating Tunable Twin Guide Laser . . . . .	58
4.2	Reflection Spectrum of Sampled Gratings with slightly different sampling period . . . . .	59
4.3	Definition of Vernier effect . . . . .	59
4.4	Two different layer structures . . . . .	60
4.5	Series resistance in BH layer structures . . . . .	62
4.6	Definition of repeat-mode spacing . . . . .	63
4.7	Threshold Simulations of a long SG-TTG laser . . . . .	67
4.8	Threshold Simulations of a short SG-TTG laser . . . . .	67
4.9	Threshold Simulations of a short SSG-TTG laser . . . . .	69
4.10	Threshold Simulations of a long SSG-TTG laser . . . . .	69
4.11	Fabrication of (S)SG-TTGs . . . . .	70
4.12	SEM picture of SG-TTGs . . . . .	71
4.13	L-I characteristic of a SG-TTG . . . . .	71
4.14	Frequency sweep of a fabricated SG-TTG laser . . . . .	73
4.15	Threshold Simulations of a fabricated SG-TTG laser . . . . .	73
4.16	Diagonal Sweep of SG-TTG . . . . .	74
4.17	Spectrum of SG-TTG . . . . .	74

---

4.18	Best points measured . . . . .	75
4.19	Modal gain . . . . .	76
4.20	Thermally tunable sampled grating DFB laser . . . . .	77
4.21	Frequency sweep of a fabricated thermal DFB laser . . . . .	77
4.22	BCB Bonded Thermally Tunable DFB laser . . . . .	78
5.1	Schematic drawing of an MG-Y laser . . . . .	82
5.2	Additive Vernier effect vs. multiplicative Vernier effect . . . . .	83
5.3	Schematic drawing of an MG-Y laser . . . . .	84
5.4	Power plane measurement . . . . .	85
5.5	SEM picture of a fabricated MG-Y . . . . .	86
5.6	Frequency and side-mode suppression of a fabricated MG-Y laser . . . . .	87
5.7	Best points measured . . . . .	88
5.8	Spectrum of MG-Y . . . . .	89
6.1	Control board MG-Y laser . . . . .	92
6.2	Wavelength Locker . . . . .	93
6.3	Injection Locking . . . . .	95
6.4	Power plane measurement . . . . .	96
6.5	Extracting a set of operating points . . . . .	97
6.6	Final set of operating points . . . . .	98
6.7	Schematic drawing of an MG-Y laser diode . . . . .	99
6.8	Link between detector current and output power . . . . .	100
6.9	Link between detector current and output power . . . . .	100
6.10	Mode stabilisation experiment . . . . .	101
6.11	Mode and frequency stabilisation experiment . . . . .	103
6.12	Mode and frequency stabilisation experiment . . . . .	104
6.13	Ratio of the right detector currents compared with the side-mode suppression . . . . .	105
6.14	Currents Flow in TTG layer structure . . . . .	106
6.15	Active Voltage Measurement . . . . .	107
6.16	Effect on output power gradient . . . . .	108
6.17	Effect of integrated detectors . . . . .	109
7.1	RIN measurements of an SG-TTG laser . . . . .	112
7.2	Damping vs. Squared resonance frequency . . . . .	113
7.3	Maximum intrinsic modulation bandwidth . . . . .	114
7.4	VI measurements and Series Resistance . . . . .	115
7.5	Indication of actual bandwidth . . . . .	116
7.6	Small signal modulation . . . . .	117

7.7	Small-signal intensity modulation at different ITU frequencies . . . . .	117
7.8	Small-signal intensity modulation at different ITU frequencies . . . . .	118
7.9	Small-signal intensity modulation at different ITU frequencies . . . . .	119

# Bibliography

- [1] G. Morthier, B. Moeyersoon, and R. Baets, "A  $\lambda/4$ -shifted sampled or superstructure grating widely tunable twin-guide laser," *IEEE Photon. Technol. Lett.*, vol. 13, no. 10, pp. 1052–1054, 2001.
- [2] R. Todt, T. Jacke, R. Meyer, J. Adler, R. Laroy, G. Morthier, and M.-C. Amann, "Sampled grating tunable twin-guide laser diodes with over 40-nm electronic tuning range," *IEEE Photon. Technol. Lett.*, vol. 17, pp. 2514–2516, December 2005.
- [3] J.-O. Wesström, S. Hammerfeldt, J. Buus, R. Siljan, R. Laroy, and H. de Vries, "Design of a widely tunable modulated grating Y-branch laser using the additive vernier effect for improved supermode selection," in *Proc. ISLC 2002*, pp. 99–100, 2002.
- [4] J.-O. Wesström, G. Sarlet, S. Hammerfeldt, L. Lundqvist, P. Szabo, and P.-J. Rigole, "State-of-the-art performance of widely tunable modulated grating Y-branch lasers," in *Proc. OFC 2004*, Paper TuE2, 2004.
- [5] M. Chacinski, M. Isaksson, and R. Schatz, "High-speed direct modulation of widely tunable MG-Y laser," *IEEE Photon. Technol. Lett.*, vol. 17, pp. 1157–1159, June 2005.
- [6] M. Isaksson, M. Chacinski, O. Kjebon, R. Schatz, and J.-O. Wesström, "10 Gb/s direct modulation of 40 nm tunable modulated-grating Y-branch laser," in *Proc. OFC 2005*, Paper TuE2, 2005.
- [7] T. Wolf, S. Illek, J. Rieger, B. Borchert, and M.-C. Amann, "Tunable twin-guide (TTG) distributed feedback (DFB) laser with over 10 nm continuous tuning range," *Electron. Lett.*, vol. 29, no. 24, pp. 2124–2125, 1993.

- [8] "Report: Internet traffic boom redux, [http://www.lightreading.com/.](http://www.lightreading.com/)"
- [9] C. A. Brackett, "Dense wavelength division multiplexing networks: principles and applications," *IEEE J. Sel. Areas in Communications*, vol. 6, pp. 948–964, August 1990.
- [10] H. Yoshimura, K. Sato, and N. Takachio, "Future photonic transport networks based on wdm technologies," *IEEE Communications Magazine*, vol. 37, pp. 74–81, February 1999.
- [11] "Recommendation g.692: "optical interfaces for multichannel systems with optical amplifiers", series g: Transmission systems and media, digital systems and networks (transmission media characteristics - characteristics of optical components and sub-systems)," tech. rep., International Telecommunication Union - Telecommunication Standardization Sector (ITU-T), 1998.
- [12] E. Desurvire, "Optical communications in 2025," in *Proc. of ECOC 2005*, Paper Mo2.1.3, 2005.
- [13] "Tunable lasers: is it time to tune in?, [http://www.fiber-systems.com/.](http://www.fiber-systems.com/)"
- [14] E. Zouganeli, A. F. Mlonyeni, O.-P. Rostad, T. Olsen, and A. Sudbo, "Wavelength routed network using widely tunable laser transmitters," in *Proc. of ECOC 2000*, vol. 4, pp. 51–52, 2000.
- [15] D. Blumenthal, B.-E. Olsson, G. Rossi, T. Dimmick, L. Rau, M. Masanovic, O. Lavrova, R. Doshi, O. Jerphagnon, J. Bowers, V. Kaman, L. Coldren, and J. Barton, "All-optical label swapping networks and technologies," *IEEE J. Lightwave Technol.*, vol. 18, no. 12, pp. 2058–2075, 2000.
- [16] J. Gripp, P. Bernasconi, C. Chan, K. L. Sherman, and M. Zirngibl, "Demonstration of a 1Tb/s optical packet switch fabric (80\*12.5Gb/s), scalable to 128 Tb/s (6400\*20Gb/s)," in *Proc. of ECOC 2000*, Paper PD2.7, 2000.
- [17] A. Kosterev, D. Weidmann, F. Tittel, O. Walsh, D. McDonald, and J. Dunne, "Multi-species QEPAS based gas sensing using a wavelength-programmable diode laser source," in *Conference on Lasers and Electro-Optics, 2004. (CLEO)*, p. 2, 2004.

- [18] T. Farrell and D. McDonald, "Tunable laser technology for sensing applications," in *Lab-on-a-Chip: Platforms, Devices, and Applications. Proceedings of the SPIE*, vol. 5594, pp. 66–80, Dec. 2004.
- [19] F. Delorme, "Widely tunable 1.55- $\mu\text{m}$  lasers for wavelength-division-multiplexed optical fiber communications," *IEEE J. Quantum Electron.*, vol. 34, pp. 1706–1716, September 1998.
- [20] S. Wang, "Principles of distributed feedback and distributed Bragg-reflector lasers," *IEEE J. Quantum Electron.*, vol. 10, no. 4, pp. 413–427, 1974.
- [21] G. Morthier and P. Vankwikelberge, *Handbook of distributed feedback laser diodes*. Artech House, Norwood, MA, 1997.
- [22] V. Jayaraman, Z.-M. Chuang, and L. A. Coldren, "Theory, design, and performance of extended tuning range semiconductor lasers with sampled gratings," *IEEE J. Quantum Electron.*, vol. 29, no. 6, pp. 1824–1834, 1993.
- [23] Y. Gustafsson, S. Hammerfeldt, J. Hammersberg, M. Hassler, T. Horman, M. Isaksson, J. Karlsson, D. Larsson, O. Larsson, L. Lundqvist, T. Lundstrom, M. Rask, P.-J. Rigole, E. Runeland, A. Saavedra, G. Sarlet, R. Siljan, P. Szabo, L. Tjernlund, O. Traskman, H. de Vries, J.-O. Westrom, and C. Ogren, "Record output power (25 mW) across C-band from widely tunable GCSR lasers without additional SOA," *Electron. Lett.*, vol. 39, pp. 292–293, February 2003.
- [24] S. Kim, Y. Chung, S.-H. Oh, and M.-H. Park, "Design and analysis of widely tunable sampled grating DFB laser diode integrated with sampled grating distributed Bragg reflector," *IEEE Photon. Technol. Lett.*, vol. 16, pp. 15–17, January 2004.
- [25] D. J. Robbins, G. Busico, L. Ponnampalam, J. P. Duck, P. J. Williams, R. A. Griffin, A. J. Ward, D. C. Reid, N. D. Whitbread, E. Barton, B. Reid, and K. Kasunic, "A high power, broadband tunable laser module based on a DS-DBR laser with integrated SOA," in *Proc. OFC 2004*, Paper TuE3, 2004.
- [26] M. C. Amann and J. Buus, *Tunable Laser Diodes*, vol. ISBN 3-540-10193-4. Artech House optoelectronics library, 1998.

- [27] G. Sarlet, *Tunable Laser Diodes for WDM communication - Methods for Control and Characterisation*. Ghent University, Phd. thesis, 2000.
- [28] F. Delorme, "1.5- $\mu\text{m}$  tunable DBR lasers for WDM multiplex spare functions," *IEEE Photon. Technol. Lett.*, vol. 12, pp. 621–623, June 2000.
- [29] T. Koch, U. Koren, and B. Miller, "High performance tunable 1.5- $\mu\text{m}$  InGaAs/InGaAsP multiple quantum well distributed Bragg reflector lasers," *Appl. Phys. Lett.*, vol. 53, pp. 1036–1038, September 1998.
- [30] C. Schanen, S. Illek, H. Lang, W. Thulke, and M.-C. Amann, "Fabrication and lasing characteristics of  $\lambda = 1.56\mu\text{m}$  tunable twin-guide (TTG) DFB lasers," *IEE Proceedings Pt. J*, vol. 137, no. 1, pp. 69–73, 1990.
- [31] T. Wolf, H. Westermeier, and M.-C. Amann, "Continuously tunable metal-clad ridge-waveguide distributed feedback laser diode," *Electron. Lett.*, vol. 26, no. 22, pp. 1845–1855, 1990.
- [32] B. Schmidt, S. Illek, R. Gessner, and M.-C. Amann, "Design and realization of a buried-heterostructure tunable-twin-guide laser diode with electrical blocking regions," *IEEE J. Quantum Electron.*, vol. 35, no. 5, pp. 794–802, 1999.
- [33] M.-C. Amann, S. Illek, C. Shanen, and W. Thulke, "Tuning range and threshold current of the tunable twin-guide (TTG) laser," *Electron. Lett.*, vol. 1, pp. 253–254, February 1989.
- [34] R. Todt, T. Jacke, J. Adler, and M.-C. Amann, "Tunable twin-guide (TTG) distributed feedback (DFB) laser diodes with over 9 nm continuous electro-optic tuning range," *Electron. Lett.*, vol. 41, pp. 1063–1065, September 2005.
- [35] C. Chang-Hasnain, "Tunable VCSEL," *IEEE J. Select. Topics Quantum Electron.*, vol. 6, pp. 978–988, November/December 2000.
- [36] L. Coldren, "Integrated tunable transmitters for WDM networks," in *Proc. of ECOC-IOOC 2003*, Paper Th1.2.1, pp. 878–881, 2003.
- [37] A. Champagne, J. Camel, R. Maciejko, K. J. Kasunic, D. Adams, and B. Tromborg, "Linewidth broadening in a distributed feedback laser integrated with a semiconductor optical amplifier," *IEEE J. Quantum Electron.*, vol. 38, pp. 1493–1502, November 2002.

- [38] G. Morthier and B. Moeyersoon, "Intensity noise and linewidth of laser diodes with integrated semiconductor optical amplifier," *IEEE Photon. Technol. Lett.*, vol. 14, pp. 1644–1646, December 2002.
- [39] B. Moeyersoon, M. Zhao, and G. Morthier, "Degradation of the mode suppression in single-mode laser diodes due to integrated optical amplifiers," in *Proc. of Optical Amplifiers and their Applications*, pp. 97–99, 2003.
- [40] J. Barton, E. Skogen, M. Masanovic, S. Denbaars, and L. Col-dren, "A widely tunable high-speed transmitter using an inte-grated SGDBR laser-semiconductor optical amplifier and mach-zehnder modulator," *IEEE J. Select. Topics Quantum Electron.*, vol. 9, pp. 1113–1117, September/October 2003.
- [41] B. Moeyersoon, *Dynamic aspects of Advanced Multi-Section Tun-able Semiconductor Lasers*. Ghent University, Phd. thesis, 2005. <http://photonics.intec.ugent.be/publications/phd.asp?ID=149>.
- [42] H. Hatakeyama, K. Naniwae, K. Kudo, N. Suzuki, S. Sudo, S. Ae, Y. Muroya, K. Yashiki, K. Satoh, T. Morimoto, K. Mori, and T. Sasaki, "Wavelength-selectable microarray light sources for s-, c-, and l-band WDM systems," *IEEE Photon. Technol. Lett.*, vol. 15, pp. 903–905, July 2003.
- [43] B. Pezeshki, E. Vail, J. Kubicky, G. Yoffe, S. Zou, J. Heanue, P. Epp, S. Rishton, D. Ton, B. Faraji, M. Emanuel, X. Hong, M. Sherback, V. Agrawal, C. Chipman, and T. Razazan, "20-mW widely tunable laser module using DFB array and MEMS selection," *IEEE Photon. Technol. Lett.*, vol. 14, pp. 1457–1459, October 2002.
- [44] D. Ton, G. Yoffe, J. Heanue, M. Emanuel, S. Zou, J. Kubicky, B. Pezeshki, and E. Vail, "2.5-Gb/s modulated widely tunable laser using an electroabsorption modulated DFB array and MEMS selection," *IEEE Photon. Technol. Lett.*, vol. 16, pp. 2573–2575, June 2004.
- [45] J. De Merlier, K. Mizutani, S. Sudo, K. Naniwae, Y. Furushima, S. Sato, K. Sato, and K. Kudo, "Full C-band external cavity wave-length tunable laser using a liquid-crystal-based tunable mirror," *IEEE Photon. Technol. Lett.*, vol. 17, pp. 681–683, March 2005.

- [46] *Intel Work - Online*. <http://www.commsdesign.com/story/OEG20030110S0053>.
- [47] K. Sato, J. De Merlier, K. Mizutani, S. Sudo, S. Watanabe, K. Tsuruoka, K. Naniwae, and K. Kudo, "Over 50-mW fibre coupled power and 40-nm tuning range of an extremely compact external cavity wavelength tunable laser," in *Proc. of ECOC 2005*, Paper Th2.5.2, 2005.
- [48] I. Christiaens, *Vertically coupled microring resonators fabricated with wafer bonding*. Ghent University, Phd. thesis, 2005. <http://photonics.intec.ugent.be/publications/phd.asp?ID=150>.
- [49] D. Rabus, Z. Bian, and A. Shakouri, "A GaInAsP-InP double-ring resonator coupled laser," *IEEE Photon. Technol. Lett.*, vol. 17, pp. 1770–1772, September 2005.
- [50] M. Takahashi, Y. Deki, S. Takaesu, M. Horie, M. Ishizaka, K. Sato, K. Kudo, K. Suzuki, T. Kaneko, X. Xu, and H. Yamazaki, "A stable widely tunable laser using a silica-waveguide triple-ring resonator," in *Proc. OFC 2005*, Paper PDP19, 2005.
- [51] S.-H. Jeong, S. Matsuo, T. Segawa, H. Okamoto, Y. Kawaguchi, Y. Kondo, H. Suzuki, and Y. Yoshikuni, "Stable and fast 100 GHz-spaced 30-channel digitally tunable operation in monolithically integrated semiconductor laser employing chirped ladder filter," *Electron. Lett.*, vol. 41, pp. 1176–1178, October 2005.
- [52] Y. Tohmori, Y. Yoshikuni, T. Tamamura, H. Ishii, Y. Kondo, and M. Yamamoto, "Broad-range wavelength tunable superstructure grating (SSG) DBR lasers," *IEEE J. Quantum Electron.*, vol. 29, pp. 1817–1823, June 1993.
- [53] A. Ward, D. Robbins, G. Busico, E. Barton, L. Ponnampalam, J. Duck, N. Whitbread, P. Williams, D. Reid, A. Carter, and M. Wale, "Widely tunable DS-DBR laser with monolithically integrated SOA: design and performance," *IEEE J. Select. Topics Quantum Electron.*, vol. 11, pp. 149–156, Jan-Feb 2005.
- [54] P.-J. Rigole, S. Nilsson, L. Backbom, T. Klinga, J. Wallin, B. Stalnacke, E. Berglind, and B. Stoltz, "114-nm wavelength tuning range of a vertical grating assisted codirectional coupler laser with

- a super structure grating distributed bragg reflector," *IEEE Photon. Technol. Lett.*, vol. 7, no. 7, pp. 697–699, 1995.
- [55] H. Kogelnik and C. Shank, "Coupled-wave theory of distributed feedback lasers," *Journal of Applied Physics*, vol. 43, no. 5, pp. 2327–2335, 1972.
- [56] P. Bienstman, *CAMFR 1.2, CAvity Modelling FRamework*. June 2004. <http://camfr.sourceforge.net>.
- [57] P. Bienstman, *Rigorous and efficient modelling of wavelength scale photonic components*. Ghent University, Phd. thesis, 2001. <http://photonics.intec.ugent.be/publications/phd.asp?ID=104>.
- [58] M. Oberg, P.-J. Rigole, S. Nilsson, T. Klinga, L. Backbom, K. Streubel, J. Wallin, and T. Kjellberg, "Complete single mode wavelength coverage over 40 nm with a super structure grating DBR laser," *IEEE J. Lightwave Technol.*, vol. 13, pp. 1892–1898, September 1995.
- [59] G. Sarlet, G. Morthier, R. Baets, D. Robbins, and D. Reid, "Optimization of multiple exposure gratings for widely tunable lasers," *IEEE Photon. Technol. Lett.*, vol. 11, pp. 21–23, January 1999.
- [60] H. Ishii, H. Tanobe, F. Kano, Y. Kondo, and Y. Yoshikuni, "Quasi-continuous wavelength tuning in super-structure-grating (SSG) DBR lasers," *IEEE J. Quantum Electron.*, vol. 32, pp. 433–441, March 1996.
- [61] D. Delbeke, *Design and fabrication of a highly efficient light-emitting diode : the grating-assisted resonant cavity light-emitting diode*. Ghent University, Phd. thesis, 2002. <http://photonics.intec.ugent.be/publications/phd.asp?ID=132>.
- [62] W. Bogaerts, *Nanophotonic Waveguides and Photonic Crystals in Silicon-on-Insulator*. Ghent University, Phd. thesis, 2004.
- [63] J. A. Nelder and R. Mead, "A simplex method for function minimization," *Computer Journal*, vol. 7, no. 4, pp. 308–313, 1964.
- [64] R. Todt and M.-C. Amann, "Influence of facet reflections on monolithic widely tunable laser diodes," *IEEE Photon. Technol. Lett.*, vol. 17, pp. 2520–2522, December 2005.

- [65] M. Farries, J. Buus, and M. Kearley, "Design and fabrication of two layer anti-reflection coatings for semiconductor optical amplifiers," *Electron. Lett.*, vol. 26, no. 19, pp. 1626–1627, 1990.
- [66] D. Marcuse, "Reflection loss of laser mode from tilted end mirror," *IEEE J. Lightwave Technol.*, vol. 7, no. 2, pp. 336–339, 1989.
- [67] I. Cha, M. Kitamura, H. Honmou, and I. Mito, "1.5/ $\mu\text{m}$  band travelling-wave semiconductor optical amplifiers with window facet structure," *Electron. Lett.*, vol. 25, pp. 1241–1242, 1989.
- [68] H. Ishii, Y. Kondo, F. Kano, and Y. Yoshikuni, "A tunable distributed amplification DFB laser diode (TDA-DFB-LD)," *IEEE Photon. Technol. Lett.*, vol. 10, pp. 30–32, January 1998.
- [69] R. Todt, *Widely Tunable Laser Diodes with Distributed Feedback*. Technical University of Munich, Phd. thesis, 2006.
- [70] R. Todt, T. Jacke, R. Meyer, and M.-C. Amann, "High output power tunable twin-guide laser diodes with improved lateral current injection structure," *Electron. Lett.*, vol. 41, pp. 190–191, April 2005.
- [71] M. Usami, S. Akiba, and K. Utaka, "Asymmetric  $\lambda/4$  shifted InGaAsP/InP DFB lasers," *IEEE J. Quantum Electron.*, vol. 23, pp. 815–821, June 1987.
- [72] P. Vankwikelberge, G. Morthier, and R. Baets, "CLADISS - a longitudinal multimode model for the analysis of the static, dynamic, and stochastic behavior of diode lasers with distributed feedback," *IEEE J. Quantum Electron.*, vol. 26, no. 10, pp. 1728 – 1741, 1990.
- [73] Photon Design. <http://www.photond.com/>.
- [74] B. Hakki and T. Paoli, "Gain spectra in GaAs double-heterostructure injection lasers," *J. Appl. Phys.*, vol. 46, no. 3, pp. 1299–1306, 1975.
- [75] R. Todt, T. Jacke, R. Meyer, and M.-C. Amann, "Thermally widely tunable laser diodes with distributed feedback," *Appl. Phys. Lett.*, vol. 87, p. 021103, June 2005.
- [76] R. Todt, T. Jacke, R. Meyer, and M.-C. Amann, "Thermally widely tunable laser diodes with distributed feedback," in *Proc. of ECOC 2005*, Paper We4.P77, 2005.

- [77] "Gert sarlet, syntune ab, private conversation."
- [78] S. L. Woodward, P. Parayanthal, and U. Koren, "The effects of aging on the Bragg section of a DBR laser," *IEEE Photon. Technol. Lett.*, vol. 5, pp. 750–752, July 1993.
- [79] H. Mawatari, M. Fukuda, F. Kano, Y. Tohmori, Y. Yoshikuni, and H. Toba, "Lasing wavelength changes due to degradation in buried heterostructure distributed Bragg reflector lasers," *IEEE J. Lightwave Technol.*, vol. 17, pp. 918–923, May 1999.
- [80] F. Delorme, G. Terol, H. de Bailliencourt, S. Grosmaire, and P. Devoldere, "Long-term wavelength stability of 1.55- $\mu\text{m}$  tunable distributed Bragg reflector lasers," *IEEE J. Select. Topics Quantum Electron.*, vol. 17, pp. 480–486, May/June 1999.
- [81] O. A. Lavrova and D. J. Blumenthal, "Accelerated aging studies of multi-section tunable GCSR lasers for dense WDM applications," *IEEE J. Lightwave Technol.*, vol. 18, pp. 2196–2199, December 2000.
- [82] G. Sarlet, G. Morthier, and R. Baets, "Control of widely tunable SSG-DBR lasers for dense wavelength division multiplexing," *IEEE J. Lightwave Technol.*, vol. 18, pp. 1128–1138, August 2000.
- [83] H. Ishii, F. Kano, Y. Yoshikuni, and H. Yasaka, "Mode stabilisation method for superstructure-grating DBR lasers," *IEEE J. Lightwave Technol.*, vol. 13, pp. 433–442, March 1998.
- [84] H. Lyu, G. Lyu, S. Park, and J. Lee, "Multichannel wavelength locking using transmission peaks of an AWG for multichannel optical transmission systems," *IEEE Photon. Technol. Lett.*, vol. 10, pp. 276–278, February 1998.
- [85] Y. Park, S.-T. Lee, and C.-J. Chae, "A novel wavelength stabilization scheme using a fiber grating for WDM transmission," *IEEE Photon. Technol. Lett.*, vol. 10, pp. 1446–1448, October 1998.
- [86] S. L. Woodward, V. Mizrahi, T. L. Koch, U. Koren, and P. J. Lemaire, "Wavelength stabilisation of a DBR laser using an in-fiber Bragg filter," *IEEE Photon. Technol. Lett.*, vol. 5, pp. 628–630, June 1993.
- [87] B. Mason, S. P. DenBaars, and L. Coldren, "Tunable sampled-grating DBR lasers with integrated wavelength monitors," *IEEE Photon. Technol. Lett.*, vol. 10, pp. 1085–1087, August 1998.

- [88] S. L. Woodward, T. L. Koch, and U. Koren, "A control loop which ensures high side-mode-suppression ratio in a tunable DBR laser," *IEEE Photon. Technol. Lett.*, vol. 5, pp. 417–419, May 1992.
- [89] M. Teshima, "Frequency stabilization of tunable DBR laser using multiwavelength light injection locking technique," *IEEE J. Light-wave Technol.*, vol. 14, pp. 2749–2756, December 1996.
- [90] B. Moeyersoon, G. Morthier, and R. Baets, "Novel optical feedback scheme for improvement of the wavelength switching behaviour of tunable lasers," in *2002 IEEE 18th International Semiconductor Laser Conference*, Paper TuP12, pp. 91–92, September 2002.
- [91] L. A. Coldren and S. W. Corzine, *Diode Lasers and Photonic Integrated Circuits*, vol. ISBN 0-417-11875-3. Wiley Interscience, 1995.
- [92] O. Kjebon, R. Schatz, S. Lourdudoss, S. Nilsson, and B. Staltnacke, "Modulation response measurements and evaluation of MQW In-GaAsP lasers of various designs," vol. 2684, pp. 138–152, SPIE, 1996.
- [93] G. Morthier, G. Sarlet, R. Baets, R. O'Dowd, H. Ishii, and Y. Yoshikuni, "The direct modulation bandwidth of widely tunable DBR laser diodes," in *Proc. ISLC 2000*, Paper P12, pp. 87–88, 2000.
- [94] K. Drögemüller and S. Illek, "Frequency modulation characteristics of tunable twin-guide (TTG) DFB lasers," in *Proc. of ECOC 1990*, pp. 181–184, 1990.
- [95] A. Saavedra, P.-J. Rigole, E. Goobar, R. Schatz, and S. Nilsson, "Relative intensity noise and linewidth measurements of a widely tunable GCSR laser," *IEEE Photon. Technol. Lett.*, vol. 10, pp. 481–483, April 1998.
- [96] M. Majewski, J. Barton, L. Coldren, Y. Akulova, and M. Larson, "Direct intensity modulation in sampled-grating DBR lasers," *IEEE Photon. Technol. Lett.*, vol. 14, pp. 747–749, June 2002.